Master's Thesis 2009

Candidate: Wei Ke

Title: CO_2 BLEVE (Boiling Liquid Expanding Vapor Explosion)

Telemark University College
Faculty of Technology

Telemark University College

Faculty of Technology

Kjølnes

3914 Porsgrunn

Norway

Lower Degree Programmes – M.Sc. Programmes – Ph.D. Programmes

Telemark University College

Faculty of Technology

M.Sc. Programme

MASTER'S THESIS, COURSE CODE FMH606

Student:	**Wei Ke**
Thesis title:	**CO$_2$ BLEVE (Boiling Liquid Expanding Vapor Explosion)**
Signature:	. . . .
Number of pages:	**139**
Keywords:	**CO$_2$ BLEVE; Pressure Wave;**
	Explosion Energy; Fragment Velocity.
Supervisor:	Professor Dag Bjerketvedt sign.:
2nd Supervisor:	Assoc. Professor Randi S. Holta sign.:
Censor:	sign.:
External partner:	StatoilHydro sign.:
Availability:	Open

Archive approval (supervisor signature)**:**   sign.:   . . . .

Date : . . . .

Abstract:

Boiling Liquid Expanding Vapor Explosion (BLEVE) has caused many accidents in industry, while research with BLEVE is still limited with scarcity of experimental data. Among all pressurized liquefied gases (PLGs), CO$_2$ plays an important role in industry. The risk of a BLEVE caused by CO$_2$ must be reduced during its storage and transportation. For this purpose, laboratory study has been performed for a deeper understanding of CO$_2$ BLEVE on its formation and prevention. A few insights have been achieved from the work with quantitative analysis of experimental data. Several possibilities of further research have also been recommended, with a same purpose of unveiling the mechanism of CO$_2$ BLEVE and increasing the safety during storage and transportation of CO$_2$.

Table of contents

Tables & Figures

Preface

The present work was carried out from late January to early June 2009 at the Faculty of Technology, Telemark University College, Porsgrunn, Norway. It requires knowledge in thermodynamics, automation, sensor technology, programming and imaging techniques. It aims to offer further insights in the safety of CO_2 storage through experimental investigations.

1 Introduction

The concept of BLEVE (Boiling Liquid Expanding Vapor Explosion) has been issued decades ago, after some catastrophic explosion accidents with fatalities and property damage occurred in the history of industry. The formation of a BLEVE was found to be related or be the main cause to some of these accidents and thus deserve thorough study.

Most research and experimental work on BLEVE so far have been focused on flammable fuels like liquid petroleum gas or other types of carbon containing fuels. BLEVEs of non-flammable fluids have not been studied as much.

Carbon Dioxide (CO_2) has a great significance to industry and plays a special role in environmental protection. When it comes to CO_2 storage and transportation, a potential of BLEVE by CO_2 would bring great risk and damage to facilities and industrial operators. Although there were several CO_2 BLEVE accidents in history, the mechanism of its occurrence remains unclear, with very limited experimental work performed.

In this work, CO_2 BLEVE experiments have been performed in laboratory. The main objective was to construct a functional experimental rig and to gain further knowledge on the mechanism and consequences of CO_2 BLEVE by analyzing experimental data. With application of new knowledge gained, CO_2 storage risk in industry may be further reduced. A set of conclusions have been reached.

The document of this work has been classified into five Chapters. Following this brief introduction, Chapter 2 introduces BLEVE with definition, consequences and main theories on the mechanism of its formation. Specific information on CO_2 BLEVE is also included. Chapter 3 describes the construction of experimental rig with experimental setup in details. Chapter 4 includes results and discussion from experimental data. Chapter 5 lists main conclusions from this work that may need further study or may be applied in industry. A few recommendations for future research are also given in Chapter 5.

2 Review on BLEVE

This Chapter introduces the concept of 'BLEVE' with related historic accidents. Main theories on the mechanism and consequences of BLEVE by other researchers have been briefly summarized. Additional information for CO_2 BLEVE is also included.

Subsection 2.1 gives a brief summary of physical and thermodynamic properties of Carbon Dioxide (CO_2). Subsection 2.2 describes BLEVE in general with definition, mechanism, consequences including pressure wave and fragments, and calculation of explosion energy. Subsection 2.3 writes more specifically for CO_2 BLEVE with an overview of its severity and CO_2 thermodynamics during an explosion.

2.1 CO_2 properties

Carbon Dioxide (CO_2) is a slightly toxic, odorless, colorless gas with a slightly pungent, acid taste. It is a small but important constituent of air. It is a main product of combustion of carbon-based fuels, respiration in animals and plants, and bacterial decomposition.

The carbon dioxide molecule (O=C=O) consists of two double bonds and has a linear shape. Its molecular weight is 44 kg/kmol. Its typical concentration in air is about 0.038% or 380 ppm. At standard temperature and pressure, the density of carbon dioxide is around 1.98 kg/m^3 and is 1.52 times heavier than air. Carbon dioxide is non-flammable and moderately reactive, but will support the combustion of metals such as magnesium.

Liquid carbon dioxide forms at pressures above 5.1 bar. The temperature determines the phase of CO_2 above this pressure. The critical point is 73.8 bar at 31.1°C. CO_2 above critical point will be in supercritical phase. Basic physical properties of carbon dioxide are summarized in Table 2-1 below.

Table 2-1: Physical properties of Carbon Dioxide (CO_2).

Molecular weight [kg/kmol]	Gas phase @[0 °C, 1 bar]			Boiling Point		Triple Point		Critical Point	
	Specific heat [kJ/kg]	Density [kg/ m^3]	Specific gravity (Air = 1)	T [°C]	P [bar]	T [°C]	P [bar]	T [°C]	P [bar]
44.01	0.85	1.98	1.54	-78.5	1	-56.6	5.17	31.1	73.8

'T' and 'P' in Table 2-1 are temperature and pressure.

A Pressure-Temperature diagram and a Pressure-Enthalpy diagram for carbon dioxide could be found in Appendix A.

2.2 BLEVE in general

2.2.1   Definition of BLEVE

BLEVE is short for Boiling Liquid Expanding Vapor Explosion. Various definitions for BLEVE exist. According to The Center for Chemical Process Safety, as sited in the work of Tasneem Abbasi et al [1], *'A BLEVE is a sudden release of a large mass of pressurized superheated liquid to the atmosphere'*. The sudden release can be caused by failure of confinement, or, *'loss of confinement (LOC)'*, which in most cases is due to fire, missile hitting, tank rupture or corrosion, etc.

The '*pressurized superheated liquid*' in the definition above refers to a pressurized liquid gas (or pressure liquefied gas, PLG) in a superheated state, a thermodynamic state when a liquid with temperature higher than its boiling point has a sudden depressurization.

2.2.2   Consequences of BLEVE

A sudden opening or failure of a vessel where a PLG is stored as liquid/vapor mixture will undergo a fast depressurization. The depressurization would cause a two-phase flow to splash out of the vessel nearly instantaneously and very likely lead to a devastating explosion with damaging pressure waves and vessel fragments. Catastrophic damages could be caused by the pressure waves generated due to the boiling and vaporization of a PLG along depressurization. The fragments of the storage vessel at high speed may be projected from explosion center at high speed and also cause serious damage to facilities and operators in industrial activities.

In general, a BLEVE may lead to the following consequences, as described by Tasneem Abbasi et al [1].

● '*Splashing of some of the liquid to form short-lived pools; the pools would be on fire if the liquid is flammable.*'

● Blast wave.

● Flying fragments (missiles).

● Fire or toxic gas release. If the pressured-liquefied vapor is flammable, as is often the case, the BLEVE leads to a fireball. If the material undergoing BLEVE is toxic, as in the case of ammonia or chlorine, there will be toxic gas dispersion [1].

A history of major BLEVE events with various causes and damages that have occurred since as early as 1920s has been summarized by Tasneem Abbasi et al [1], as cited in a full version in Appendix B.

2.2.3 Mechanism of BLEVE

Theories on BLEVE mechanism are few and often rely on very limited experimental data. Among them, a comprehensive summary about key steps involved in a typical BLEVE has been summaried by Tasneem Abbasi et al [1] and is paraphrased as below.

(a) Failure of vessel. Various causes including overload heating, external hitting or vessel corrosion may lead to a failure and sudden opening of the vessel.

(b) Phase transition. When the vessel fails, an instantaneous depressurization occurs to the pressure liquefied gas stored inside. The pressurized liquid/vapor mixture initially in a saturated thermodynamic state with a temperature higher than its boiling point becomes superheated when the original vessel pressure decreases to atmospheric pressure in few milliseconds.

(c) Bubble nucleation. According to 'Superheat Limit Temperature' theory as is described with details later in this page and next page, the pressurized liquid can endure with being superheated when temperature inside the vessel is well below the superheat limit temperature (SLT) of the liquid. However, if the temperature is above SLT, fast bubble nucleation will start inside and finally lead to violent splashing of liquid/vapor mixture out of the vessel into atmosphere.

(d) Explosion due to depressurization and bubble nucleation. As intense phase transition in superheated state happens, the boiling of the liquid followed by bubble nucleation, the expanding vapor from both vaporization of the liquid and the initial vapor stored in the vessel will together lead to an explosion (Boiling Liquid Expanding Vapor Explosion, BLEVE).

(e) Blast wave formation. With an increase in total volume of the expanding vapor, by a factor of a hundred to over a thousand fold, a powerful blast wave will form and bring damage to facilities nearby.

(f) Vessel rupture. Due to the powerful blast wave, the vessel ruptures and its pieces/fragments fly outwards everywhere like rocket missiles.

(g) Fireball or dispersion of toxic fluid. Discussion on fireball or toxic dispersion in a BLEVE has been developed with theoretical models and will not be described here. If the substance undergoing a BLEVE is not toxic or flammable, such as carbon dioxide discussed in this work, the blast wave and the vessel fragments will be the only effects of the explosion.

C.R.Reid [2] suggested that BLEVEs are essentially superheat explosions and thus can be predicted with superheat. Reid's 'Superheat Limit Temperature' theory is illustrated with Figure 2-1, as cited in the work of G.A.Pinhasi [3].
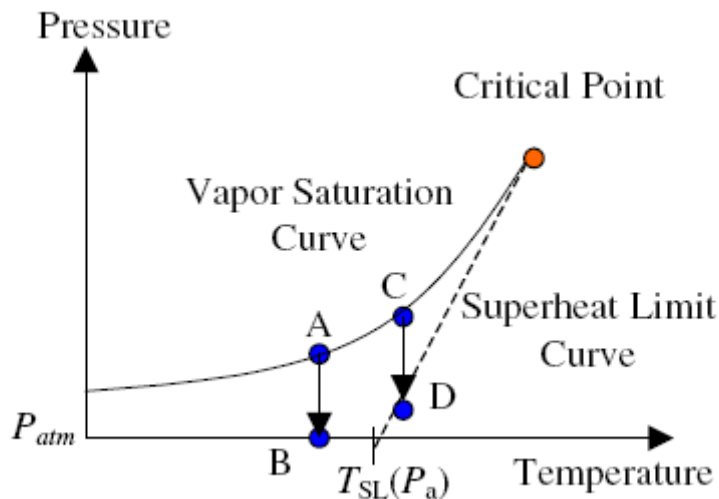
Figure 2-1: Reid's 'Superheat Limit Temperature' theory for BLEVE formation [3].

Initially, prior to the failure of vessel, the vessel contains both pressurized vapor and liquid at saturated state. Then, the depressurization starts with a sudden opening of the vessel. This opening process is expected to be so fast that the saturated temperature is assumed to remain unchanged, as shown in Figure 2-1 the routes from point A to point B or point C to point D.

With this isothermal assumption, there are in total two possible routes for the depressurization process.

The first route is when a relatively low initial temperature at the beginning of depressurization, as from point A, the pressure drops to atmospheric pressure, to point B. Violent liquid boiling could be observed from this depressurizing process. However, a BLEVE will not occur since the superheat-limit curve (the dotted line) is not yet reached.

The second route is when the initial temperature is higher, for example, starting from point C, and similarly, pressure drops to atmospheric pressure, through point D. In this case, the superheat limit curve is reached by point D and thus an explosion is expected to occur.

Basically, Reid's 'Superheat Limit Temperature' theory assumes that the superheat limit temperature for a fluid is the temperature threshold to the occurrence of a BLEVE. The theory has been supported by some BLEVE researchers. However, Prugh [4] stated that, a BLEVE can also occur with an initial temperature of the two phase mixure lower than the super heat limit temperature. He also commented that a difference between such a low temperature BLEVE and BLEVEs that occur with initial temperature higher than SLT is that the TNT equivalent of the blast wave (explosion energy) of the former case is considerably lower than the later one.

The SLT theory has been tested and confirmed with some fluids and is assumed to be applicable to other fluids as well.

'When it comes to pressurized liquefied gas, a substance that would be in gaseous state at atmospheric pressure but is held as liquid in a pressurized container, the SLT theory seems to be implicit. Numerous industrial chemicals such as liquid petroleum gas, compressed natural gas, liquefied chlorine, etc. have confirmed to this theory, so does superheated water in a boiler.' [1].

Still, more experiments with various fluids can be tested with experiments to further confirm or improve the theory.

An alternative to look into SLT theory is to observe the degree of superheat. The degree of superheat is the temperature range from the initial temperature when the sudden opening of a vessel starts to the boiling point of the liquid. A 'Nominal degree of Superheat' is often used as a reference and it means the temperature difference between the Superheat limit temperature (SLT) and the boiling point of the liquid.

Tasneem Abbasi et al [1] in their work gave an illustrative example with ammonia, chlorine and butane with analysis of the degree of superheat. They have calculated the available degree of superheat when vessels containing these PLGs accidentally rupture at 308 K or 350 K. They described the result with Figure 2-2. The figure also gives the pressure-temperature curves for the three PLGs along with the corresponding superheat limit curves (tangents drawn from critical points).
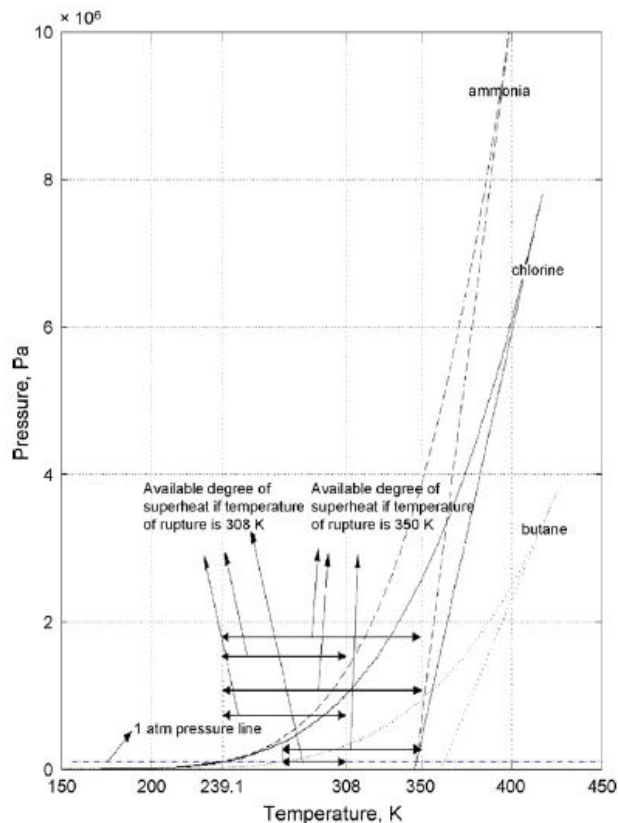
Figure 2-2: Pressure-temperature curves and superheat limit curves for ammonia, chlorine and butane, with degrees of superheat at two rupture temperatures (308 K/350 K) [1].

The values of boiling point (BP) and superheat limit temperature (SLT) at 1 atm for ammonia is 239.8 K and 347.21 K respectively. For chlorine, BP = 239.1 K, SLT = 247.22 K. For butane, BP = 272.7 K, SLT = 362.61 K. The different available degrees of superheat with different temperature of rupture (initial temperature) for these three PLGs are indicated in Figure 2-2.

An assumption applied with the degree of superheat is that this temperature difference decides the intensity of the blast wave generated from an explosion. The higher the degree of superheat is available for a pressure liquefied gas in a storage vessel, the more possible a BLEVE would occur.

2.2.4 Explosion Energy in a BLEVE

Three main methods used to estimate the explosion energy with a BLEVE have been developed, as summarized by Tasneem Abbasi et al [1]:

a) The 'TNT equivalent method'. The expanding vapor is treated as an ideal gas. This method is developed by Prugh [4].

b) The 'SVEE Method'. It relies on entropy, enthalpy and specific volume data while treating the expanding vapor as non-ideal gas. This method is developed by Prugh [4], CCPS, Lees and TNO together, as cited in the work of Tasneem Abbasi [1].

c) The 'Irreversible adiabatic expansion Method'. It treats the flashing of vapor-liquid mixture in a BLEVE as irreversible, adiabatic expansion rather than as isentropic expansion as in the 'TNT equivalent Method' and thus is considered to be closer to reality. This method is developed by Planas-Cuchi et al, as cited by Tasneem Abbasi [1].

A table on these three methods of estimating explosion energy in a BLEVE has been summarized by Tasneem Abbasi et al [1] and a full version has been cited and attached as Appendix C.

2.2.5 Fragments

One consequence of a BLEVE is fragments, or, rocket missiles flying out from the explosion center. M.R.Baum [5] has discussed in his work in great details with development of theoretical models for calculation of rocket missiles. He also performed experiments with a horizontal pressure vessel containing high temperature liquid. Peak velocity of fragments is usually used for calculation of the kinetic energy. The kinetic energy could then be related to the overall explosion energy as calculated with models described in Subsection 2.2.4. Sometimes for simplicity, researchers may use a coarse estimation that a certain percentage of the overall explosion energy, 10% or 20% for example, is transformed into the kinetic energy of fragments. This would make the estimation of explosion energy in a BLEVE much easier.

2.3 CO_2 BLEVE

With a brief description on general BLEVEs and a main theory ('Superheated Limit Temperature' theory) for BLEVE formation introduced in Subsection 2.2, this Subsection is written more specifically for CO_2 BLEVE, to know more about its severity and CO_2 thermodynamics during an explosion.

2.3.1 Overview

Most publications and general literatures on BLEVE have been discussing hydrocarbon substances like LPG, propane, etc with emphasis on safety issues like ignition and the combustion process. Literature on CO_2 BLEVE is very limited. CO_2 BLEVE has not been studied as much as BLEVEs of flammable PLGs. Experimental data on CO_2 is also very limited.

Severe fatalities and property damage can also occur when vessels contain non-flammable and non-toxic chemicals like CO_2. With a special importance to industry, the CO_2 storage and transportation should be assured safe and reduce risks of accidents, like a BLEVE.

The public may have a wrong impression on the severity of BLEVEs caused by flammable or non-flammable fluids. An analogy drawn from everyday experience that may not be accurate in science may explain why they would think as granted that a BLEVE with non-flammable fluids will cause much less fatalities or damage than a BLEVE with flammable fluids. Think of a balloon played by kids for fun and a lighter used by men for smoking. If asked to choose one with more danger, the public will probably choose the lighter, because the small, twinkling flame above the lighter they see looks more dangerous than a sound of 'P-O-O' they hear from a cracked balloon.

The truth is, large amount of CO_2 is usually stored in high strength, fine grain carbon steel vessels in industry. There will be, if a BLEVE occurs, large-scale damages and fatalities caused by both blast waves with high explosion energy and vessel fragments at high speed. As marked in the list of BLEVE accidents in industrial history in Appendix B, at least two severe BLEVE accidents were caused by failure of CO_2 storage, one in January 2, 1969, Hungary and the other in November 27, 1972, USA. Take the accident in Hungary for example, 9 people were killed when a 35-t vessel containing carbon dioxide BLEVEd due to over filling. The fatality severity in this accident was even worse than some BLEVEs of flammable PLGs.

2.3.2 Thermodynamics

When it comes to CO_2 BLEVE, the uniqueness of its thermodynamic properties also makes it more interesting and more complex to study. Normally carbon dioxide is stored in vessels

with a pressure of no less than 5 atm. The CO_2 inside the vessel is at equilibrium state (saturated) as a mixture of liquid and vapor. When the vessel fails, the instantaneous depressurization to atmospheric pressure gives rise to a rapid phase change of the two-phase CO_2 mixture. Compared with other PLGs, thermodynamics of this phase transition is unique and explained below.

Start from SLT theory. The theory has for simplicity assumed the superheat limit temperature of a fluid is the temperature threshold to the occurrence of a BLEVE, as shown in Figure 2-1 on page 15 while the depressurization process is considered isothermal. Figure 2-3 plots the vapor pressure line (Saturation line) of CO_2 with superheat limit curve. The SLT of CO_2 is found to be -13.8 °C (T_{SL_CO2}). The saturation pressure with this temperature is 23.7 bar. The pressure range between 1 bar (atmospheric pressure) and 73.8 bar (Critical pressure) is of our interest to consider the phase transition. It corresponds from the boiling point to the critical point.
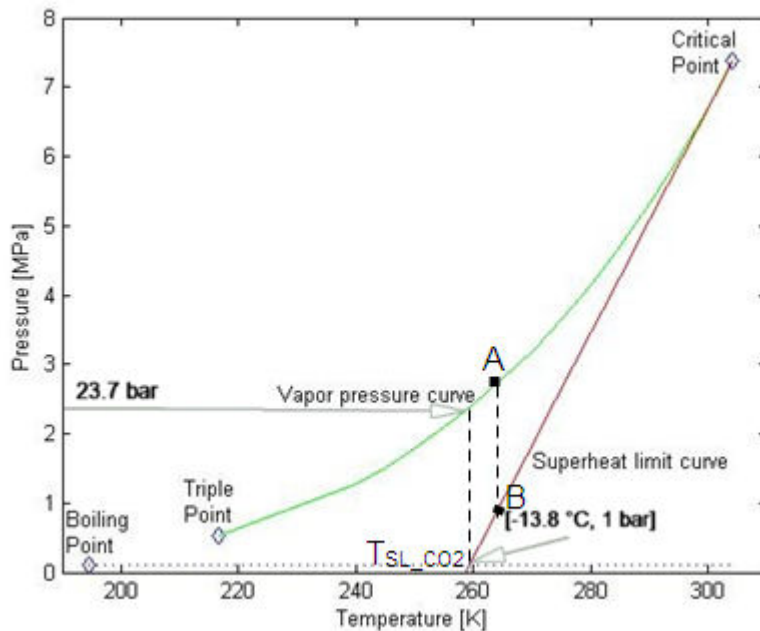
Figure 2-3: Saturation curve and Superheat limit curve of CO_2.

A saturation state is chosen randomly for an imagined CO_2 storage vessel. For example, the vessel is initially at 27.9 bar and -8 °C, shown as point A in Figure 2-3 (CO_2 storage pressure varies in industry depending on the design of storage vessel, normally above 20 bar).

If the vessel fails at this moment, according to SLT theory, the superheat limit curve has been reached at point B, when

$T_A = T_B$ = -8 °C > T_{SL_CO2} = -13.8 °C

The sudden depressurization from P_A (27.9 bar) to atmospheric pressure (1 bar) will lead to violent vaporization of liquid CO_2 and an explosion is expected with vapor expansion in

volume with several hundred or even higher fold. This 'A→B' route is given a name 'Expansion Route' when discussed in this report.

Interestingly, things may not end here. After the opening of this imagined vessel with pressurized two-phase CO_2, part of the liquid CO_2 may not vaporize but possibly, go to solid phase as dry ice. CO_2 Pressure-Temperature diagram as shown in Figure 2-4 is used here to clarify this assumption as a second route of phase transition, which is also given a name, 'Icing Route'.
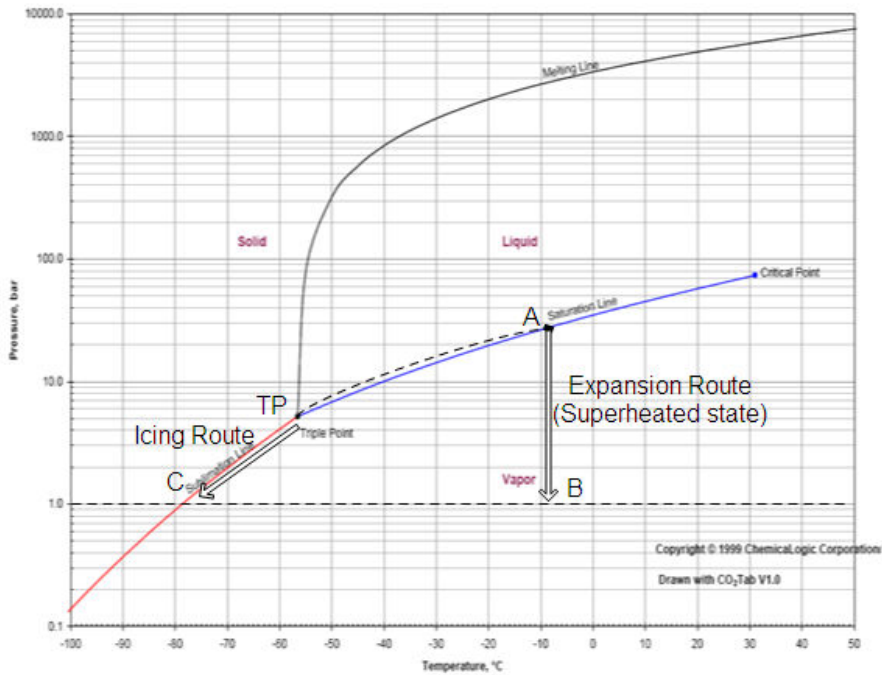
Figure 2-4: Pressure – Temperature diagram of CO_2.

CO_2 triple point [-56.6 °C, 5.17 bar] is indicated in figure above as TP. Both 'Expansion Route' and 'Icing Route' are shown for comparison.

SLT assumes that the temperature does not have a chance to decrease when the depressurization process has been considered infinitely fast, as from point A to point B. As a result, only vapor CO_2 will form by vaporization of liquid CO_2.

What will happen if depressurization takes such a long time that it can no longer be assumed 'infinitely fast'? The pressure will decrease. So will the temperature, due to continuous vaporization of liquid CO_2. The decreasing pressure and temperature of newly generated vapor may not necessarily follow the saturation line. It might be heated by ambient air of higher temperature through a contact surface. For simplicity, this heat inflow from air is neglected and we assume that the vapor is in a 'quasi-equilibrium' state that it tolerably follows the saturation curve with decrease in both pressure and temperature. Point A to point TP in Figure 2-4 shows this process.

The arrival of triple point gives the vapor an opportunity to form dry ice through the sublimation line backwards, as shown from point TP to point C. Point C is dry ice at boiling

point (-78.5 °C, 1 bar). Dry ice will start to form from TP, not the arrival of point C, although the pressure will surely decrease to 1 bar in the end. This process of potential is the 'Icing Route'. It is so far only an assumption and needs confirmation with CO_2 experiments.

3 Experimental setup

This chapter describes the experimental setup used to perform CO_2 tests. An overview in Section 3.1 with an instrumental diagram and a flow chart of experimental procedures goes first for the overall Chapter. Section 3.2 describes the construction of testing rig by dividing it into six operating units which support each other and together function organically. Section 3.3 introduces methods and programming files for post processing of experimental data. Technical information of devices in details is included in Appendix D.

3.1 Overview

The experimental setup work was carried out to establish a platform where CO_2 BLEVE tests could be performed. Various devices have been integrated into the experimental rig through which experimental data could be collected and stored in a proper way and used for further analysis.

Figure 3-1 is a photograph showing a vertical steel pedestal mounted on a side of wall. A tie rod air cylinder mounted on top of the pedestal and an experimental plastic pipe fixed with an aluminum pedestal at the rig bottom is the 'Experimental Center' area.
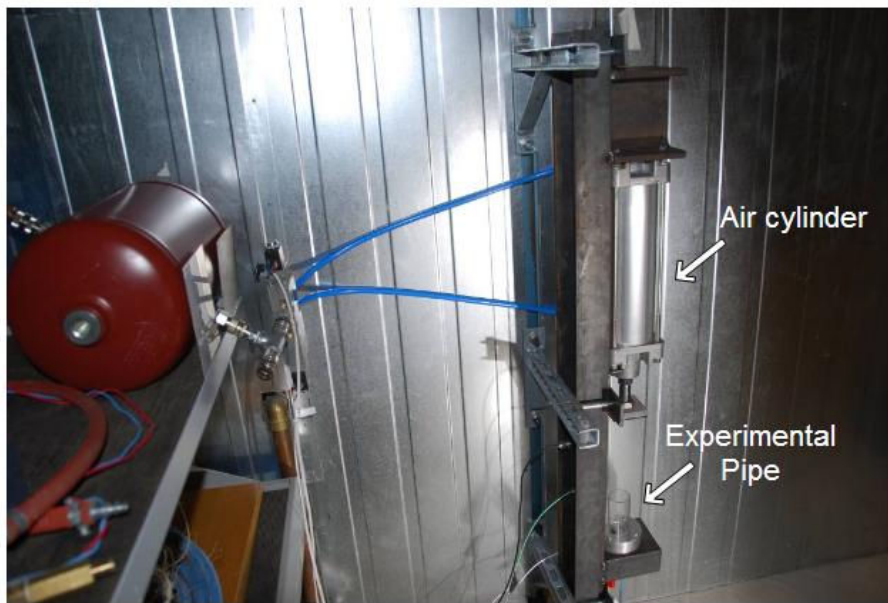
Figure 3-1: The 'Experimental Center' with an air cylinder and an experimental pipe.

Two kinds of pressure transducers together with their corresponding signal amplifiers were used to measure overpressures in varied places on or around the testing rig. The pressure signals recorded by these pressure transducers can be analyzed to find out the pressure peaks and the speed of blast wave propagation. The overpressures of each experiment were plotted as a function of time. This kind of plots was one of the main information sources for further analysis.

Besides pressure recordings, experimental videos were also recorded by a high-speed camera. These video recordings were important for the timing check of event scenarios with pressure signals, the analysis of bubble nucleation inside testing pipes, formation of fragments and estimation of their kinetic energy. Other important experimental information that could not be seen in pressure recordings may also be found in videos and thus gain extra insights.

An instrumental diagram of the experimental rig is shown in Figure 3-2.
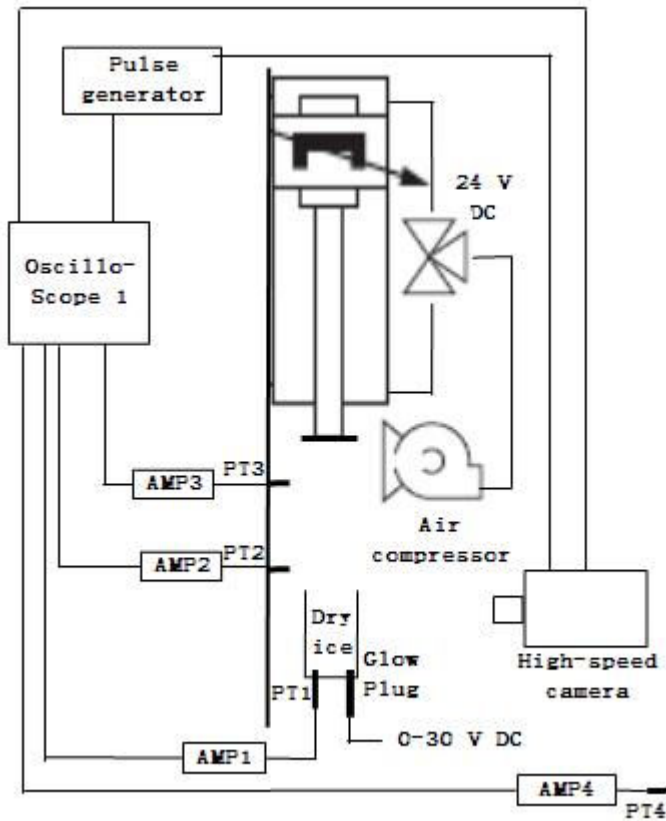
Figure 3-2: An instrumental diagram of the experimental rig.

As shown in Figure 3-2, dry ice was adopted as source of CO_2 filling. Four pressure transducers (from PT 1 to PT 4) together with their signal amplifiers (from AMP 1 to AMP 4) have been mounted to measure overpressures at varied locations. A high-speed camera was used to record videos of experiments. An oscilloscope was used to show voltage signals from pressure transducers and also served as a work station to store experimental data. Since all voltage signals from pressure transducers would easily be transformed later into overpressures with MATLAB programming scripts, they would be called 'pressure recording' or 'pressure records' in the following text. An air compressor and a pneumatic valve controlled the movement of piston in the air cylinder by changing the direction of pressurized air flow.

A standard flow chart of experimental procedures is shown in Figure 3-3.
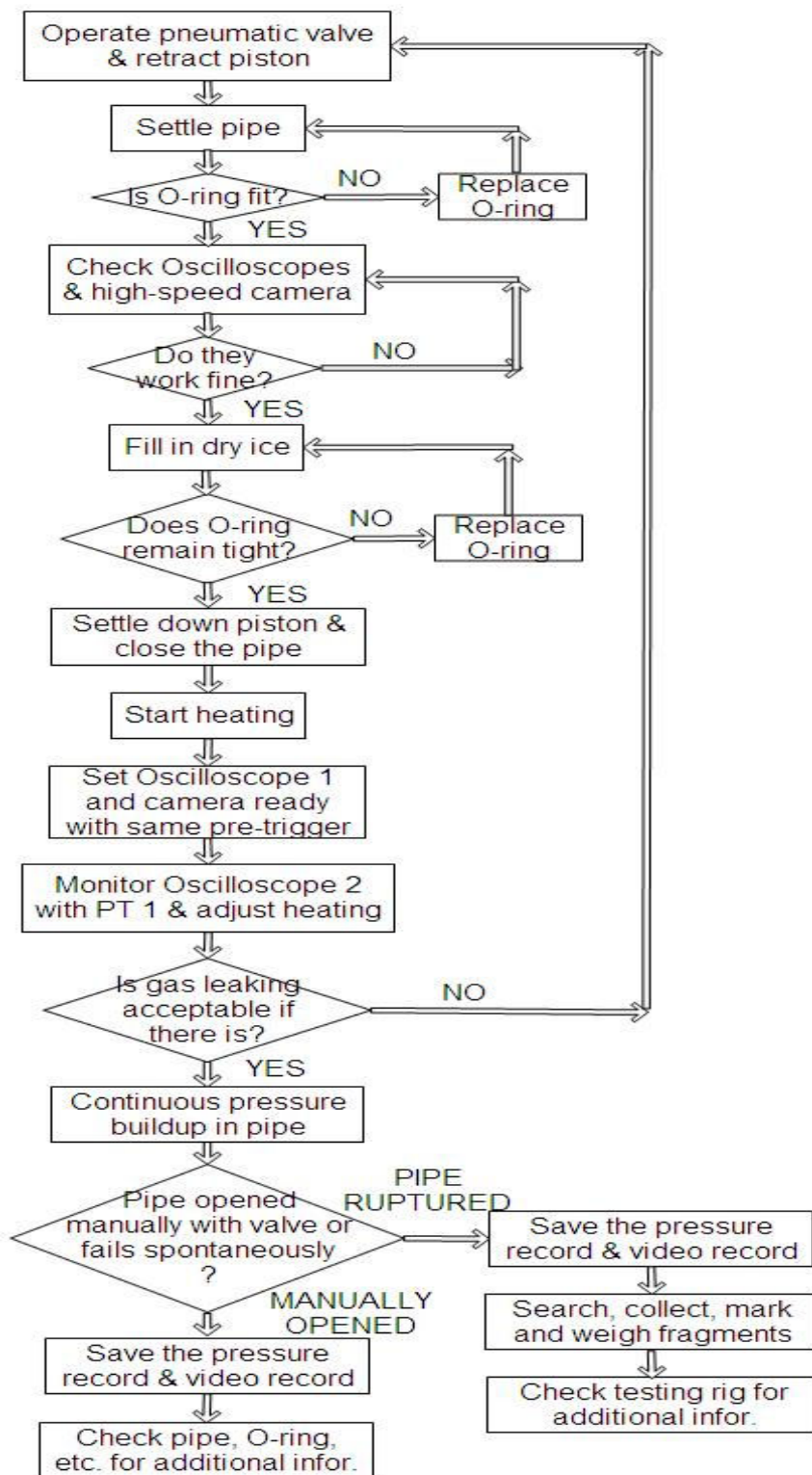
Figure 3-3: A standard flow chart of experimental procedures.

One thing that particularly worth mentioning in Figure 3-3 is that: when an experiment goes into the step of 'Continuous pressure buildup in pipe', two options of pipe opening are possible.

Option I: Open the pipe manually by manipulating the pneumatic valve and retract the piston. With this option, there might or might not be a BLEVE and the experimental pipe could normally endure the sudden pressure drop and no fragments would form.

Option II: Allow the pressure inside the pipe build up continuously and NOT redirect the valve / retract the piston UNLESS the pipe itself at some point suddenly ruptures. With this option, still, there might or might not be a BLEVE. The difference with Option I is that the pipe is not really 'opened' but 'cracked', and the fast cracking would generate a large number of fragments of small pieces. These fragments may be marked, collected and weighed as one additional approach to estimate the explosion energy.

Based on experimental setup described in this chapter and following the experimental procedures in Figure 3-3, a total of 21 CO_2 BLEVE tests have been performed. A complete set of experimental data has been collected and stored in a proper way for further analysis. The two options on pipe opening/rupturing make it necessary to classify the 21 CO_2 tests into two SETs, in order to make the description and discussion of each clearer.

SET 1 follows Option I and consists of test 1 to test 20. Among them, test 1 was a background test with no CO_2 filling, to reveal the magnitude of noise signals from the experimental system. It has pressure record and no video record. SET 2 follows Option II and consists of only test 21. Pressure record and video record are available for test 21. This classification of all tests is summarized as Table 3-1 below.

Table 3-1: Classification of CO_2 BLEVE tests.

SET No.	Test No.	CO_2 filling?	Pressure record?	Video record?	**Fragment?**
1	1-20	YES except test 1	YES	YES, except test 1 & test 3	**NO**
2	21	YES	YES	YES	**YES**

Six different operating units have been integrated into this overall, functional experimental rig. These six operating units are summarized and described in details in Subsection 3.2 'Rig construction'.

The methodology of HAZOP (Hazard and Operability Study) has been applied to the experimental rig. The purpose was to locate potential hazards during experiments, find out ways of prevention of these hazards as well as ways of protection to experimental operators, to reduce experimental risks as much as possible. A report of HAZOP Study has been attached as Appendix E.

3.2 Rig construction

Figure 3-1 on page 21 only shows the center area of an experiment, which was the experimental pipe where dry ice as CO_2 filling source was placed and heated, and a tie rod air cylinder with a piston for closing the pipe. In fact, the overall experimental setup includes six different, inter-connected operating units. These units are: Experimental pipes, Pipe closing/opening unit, Heating unit, Signal acquisition and recording unit, Video recording unit and Triggering unit.

Experimental pipes are described in Subsection 3.2.1. Subsection 3.2.2 describes the pipe closing/opening unit. Subsection 3.2.3 describes the heating unit. Signal acquisition and recording unit is described in Subsection 3.2.4. Subsection 3.2.5 describes the video recording unit and finally Subsection 3.2.6 describes the triggering unit. All six units work together to make sure an experiment goes smooth and experimental data including pressure records and video records is well collected with accurate timing and properly stored for further analysis.

3.2.1 Experimental pipes

Circular, polycarbonate pipes of two sizes were used in experiments. Table 3-2 gives the pipe parameters. The size of a pipe determines also the pipe volume and can be used later to calculate the weight of liquid CO_2 and vapor CO_2 respectively.

Table 3-2: Experimental polycarbonate pipe sizes.

Pipe No.	Used in:	Pipe Length [mm]	Inner Diameter [mm]	Outer Diameter [mm]	Volume [cm3]
1	Tests 1-5; test 21	80	36	40	82
2	Tests 6-20	100	32	40	80

An experimental pipe was sealed at one side with aluminum pedestal. Rubber rings (O-rings) with a same outer diameter as experimental pipes (40 mm) were placed tightly around inside the aluminum pedestal to prevent gas leakage from the bottom of the pipe. Figure 3-4 and Figure 3-5 show the aluminum pedestal and the O-ring used in experiments.

Figure 3-4: Aluminum pedestal.

Figure 3-5: O-ring for preventing gas leakage.

3.2.2   Pipe closing/opening unit

As shown in Figure 3-4 and Figure 3-5, the experimental pipe was sealed at bottom side with aluminum pedestal, with use of O-ring to prevent gas leaking from the bottom of the pipe. On the other hand, the Pipe closing/opening unit in this Subsection describes how the closing and opening of the pipe's top side was realized. This operating unit includes four elements with pressurized air flow, as shown in Figure 3-6 and Figure 3-7. Each of them is described below, in an order consistent with the flow direction of pressurized air.

Figure 3-6: Pipe closing/opening unit (Part 1).
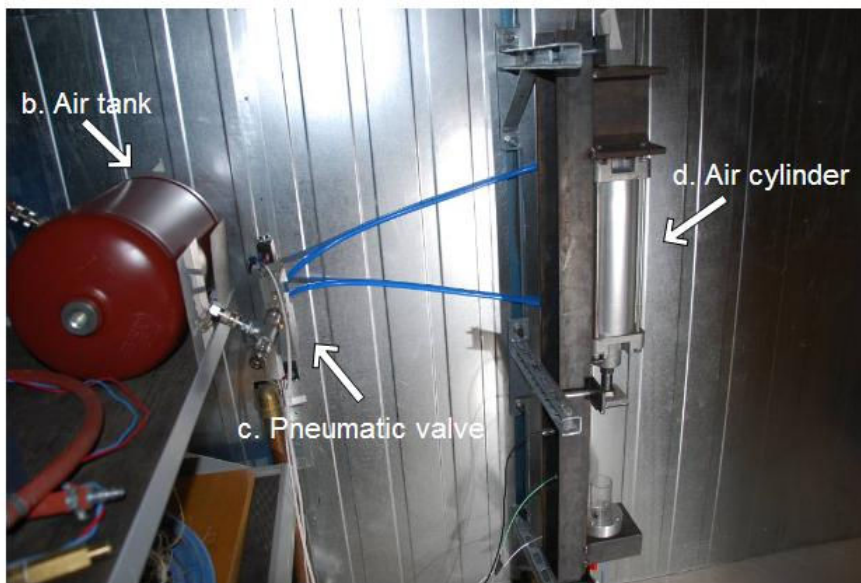
Figure 3-7: Pipe closing/opening unit (Part 2).

a) Air compressor.

The air compressor produces pressurized air and sends it to the air tank for storage. The air compressor shown in Figure 3-6 was named Compressor 1. Compressor 1 has a maximum internal pressure of 8 bar and adjustable outlet pressure of 0 − 8 bar. This compressor was used in tests 1 to 20, with an outlet pressure of 4 bar. This outlet pressure was increased to 10 bar as in test 21 by using Compressor 2. As shown in Figure 3-8, Compressor 2 has a maximum outlet pressure of 16 bar. The usage and main parameters of Compressor 1 and Compressor 2 are summarized in Table 3-3.

Figure 3-8: Air compressor 2 used in test 21.

Table 3-3: Compressor 1 & Compressor 2.

Compressor No.	Used in	Outlet pressure applied [bar]	Maximum outlet pressure [bar]
1	Tests 1-20 (SET 1)	4	8
2	Test 21 (SET 2)	10	16

b) Air tank.

The air tanks showed in Figure 3-6 and Figure 3-7 were used to store pressurized air from Compressor 1 or 2 and fill it into air cylinder with control of a pneumatic valve. The tank has a volume of 1.5 L and a maximum pressure of 10 bar. Same as Compressor 2, this air tank was only used in test 21 (SET 2); as in tests 1 to 20 (SET 1), the air compressor was connected directly with the pneumatic valve through which the air filling into air cylinder was controlled.

c) Pneumatic valve.

The pneumatic valve was a key element to switch the direction of air filling into the air cylinder so the movement of piston was controlled. More specially, this Bosch Rexroth 5/3 – way valve is driven by both electrical charge and pressurized air. The nominal voltage is 24 V. The minimum air pressure to drive the valve is around 4 bar. Figure 3-9 shows the connection of the pneumatic valve. Figure 3-10 shows its mechanism of switching the direction of pressurized air flow.
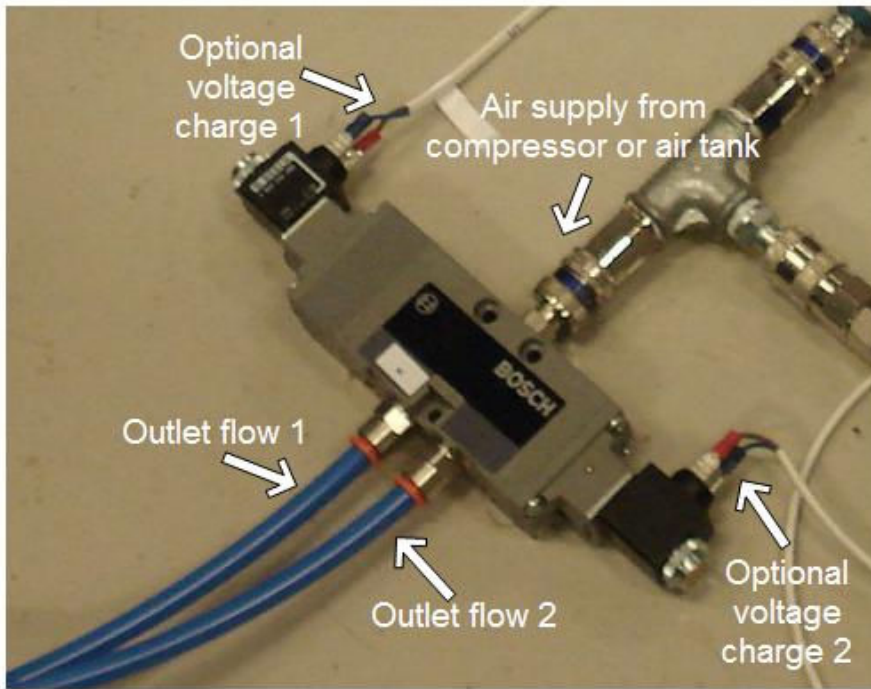
Figure 3-9: Connections of Bosch Rexroth 5/3 –way pneumatic valve.
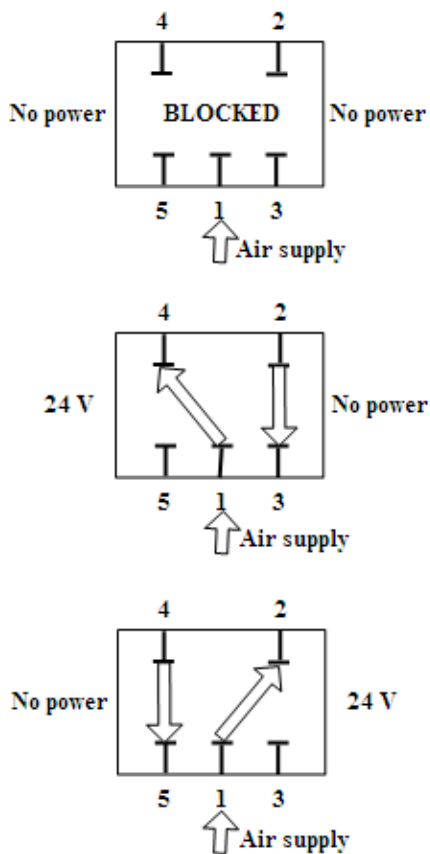
Figure 3-10: Mechanism of pneumatic valve for switching pressurized air flow.

The pneumatic valve is driven by 24 V voltage at either side, as marked in Figure 3-9, 'Optional voltage charge 1' or 'Optional voltage charge 2'. Meanwhile, it requires a minimum pneumatic air pressure of around 4 bar. The air supply from compressor or air tank marked in

Figure 3-9 corresponds to positon 1 in Figure 3-10. The outlet flow 1 and outlet flow 2 in Figure 3-9 correspond to position 2 and 4 in Figure 3-10. With a pneumatic pressure of no less than 4 bar through the valve, the valve redirects the pressurized air flow from air compressor to one of the inlets into the air cylinder by charging 24 V voltage to one specific side, which consequently builds up pressure from one side of the air cylinder and moves the piston either upwards or downwards.

The voltage switch was realized by a power supply with nominal voltage of 24 V and a physical switch as shown in Figure 3-11. The 'Up' position of the physical switch corresponds to the upward movement of the piston and opening of the experimental pipe; the 'Down' position of the switch leads to the downward movement of the piston and closing of the experimental pipe.
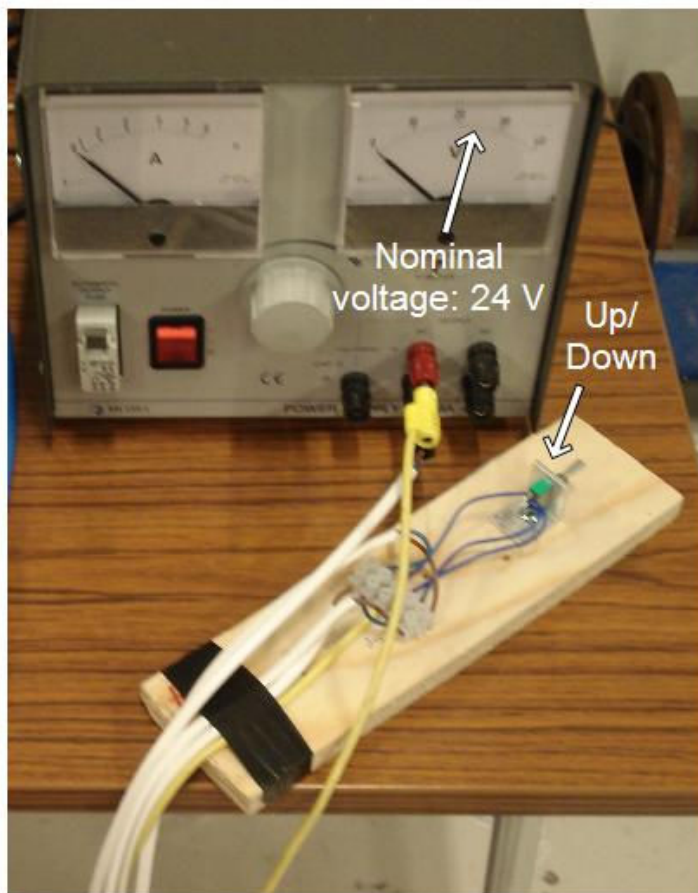
Figure 3-11: A physical switch and a power supply for the pneumatic valve.

More specific technical information of this 5/3 –way pneumatic valve could be found in Appendix D.1 .

d) Air cylinder.

A Bosch Rexroth Series 167: 80/200 mm tie rod cylinder was used in the experiments. As shown in Figure 3-12 below and also Figure 3-7, the air cylinder with two air flow inlets/outlets offers the possibility of pressure buildup inside from opposite directions. This is achieved with help of a pneumatic valve, as explained in c) above. When the inlet air flow

into air cylinder is switched by the pneumatic valve, the piston will either goes downwards or upwards, due to the pressure buildup inside air cylinder in either direction. When the piston goes downwards, it covers the top of the experimental pipe tightly and closes it. When the piston goes upwards, the pipe is opened, causing a sudden pressure drop if initially there is a pressure buildup inside the pipe.
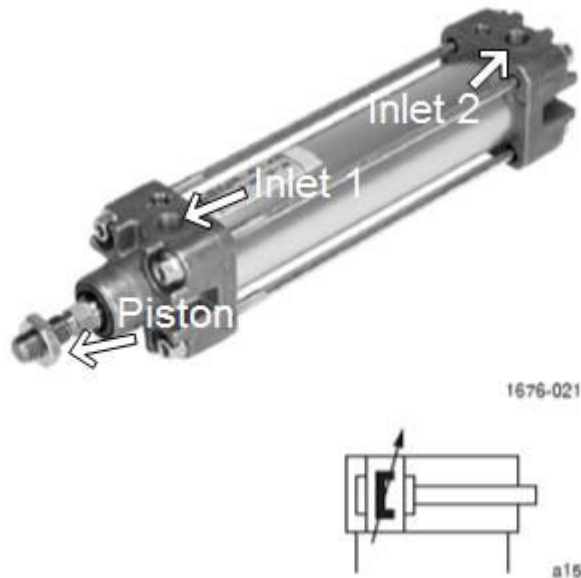
Figure 3-12: Bosch Rexroth Series 167: 80/200 mm tie rod cylinder.

O-rings were used to prevent gas leakage from the bottom of experimental pipes. Similarly, a plastic square with gasket as shown in Figure 3-4 on page 28 was used between the piston and the pipe top to prevent gas leakage from the top of the experimental pipes.

Detailed technical information for this type of air cylinder can be found in Appendix D.2.

3.2.3   Heating unit

With experimental pipes and pipe closing/opening unit ready, as described in previous Subsection 3.2.1 and Subsection 3.2.2, a heating unit was mounted. A Beru GN 857 glow plug used in diesel engines served together with a power supply as a heating unit to heat up dry ice of controlled weights and get pressurized liquid/vapor CO_2 mixtures. By adjusting the voltage applied to the glow plug and varying the time of heating, the speed of pressure buildup inside the experimental pipe was controlled. The glow plug was mounted through the aluminum pedestal and stayed inside the pipe during the whole experimental process. Figure 3-13 shows the glowing part (heating filament) of the glow plug inside the experimental pipe before CO_2 filling. Figure 3-14 shows the structure of a Beru GN 857 glow plug.

Figure 3-13: Glowing part of the glow plug inside experimental pipe.
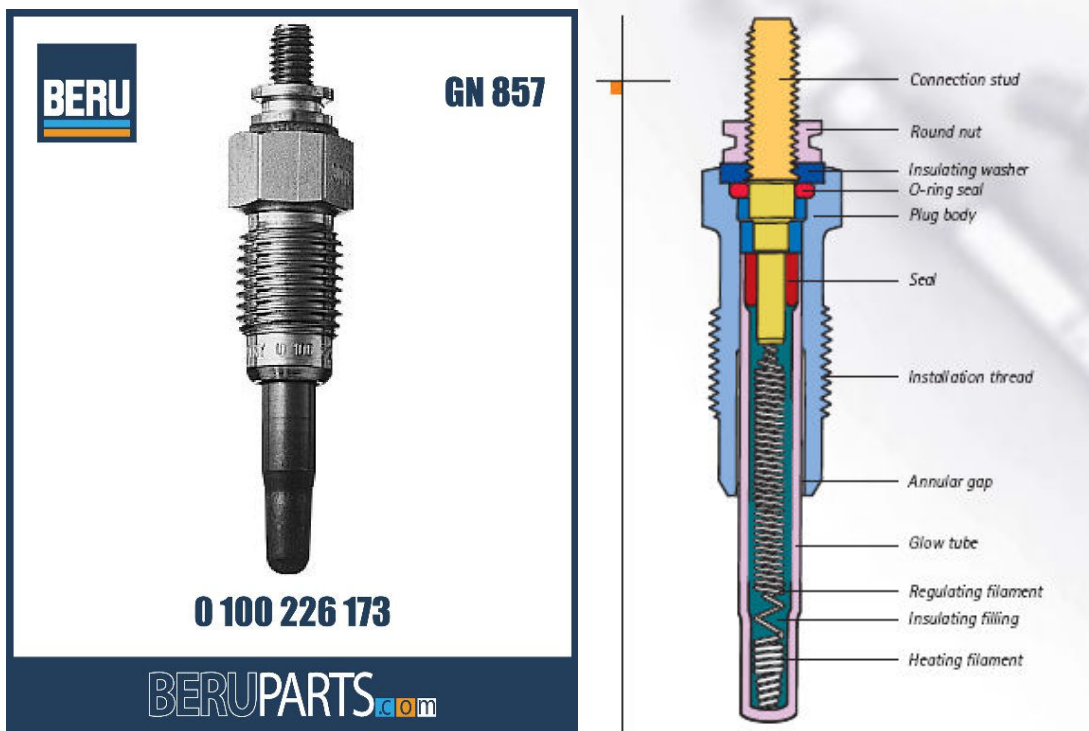
Figure 3-14: Structure of a Beru GN 857 glow plug.

The electrical resistance of the glow plug,

$R = 0.5\ \Omega$.

The power,

$P = U^2 / R$ depends on the voltage applied. For example, a voltage of 2 V provides a power supply of 8 W. For most experiments described in Chapter 4, a voltage of less than 1 V was applied to the glow plug, so the current flow,

$I = U / R$ was less than or around 2 A.

Figure 3-15 below shows the electrical cables to charge the glow plug. The power supply which was connected with the cables in the other side was similar to the power supply in Figure 3-11 on page 32 and was not shown here. Figure 3-15 also points out the locations of three pressure transducers mounted on the testing rig for measurement of overpressures. These pressure transducers are further described in the following Subsection 3.2.4.
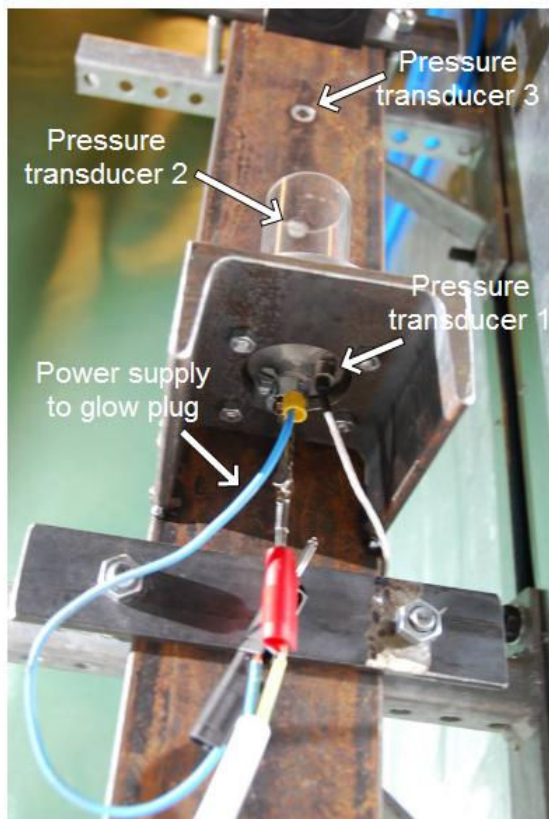
Figure 3-15: Power supply to glow plug and three pressure transducers.

It is unnecessary to charge a high voltage to the glow plug. The purpose of setting up this heating unit is simply to speed up the melting of dry ice initially placed in the experimental pipe and help the liquid/vapor CO_2 mixture go up faster in pressure and temperature along the saturation curve. Considering also heat inflow from ambient air, the time it took for dry ice to fully melt in most experiments was less than 3 min.

More information of the Beru GN 857 glow plug could be found in Appendix D.3.

3.2.4   Signal acquisition and recording unit

The signal refers to overpressures during experiments. They were recorded by pressure transducers at different places and were the most important experimental data for analysis of pressure peaks, speed of wave propagation and discussion of BLEVE formation with initial pressures. The initial pressure and initial temperature are defined as the saturation pressure and temperature prior to the controlled opening or sudden failure of an experimental pipe.

This operating unit includes two types of pressure transducers with their corresponding signal amplifiers and two oscilloscopes of the same type. A total of 4 pressure transducers were mounted in the testing rig. These elements were described separately below and all of them together made the signal acquisition and recording feasible.

a)   Pressure transducer 1 and its signal amplifier.

Pressure transducer 1, a Kulite Semiconductor XT-190-500SG, as shown in Figure 3-15 above and Figure 3-16 below, was mounted through the aluminum pedestal and stayed inside the experimental pipe, close to the glow plug. It was responsible of recording overpressures inside the pipe since the dry ice started to melt. For simplicity, the name 'Pressure Transducer' was called 'PT' in the following text. For example, PT 1 refers to pressure transducer 1.

Figure 3-16: *Kulite Semiconductor (Pressure transducer 1).*

A M1064 signal amplifier for PT 1 and the connections are shown in Figure 3-17 and Figure 3-18, with signal input from PT 1 and voltage output from the amplifier. The signal input connection was by a standard 7-pin connector. The voltage output was connected with a BNC connector to one of the input channels of an oscilloscope to make visible the real-time voltage signals. Similar settings were applied to other pressure transducers.
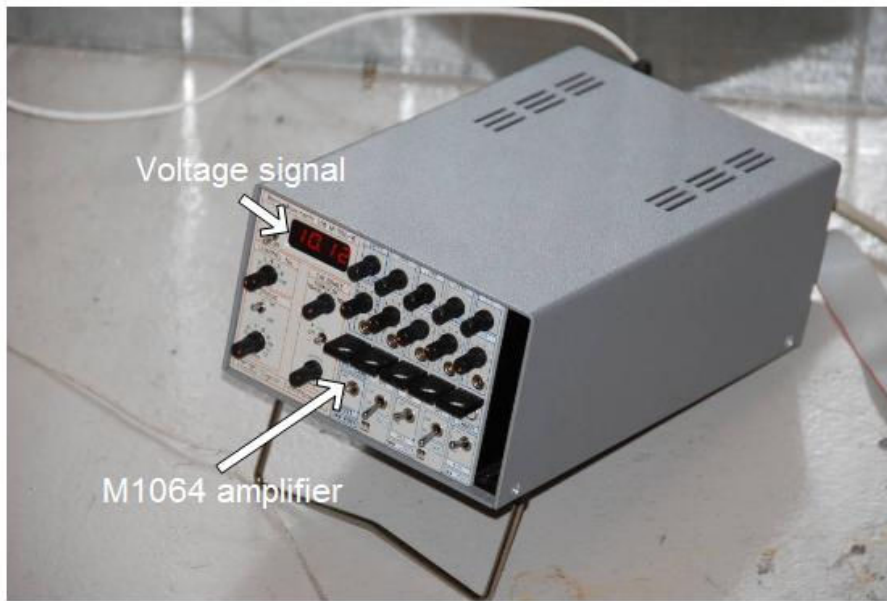
Figure 3-17: Front panel of M1064 amplifier for Pressure transducer 1.
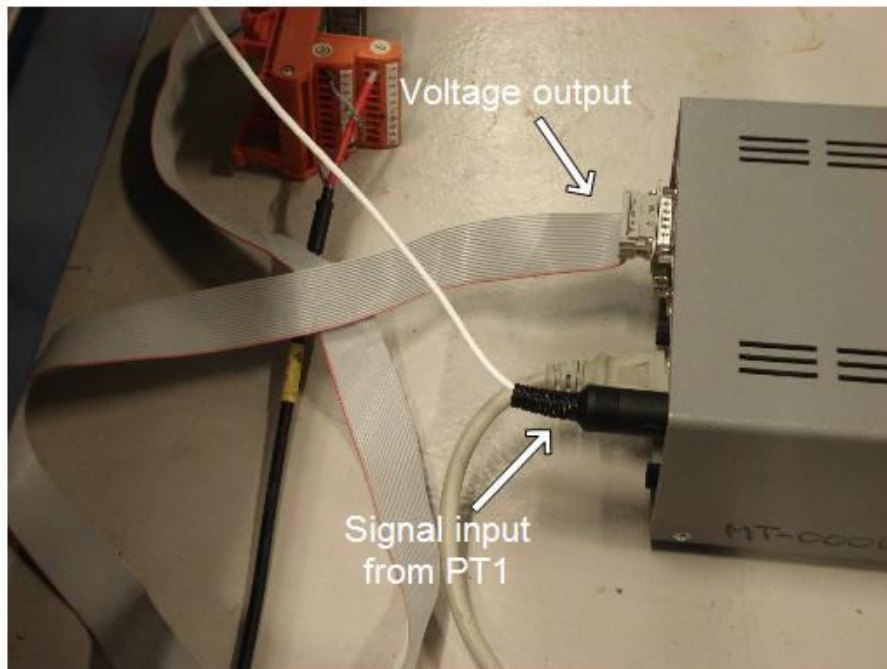
Figure 3-18: Amplifier connections for Pressure transducer 1.

This M1064 amplifier for PT 1 was named AMP 1 for simplicity. Similarly, the signal amplifiers for PT 2, PT 3 and PT 4 were named AMP 2, AMP 3 and AMP 4. Detailed technical information of PT 1 could be found in Appendix D.4.

b) Pressure transducers 2, 3, 4 and their signal amplifiers.

PT 2, PT 3 and PT 4 were pressure transducers of a same type, Kistler 7001, as shown in Figure 3-19. The locations of PT 2 and PT 3 are shown in Figure 3-15 on page 35. PT 2 was mounted 8 cm above the top of a 80 mm long experimental pipe. PT 3 was mounted 10 cm above PT2. PT 1, PT 2, PT 3 were used to measure overpressures throughout all experiments. PT 4 is shown in Figure 3-20, mounted with a plastic sheet on the ground and a distance of

2.1 m from the experimental pipe (not shown in the figure). PT 4 was only used in test 21, to measure side-on pressures in a longer distance.
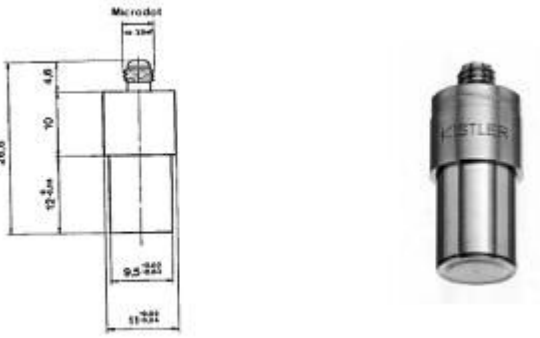
Figure 3-19: Kistler pressure transducers: Type 7001.
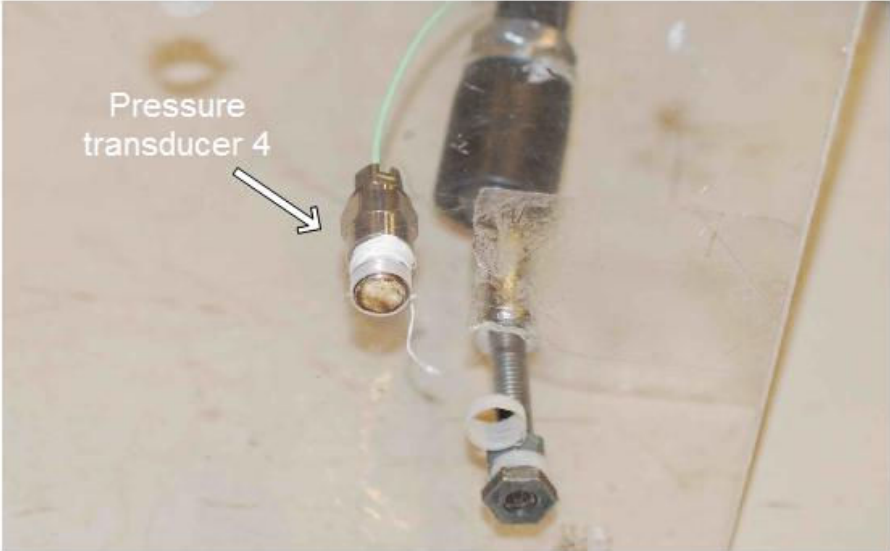
Figure 3-20: mounting of Pressure transducer 4, 2.1 m from the experimental pipe.

Kistler amplifiers for PT 2, PT 3 and PT 4 were named AMP 2, AMP 3 and AMP 4 for simplicity. They are similar physical units with different settings on sensitivity. The physical appearance of a typical Kistler amplifier is shown in Figure 3-21.
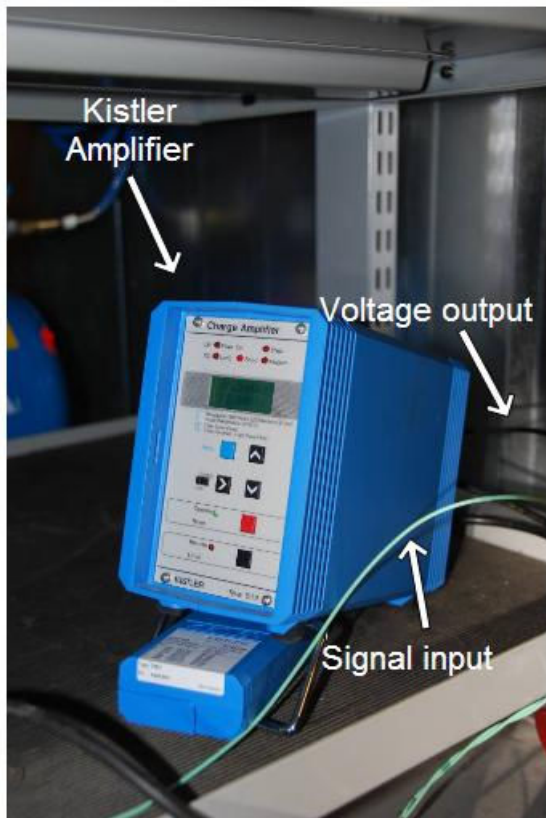
Figure 3-21: A typical Kistler amplifier used for Pressure transducers 2, 3 and 4.

The connections for this type of amplifier are similar as those of M1064 amplifier (AMP 1), as shown in Figure 3-18 on page 37. The signal input was connected to a Kistler transducer. The voltage output was connected to an oscilloscope with a BNC connector to show real-time voltage signals.

Basic parameters of all pressure transducers described above for experimental setup and data processing are summarized in Table 3-4.

Table 3-4: Parameters of pressure transducers.

Pressure transducer	Nominal voltage [V]	Working temperature range [°C]	Maximum pressure [bar]	**Overall scale [bar/V]**
PT 1	10	[-55, 175]	50	For all tests: 24
PT 2	10	[-196, 350]	250	For tests 1-20: 0.2; for test 21: 2
PT 3	10	[-196, 350]	250	For tests 1-20: 0.2; for test 21: 2
PT 4	10	[-196, 350]	250	Only for test 21: 0.02

The most important parameter in Table 3-4 is the 'Overall scale'. This scale was computed based on both the sensitivity of each pressure transducer and the times of amplification of the corresponding amplifier. The value of an overall scale transforms a

voltage signal into a pressure data. For example, the overall scale for PT 1 in all tests was 24 bar/V. If a decrease of voltage signal from PT 1 inside the experimental pipe is observed to be 200 mV, it suggests a pressure drop of 200 mV * 24 bar/V = 4.8 bar. Similar calculations apply to PT 2, PT 3 and PT 4.

c) Oscilloscopes

Two Sigma 90 Transient Oscilloscopes were used in experiments, as shown in Figure 3-22. They were mainly used to receive voltage signals from amplifiers of pressure transducers (AMP 1, AMP 2, AMP 3, AMP 4) with BNC connections.
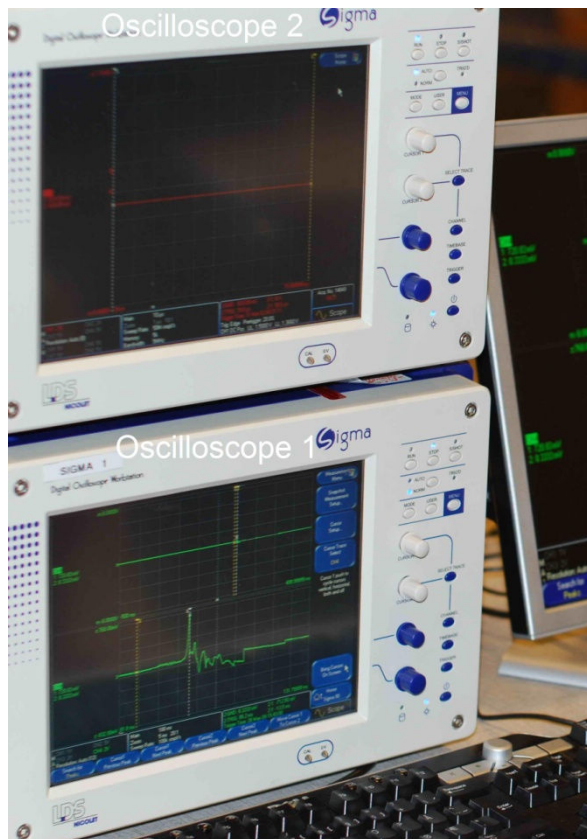
Figure 3-22: Sigma 90 Transient Oscilloscopes.

The two oscilloscopes were used for different purposes. Oscilloscope 1 was the main work station with Windows Operating System. Both pressure recordings and video recordings would be stored in this oscilloscope. Besides, it would accept a trigger signal from a pulse generator, with same pre-trigger setting as the high-speed camera. In this way, it was guaranteed that the pressure recordings and video recordings were done with the same timing and recording period.

When Oscilloscope 1 was set to be 'Waiting for trigger', there was no real-time voltage signal showing in its screen. As during experiments, the overpressure inside the experimental pipe ought to be monitored real time. For this purpose, Oscilloscope 2 was used with a BNC splitter to connect also to the M1064 amplifier of PT 1 so the real-time voltage signal of PT 1 was visible. With a correct overall scale of PT 1 of 24 bar/V, the real-time overpressures

inside the experimental pipe were monitored until the moment of pipe opening by switching the pneumatic valve or a sudden failure of the pipe itself.

Each oscilloscope has a total of 8 signal input channels from 1 to 8 that could be connected directly with pressure transducers or through signal amplifiers, as shown in Figure 3-23. Since Oscilloscope 1 was used as work station and aimed to store pressure records, the channel connections and usages of Oscilloscope 1 are summarized in Table 3-5.
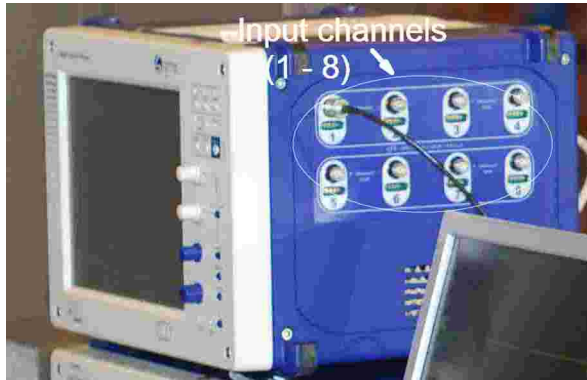
Figure 3-23: Input channels of a Sigma 90 Transient Oscilloscope.

Table 3-5: Channel connections of Oscilloscope 1 (Work station).

Channel No.	Connects to	Usage
1	'EXT/GATE' in pulse generator	Waiting to be trigged
2	AMP 1	Receive and store pressure signals from PT 1
3	AMP 2	Receive and store pressure signals from PT 2
4	AMP 3	Receive and store pressure signals from PT 3
5	AMP 4	Receive and store pressure signals from PT 4

The connection of channel 1 with 'EXT/GATE' in pulse generator is described in Subsection 3.2.6 'Triggering unit'.

More technical information of Sigma 90 Transient Oscilloscope could be found in Appendix D.5.

3.2.5   Video recording unit

Beside the recording of pressure signals with pressure transducers, signal amplifiers and oscilloscopes for monitoring and data storage, a video recording unit was established as equally important for further analysis of experimental data. This operating unit includes two main elements, a high speed camera and an illumination system, to record experimental videos of CO_2 tests with same and accurate timing as in Oscilloscope. The correct timing was achieved with same pre-trigger settings, as will be described in Subsection 3.2.6. A view of this recording unit is shown in Figure 3-24.
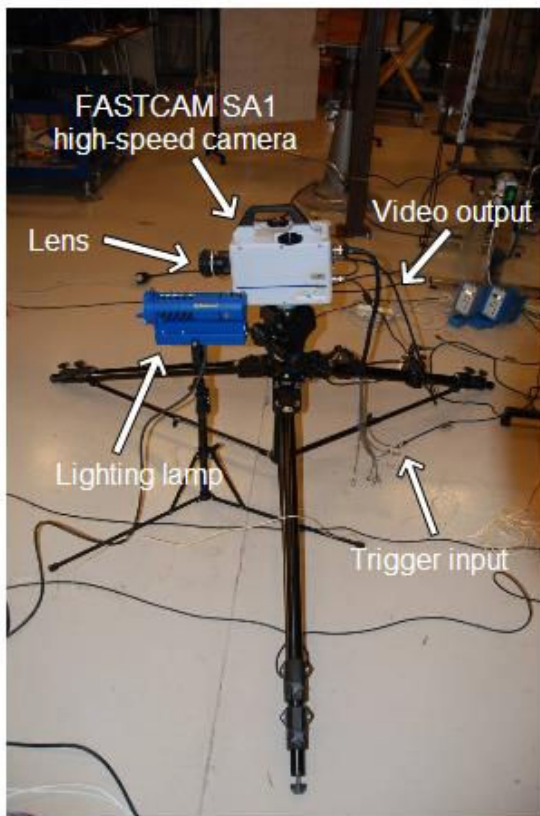
Figure 3-24: Video recording system.

A Photron color FASTCAM SA1 high-speed camera was used in the experiments to record test videos. As shown in Figure 3-24, the 'trigger input' receives triggering signal from a pulse generator, as will be described in Subsection 3.2.6. The 'video output' sends test videos with through an internet cable to the work station (Oscilloscope 1) for storage and analysis. A Nikon 50mm f/1.2 lens was used for imaging. Figure 3-24 shows a single lighting lamp for illumination. In fact, a pair of lighting lamps was more often adopted, to improve the illumination conditions. Figure 3-25 shows the high-speed camera with a pair of Dedocool lighting lamps.

Figure 3-25: A pair of Dedocool lighting lamps for illumination.

As described in Chapter 4, there were in total 21 CO_2 tests with this video recording unit. The main parameters of Camera setting during all tests are summarized in Table 3-6.

Table 3-6: Camera settings in CO_2 tests.

Test No.	Camera Settings			
	Pre-trigger	Frame speed [fps]	Shutter [s]	Resolution
1-5	10%	5400	1/62000	1024*1024
6-20	80%	5400	1/57000	1024*1024
21	50%	5400	1/57000	1024*1024

The column 'Pre-trigger' of camera settings in Table 3-6 also applied to Oscilloscope 1, so the pressure recordings and the video recordings were at same timing. More description on the pre-trigger setting is included in Subsection 3.2.6. More technical information of the FASTCAM SA1 high-speed camera and the lens could be found in Appendix D.6.

Test videos could help analyze the entire process of thermodynamic change starting from dry ice inside the experimental pipe, during heating and sudden opening of the pipe. Key information from the videos may include the phase change of CO_2 with time and equilibrium pressure/temperature inside, the boiling and vaporizing process, the nucleation of bubbles with pressure build-up, and the way of splashing of vapor-liquid mixture out of pipe.

One methodology was to combine information from pressure signals and videos to help clarify the entire process. A typical example of doing this was the way the phase composition of CO_2 at equilibrium state prior to the opening of testing pipe was calculated. The loss of

CO_2 due to leaking could also be calculated. The calculation process and results are described in Chapter 4.

3.2.6   Triggering unit

As mentioned in previous Subsections, it is crucial to make sure that a pressure recording a video recording were always captured and stored with same and accurate timing. Only with this confirmed did the combined analysis of pressure signals and test videos make real sense.

A Quantum Composers series 9500 pulse generator as shown in Figure 3-26 was used in experiments to achieve this goal. It was capable of offering simultaneous triggering signals to both Oscilloscope 1 (also the work station) and the high-speed camera. Beside this simultaneous triggering signal, a same pre-trigger setting was also applied to both the camera and Oscilloscope 1 in each experimental test. The pre-trigger setting was necessary because any loss of experimental information including pressure signals and video information should try to be avoided.
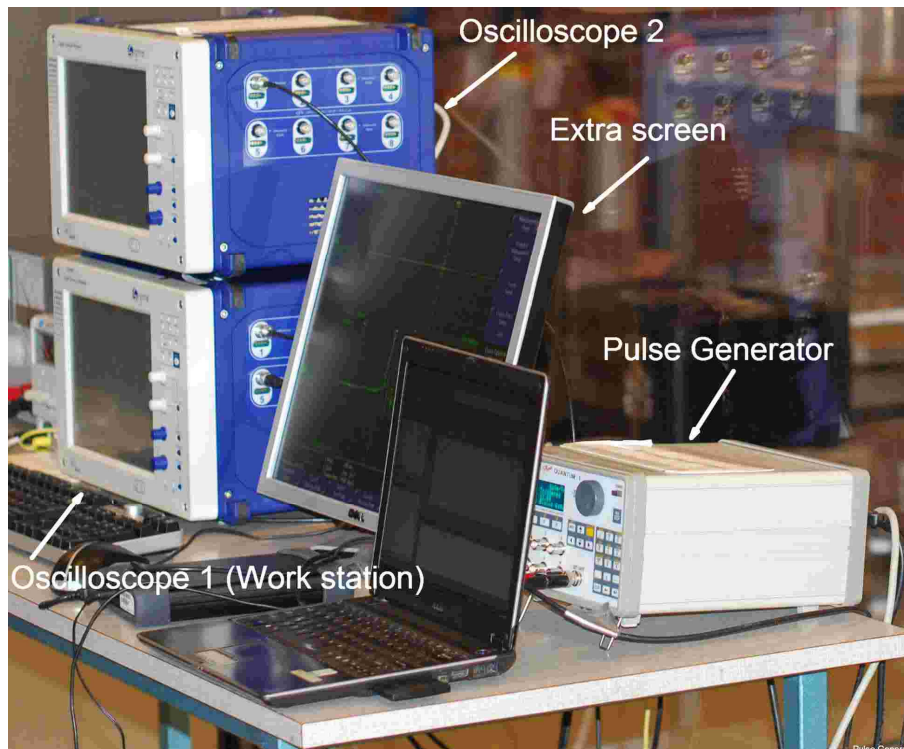
Figure 3-26: Pulse generator (Quantum Composers, series 9500, model 9518) in work.

The pre-trigger setting for different tests has been summarized in Table 3-6, while camera settings were introduced: For test 1-5, test 6-20 and test 21, 10%, 80% and 50% pre-trigger were applied respectively. To make it clear, a total recording time of 1 s with a 10% pre-trigger means that the 1 s recording time consists of 0.1 s prior to the trigger and 0.9 s after the trigger.

The trigger mode in pulse generator was selected to be 'External trigger'. This literally means that under this mode the pulse generator itself needs an external electrical signal to

initiate and start sending pulses to trigger the high-speed camera and Oscilloscope 1. This external electrical signal as input into pulse generator was a signal from the physical switch of the pneumatic valve, as shown in Figure 3-11 on page 32. Whenever the switch changes the flow direction through the pneumatic valve, forces the piston to draw back and opens the experimental pipe, it sends an electrical signal also to the pulse generator, completing the 'External trigger' mode.

The pulse generator has a total of 8 signal outputs from A to H and a signal input named 'EXT/GATE', as shown in Figure 3-27 below. The connections and usages of its input/output with other experimental devices are summarized In Table 3-7.
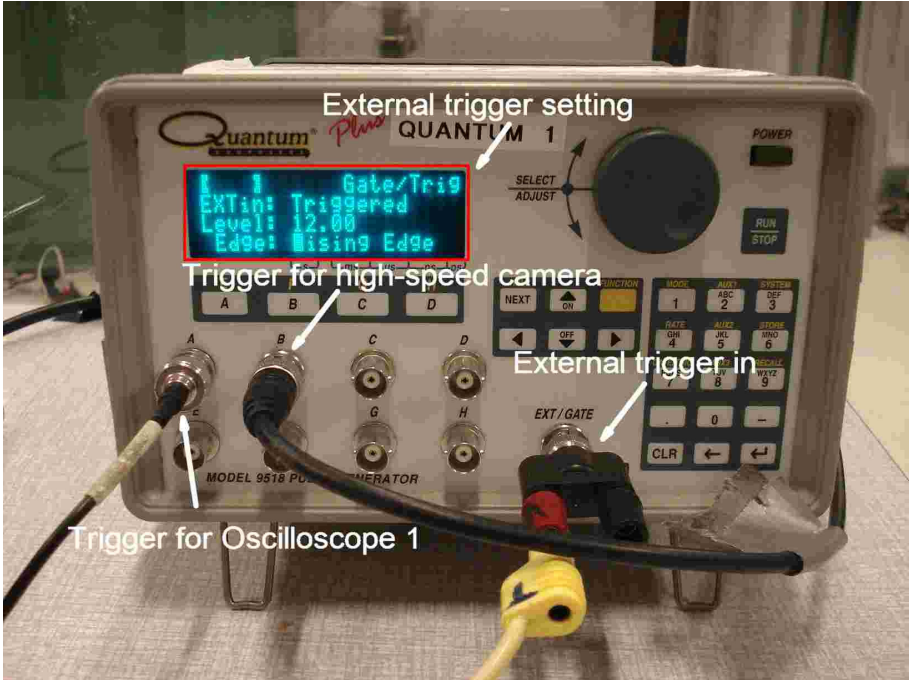
Figure 3-27: Channels (I/O) and connections of the pulse generator.

Table 3-7: Connections and usages of Pulse generator channels.

Channel (I/O)	Connects to	Usage
A	Oscilloscope 1 (Work station)	To trigger Oscilloscope 1 for pressure recording
B	FASTCAM SA1 high-speed camera	To trigger high-speed camera for video recording
EXT/GATE	Physical switch of pneumatic valve	To receive external signal from the switch as 'External trigger'

More technical information on the Quantum Composers series 9500 pulse generator under 'External trigger' mode could be found in Appendix D.7.

3.3 Data post processing

The post processing of experimental data mainly consisted of two parts: to process pressure records and to process video records. Various versions of MATLAB scripts have been written for reading pressure signals from experimental tests, due to the differences in the pre-trigger setting, the overall scale of pressure transducers and plotting requirements. Photron FASTCAM Viewer, a software developed by Photron, the same company supplying the high-speed camera, has been used to process experimental videos.

Take test 18 for example, a typical .txt file recorded with voltage signals by Oscilloscope 1 from one of the pressure transducers in this test starts as following, with line numbers added in front:

CH2_02h.TXT

```
1       Nicolet Sigma 90
        15:53:24 Trigger Time
        Trace Type
        YT
5       Time of First sample wrt trigger (s)
        -0.8
        Time per sample (s)
        1e-005
        Units
10      V
        Number of Samples
        100000
        DATA START
14      0.265625
        0.276042
…
```

The file name 'CH2_02h' reveals that this was a pressure record from channel 2 which was from pressure transducer 1 (PT 1). Line 2 shows the local time of triggering. Line 6 indicated the pre-trigger setting: -0.8 means there was in total 0.8 s before the trigger, so the pre-trigger setting for this test was 80%. Line 12 suggested the total sampling numbers of 100000 during the recording time. The product of the number of sampling and the 'Time per sample' of 1e-005 suggested a total recording time of 1 s. voltage data started from line 14.

To make the description consistent along the context, a MATLAB script written for test 18 to read overpressures in the experiment has been attached as Appendix F. Tiny changes are necessary when using this script to read pressure signals from other tests while resulting in similar Pressure – time figures. The changes necessary to be made in the programming script are mainly according to different settings of pre-trigger and the overall scale of pressure transducers. They are summarized separately in Table 3-6 and Table 3-4 on page 43 and 39.

The processing of experimental videos was achieved by software Photron FASTCAM Viewer. A quick look on the operating areas of Photron FASTCAM Viewer is shown in Figure 3-28.

Figure 3-28: *Operating areas of Photron FASTCAM Viewer.*

4 Results and discussion

This chapter describes and discusses experimental results of CO_2 BLEVE tests based on the experimental setup in Chapter 3. The purpose was to analyze the experimental data of both pressure records and video records in depth to attain more insights on the formation and consequences of a CO_2 BLEVE.

A total of 21 CO_2 BLEVE experiments have been performed to gain more understanding on the propagation of pressure waves and release of explosion energy with fragments. Experimental data of all CO_2 BLEVE tests could be found in Appendix G. Appendix H gives thermodynamic data of reference as well as of all tests required for thermodynamic calculations. Pressure records are given in Appendix I.

Subsection 4.1 reviews two ways of classification of tests in order to make descriptions and discussion clearer. Subsection 4.2 describes a balloon test prior to CO_2 BLEVE tests to make sure that the experimental rig as a whole and especially the pressure transducers could work fine with correct timing. Subsection 4.3 describes results of phase composition calculation of liquid/vapor CO_2 mixture prior to the opening of experimental pipe. Subsection 4.4 and 4.5 describe the two sets of tests by 'Classification I' defined in Subsection 4.1 in details and in order. Subsection 4.6 discusses the fitness of experimental results with the 'Superheat limit temperature' theory that was introduced in Chapter 2 for predicting the occurrence of a BLEVE. Subsection 4.7 describes dry ice formation after pipe opening with experimental observations and thermodynamic analysis.

4.1 Experiment classifications

A list of 21 CO_2 BLEVE tests is given in Table 4-1.

Table 4-1: List of CO_2 BLEVE tests.

Test No.	Test Time	Signal file folder	Video file
1	2009-4-23 14:39	D:\...\09_KeW_P101_ T 00001	/
2	2009-4-23 13:55	D:\...\09_KeW_P101_ T 00002	S0002.avi
3	2009-4-23 15:02	D:\...\09_KeW_P101_ T 00003	/
4	2009-4-23 15:18	D:\...\09_KeW_P101_ T 00004	S0004.avi
5	2009-4-23 16:04	D:\...\09_KeW_P101_ T 00005	S0005.avi
6	2009-4-24 11:05	D:\...\09_KeW_P101_ T 00006	S0006.avi
7	2009-4-24 11:25	D:\...\09_KeW_P101_ T 00007	S0007.avi
8	2009-4-24 11:39	D:\...\09_KeW_P101_ T 00008	S0008.avi
9	2009-4-24 12:01	D:\...\09_KeW_P101_ T 00009	S0009.avi
10	2009-4-24 12:17	D:\...\09_KeW_P101_ T 00010	S0010.avi
11	2009-4-24 13:09	D:\...\09_KeW_P101_ T 00011	S0011.avi
12	2009-4-24 13:26	D:\...\09_KeW_P101_ T 00012	S0012.avi
13	2009-4-24 13:42	D:\...\09_KeW_P101_ T 00013	S0013.avi
14	2009-4-24 14:00	D:\...\09_KeW_P101_ T 00014	S0014.avi
15	2009-4-24 14:23	D:\...\09_KeW_P101_ T 00015	S0015.avi
16	2009-4-24 14:51	D:\...\09_KeW_P101_ T 00016	S0016.avi
17	2009-4-24 15:13	D:\...\09_KeW_P101_ T 00017	S0017.avi
18	2009-4-24 15:53	D:\...\09_KeW_P101_ T 00018	S0018.avi
19	2009-4-24 16:14	D:\...\09_KeW_P101_ T 00019	S0019.avi
20	2009-4-24 16:38	D:\...\09_KeW_P101_ T 00020	S0020.avi
21	2009-5-26 16:07	D:\...\09_KeW_P101_ T 00021	S0021.avi

A table with detailed experimental data and additional experimental information could be found in Appendix G. To make description and discussion of these tests clearer, two kinds of classification were made to all tests, based on different criteria or assumption.

4.1.1 Classification I

Tests were classified into two SETs based on different ways of opening the experimental pipe. This classification is also the one used to describe tests in order as in Subsections 4.4 and 4.5.

SET 1: The pipe was opened manually by manipulating the pneumatic valve and retracting the piston. With this option, there might or might not be a BLEVE and the experimental pipe could normally endure the sudden pressure drop with no fragments formed.

SET 2: The pressure inside the pipe was allowed to build up without control and the valve was NOT redirected/the piston was NOT retracted UNTIL the pipe itself at some point suddenly ruptured. With this option, still, there might or might not be a BLEVE. The difference with Option I is that the pipe was not really 'opened' but 'cracked', and the fast cracking generated a large number of fragments of small pieces. These fragments were marked, collected and weighed as one additional approach to estimate the energy released by the explosion.

SET 1 consists of test 1 to test 20. Among them, test 1 was a background test with no CO_2 filling, in order to reveal the magnitude of noise signals from the experimental system. It has pressure record and no video record. SET 2 consists of only test 21. Pressure record and video record are available for test 21.

This classification of tests is named 'Classification I' and is the one used to describe experimental results in order. It is summarized in Table 4-2 below.

Table 4-2: Classification I of CO_2 BLEVE tests.

SET No.	Test No.	CO_2 filling?	Pressure record?	Video record?	**Fragment?**
1	1-20	YES except test 1	YES	YES, except test 1 & test 3	**NO**
2	21	YES	YES	YES	**YES**

As in laboratory experiments, a test of SET 2 was much more difficult to perform than other tests. This is to say, it was not easy to have such a spontaneous pipe rupture with fragments. It was even harder to capture and store the pressure signals and test videos in such a situation. The reason is that a sudden explosion like this would not give any warning to the experimental operator at all until it does happen. It requires both an appropriate pre-trigger setting (50% pre-trigger in test 21) and a fast response of the experimental operator to trigger both Oscilloscope 1 (work station) and the high-speed camera AFTER the explosion to record the pressure data and test video with no loss of key information. And that is why explosions of SET 2 have been observed three times in laboratory while test 21 is the only one with experimental data saved.

4.1.2 Classification II

Beside Classification I as in Table 4-2, a second way of dividing CO_2 BLEVE tests into two SETs was also used based on such an assumption: A test in which overpressure peaks detected by pressure transducer 2 (PT 2) and/or pressure transducer 3 (PT 3) were higher than 0.1 bar was considered to have an explosion. On the contrary, a test where both PT 2 and PT 3 were lower than 0.1 bar was with no explosion. This 'Classification II' simplified the judgment on whether an explosion occurred in a specific experiment. Plots of overpressures in

this Chapter have followed this classification with use of legends 'Explosion' and 'No explosion'. Classification II is summarized in Table 4-3.

Table 4-3: Classification II of CO_2 BLEVE tests.

SET No.	Test No.	CO_2 filling?	Pressure record?	Video record?	**Explosion?**
1'	1,2,3,5,7,8,10,12,13,14,20	YES except test 1	YES	YES, except test 1 & test 3	**NO**
2'	4,6,9,11,15,16,17,18,19,21	YES	YES	YES	**YES**

One thing that worth mentioning here is that it is unwise to equalize a BLEVE with an explosion according to this classification, partly because the assumption for 'Classification II' itself is very coarse, but more important reason is, there are not yet clear judgment criteria for the occurrence of a BLEVE.

4.2 Balloon test

4.2.1 Introduction

Before carrying out CO_2 BLEVE tests, the matching of time scenario in a pressure recording and the corresponding video recording must be confirmed so that combined analysis of pressure signals with test videos could make sense. Compared with the continuity of PT 1 (pressure signal from inside the experimental pipe), transducers mounted outside (PT 2, PT 3, PT 4) to record the instantaneous over pressures above or close to the experimental pipe were more urgent to be confirmed, with correct timing. Being transducers of the same type (Kistler), a confirmation with one of them would be enough.

A simple test with balloon was designed for this purpose. The idea was to punch a balloon broken close to the experimental pipe with pressure transducers PT 2 and PT 3 mounted nearby. By analyzing events along time scenarios before and after the balloon breaking with the pressure record and the test video, the correctness of experimental timing and readiness of pressure transducers could be confirmed.

4.2.2 Results

Three images intercepted from the balloon test video are shown in Figure 4-1, Figure 4-2 and Figure 4-3, with 'Current time' and position of PT 3 indicated. Figure 4-1 shows the moment when the balloon's breaking started from the very beginning. Figure 4-2 shows the moment when overpressure measured by PT 3 started to increase. Figure 4-3 shows the moment when the overpressure reached the peak. Besides, Figure 4-4 shows the pressure record of PT 3 within the time period [0.35 s, 0.4 s] for comparison with video pictures. PT 2 did not work as in this test.
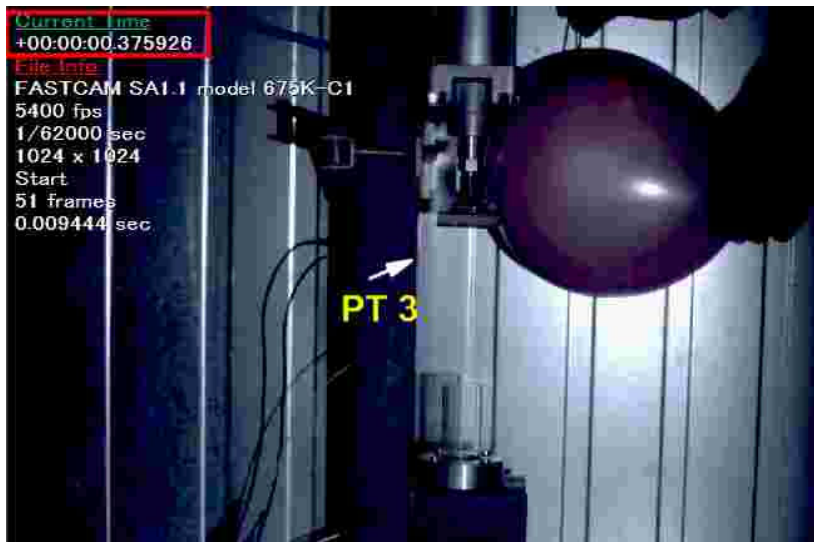
Figure 4-1: The beginning of balloon's breaking. $t_1 = 0.375926$ s.
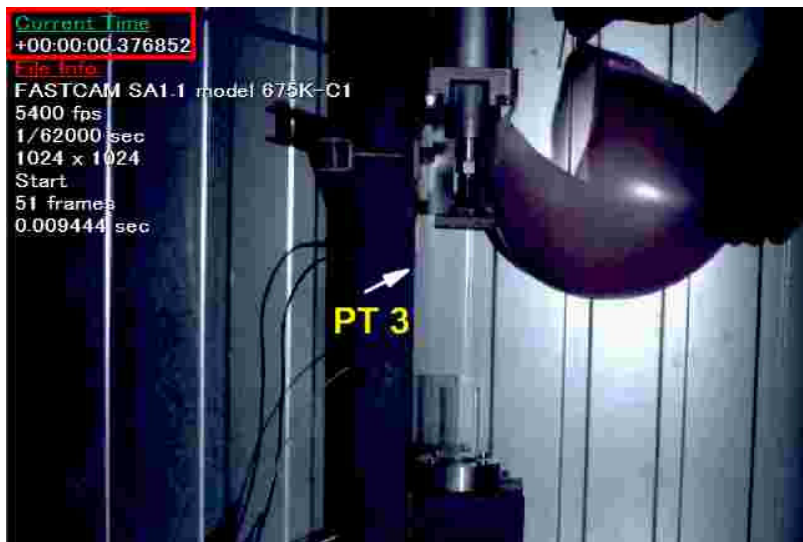
Figure 4-2: The moment when PT 3 started increasing. $t_2 = 0.376852$ s.
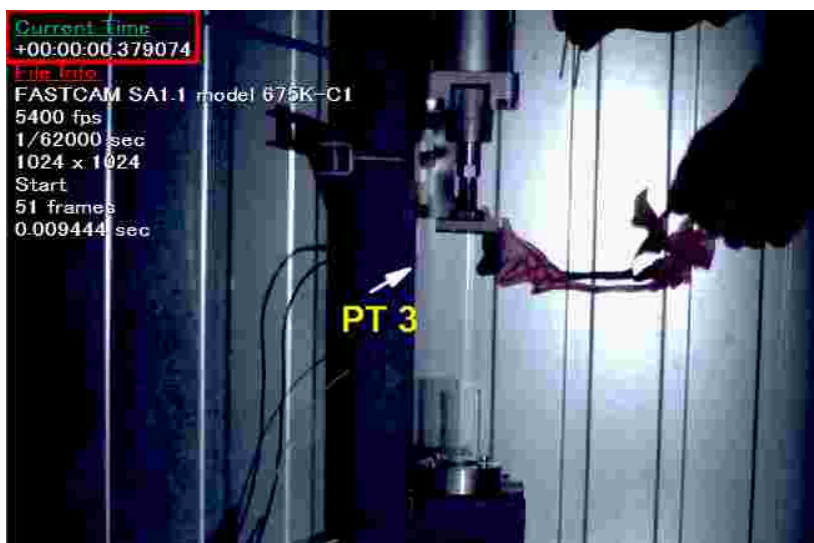
Figure 4-3: The moment when PT 3 reached its peak. $t_3 = 0.379074$ s.
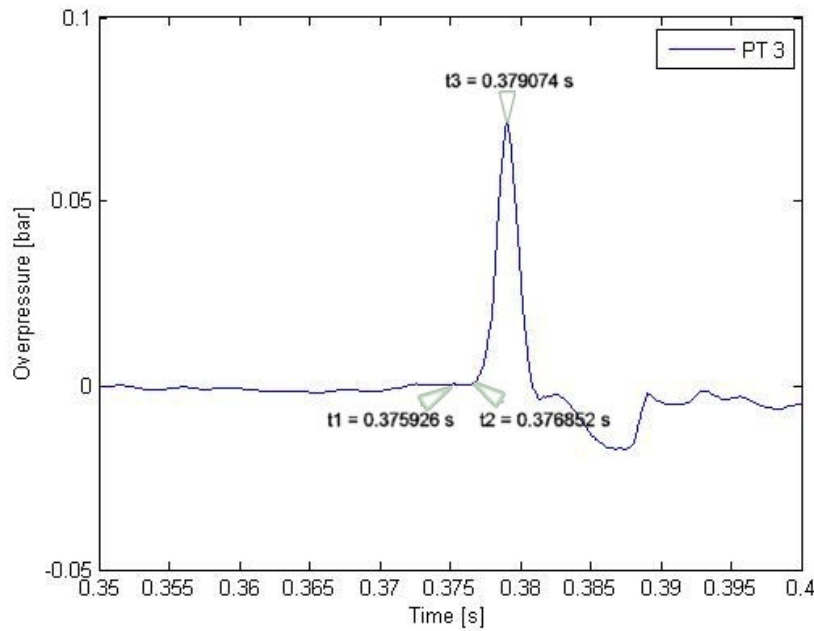
Figure 4-4: PT 3 from 0.35 s to 0.4 s in balloon test.

As shown in Figure 4-1, the balloon started to break from 0.375926 s (t_1), when there was no increase in over pressure yet. At this time, the pressurized air inside balloon has not come out and reached pressure transducer 3. At 0.376852 s (t_2), PT 3 started to increase, indicating that the air wave from balloon breaking has been detected. The time difference,

$$\Delta t_1 = t_2 - t_1 = 0.926 \text{ ms.}$$

With a sound speed of 340 m/s at room temperature of around 20 °C and a distance between the balloon center and PT 3 of 26 cm (computed by pixel scaling), the time it was expected to take for pressurized air in balloon to reach PT 3,

$$\Delta t = 26 \text{ cm}/(340 \text{ m/s}) = 0.765 \text{ ms.}$$

The time delay for transducer 3's response is $\Delta t_1 - \Delta t = 0.16$ ms. A response delay of same magnitude is expected for PT 2 and PT 4 also and is considered negligible.

At 0.379074 s (t_3), PT3 reached its peak of around 0.07 bar, as told by the pressure signal. The time it took from the beginning of pressure increase to the pressure peak,

$$\Delta t_2 = t_3 - t_2 = 2.2 \text{ ms.}$$

Time differences very close to this Δt_2 were found in all the other tests from test 2 to 21.

And within this time period of pressure increase, the blast wave, if there was, would have been travelled a distance through air,

$$\Delta d_{air} = 2.2 \text{ ms} * 340 \text{ m/s} = 0.68 \text{ m.}$$

If the medium is CO_2 instead of air, the sound speed in a large range of pressure is around 220 m/s. And the blast wave would have been travelled a distance,

$$\Delta d_{CO2} \sim 2 \text{ ms} * 220 \text{ m/s} = 0.44 \text{ m.}$$

This distance is within the scale of experimental videos.

4.2.3 Conclusion

The balloon test proved that the overall experimental rig was capable of running with correct timing and negligible response delay in pressure transducers. Blast wave brought by an explosion is supposed to be tracked by experimental videos.

4.3 Phase composition of CO_2 mixtures

4.3.1 Introduction

This Subsection describes with an example the calculation method and result of phase composition of liquid/vapor CO_2 mixture for each test, prior to the opening of the experimental pipe. The mixture composition at this moment is of special interest since it relates directly to the formation of an explosion. It might help to gain more insights on contributions liquid and vapor CO_2 could make respectively to an explosion.

4.3.2 Calculation Procedure and results

The calculation on phase composition of CO_2 mixtures was achieved by analyzing the experimental videos. Test 1 as the background test had no CO_2 filling. Test 3 had only pressure record with the video missing. The calculation was done to the rest 19 tests.

Test 18 is given as an example for calculation and a complete table with phase composition information for all tests is given in the end of this Subsection. The procedure normally goes as following.

a) Selected experimental data of test 18 is listed in Table 4-4.

Table 4-4: A selection of experimental data in test 18.

Test No.	D_{pipe} [mm]	L_{pipe} [mm]	V_{pipe} [cm^3]	m_{CO2} [g]	P_1 [bar]	T_1 [K]	ρ_{liq} [g/cm^3]	ρ_{vap} [g/cm^3]
18	32	100	80	62	30.4	268	0.956	0.083

In Table 4-4, D_{pipe}, L_{pipe}, V_{pipe} were the diameter, length and volume of the experimental pipe. $V_{pipe} = (1/4)*\pi D_{pipe}^2*L_{pipe.}$ m_{CO2} was the weight of dry ice initially placed into the pipe. P_1 and T_1 were the initial absolute pressure and temperature prior to the opening of the pipe. ρ_{liq} and ρ_{vap} were the densities of liquid and vapor CO_2 respectively under P_1 and T_1.

b) The start of first opening of the pipe could be found from pressure record of test 18, as shown in Figure 4-5. All pressure values are overpressures as indicated in y-axis.
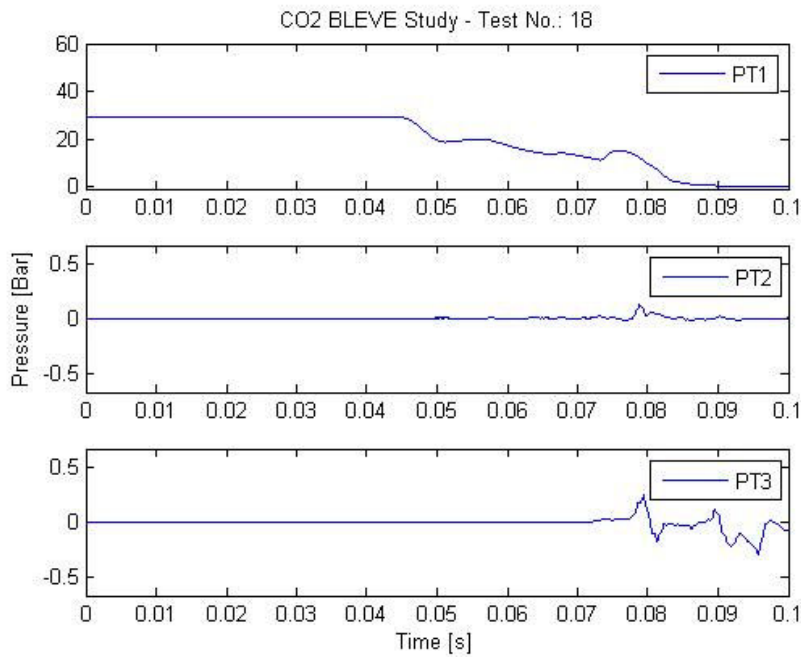
Figure 4-5: Pressure record of test 18 with channels PT 1, PT 2 and PT 3.

Pressure records of all tests including test 18 above could be found in Appendix I. Relevant thermodynamic data used for calculation is also attached as Appendix H.

In Figure 4-5, the first opening of the pipe was indicated by the first pressure drop started from 44 ms after trigger. With a frame speed of 5400 fps, this time corresponded to frame No.238 in the video of test 18. A picture of the pipe at this moment (44 ms, frame 238) was intercepted and shown as Figure 4-6 below. The liquid surface was indicated by the yellow, horizontal line and above that was pressurized CO_2 vapor.

Figure 4-6: The experimental pipe in test 18 at 44 ms after trigger (frame No.:238).

c) With help of counting pixel numbers to indicate distances in axis x and y, as shown in Figure 4-6 above (current position X:0364 Y:0442), it becomes easy to know the heights of both liquid CO_2 (L_{liq}) and vapor CO_2 (L_{vap}). A scale between pixel numbers and physical distance in a form of 'mm/pixel' could transform pixel numbers into physical heights and one step further, the volumes (V_{liq}, V_{vap}). In this case,

$L_{liq} = 48.6$ mm,

$L_{vap} = 100 - 48.6 = 51.4$ mm.

$V_{liq} = (48.6 / 100) * V_{pipe} = 39$ cm^3,

$V_{vap} = V_{pipe} - V_{liq} = 41$ cm^3.

d) With the densities of liquid and vapor CO_2 as shown in Table 4-4:

$\rho_{liq} = 0.956$ g/cm^3.

$\rho_{vap} = 0.083$ g/cm^3

The weight of liquid CO_2 (m_{liq}), vapor CO_2 (m_{vap}) and weight of the mixture (m_{total}) were calculated:

$m_{liq} = \rho_{liq} * V_{liq} = 37.3$ g.

$m_{vap} = \rho_{vap} * V_{vap} = 3.4$ g.

$m_{total} = m_{liq} + m_{vap} = 40.7$ g.

Liquid CO_2 took a percentage of $m_{liq} / m_{total} = 91.6\%$ and

Vapor CO_2 took a percentage of 8.4%.

The loss of CO_2 by leakage during this experiment before trigger and opening of the pipe,

$Loss_{CO2} = 1 - m_{total} / m_{CO2} = 34.4\%$.

Following the same procedures from a) to d) above, the pipe volume, dry ice filling, saturation pressure and temperature and phase composition of CO_2 mixtures for all tests at equilibrium state prior to the trigger and opening of the pipe were computed and summarized as in Table 4-5.

Table 4-5: Phase compositions of CO_2 mixtures in all tests prior to the pipe opening.

Test No.	Pipe Volume [cm3]	Dry ice [g]	PT 1 [bar]	T [°C]	Phase composition at PT1 / T				
					Liquid CO2 [g]	Percentage [wt-%]	Vapor CO2 [g]	Percentage [wt-%]	CO2 loss by leakage [wt-%]
1	82	0	0.05	-78.5	0	0	0	0	0.0
2	82	22	16.2	-24.2	20.5	93.2	1.5	6.8	0.0
3	82	30	17.1	-22.6	/	/	/	/	/
4	82	45	17	-22.7	43.5	96.7	1.5	3.3	0.0
5	82	9.7	20.4	-17.2	5.1	54.6	4.2	45.4	3.7
6	80	20	18.4	-20.4	17.8	89.4	2.1	10.6	0.5
7	80	20	19.7	-18.2	16.8	84.0	3.2	16.0	0.0
8	80	30	20.1	-17.5	27	90.0	3.0	10.0	0.0
9	80	45	15.8	-25	38	95.0	2.0	5.0	11.1
10	80	30	18.4	-20.4	18.6	85.1	3.3	14.9	27.1
11	80	30	19.3	-18.7	24.6	88.8	3.1	11.2	7.6
12	80	20	18.4	-20.4	16.5	83.1	3.4	16.9	0.7
13	80	10	18.3	-20.6	5.2	57.2	3.9	42.8	9.0
14	80	30	20	-17.8	27.2	90.7	2.8	9.3	0.0
15	80	60	12.5	-31.6	56.3	98.2	1.1	1.8	4.4
16	80	62	21.8	-15.1	53.5	96.8	1.8	3.2	10.9
17	80	60	22.3	-14.3	52.3	96.6	1.9	3.4	9.7
18	80	62	29.4	-5	37.3	91.6	3.4	8.4	34.4
19	80	60	27.3	-7.5	22.3	83.1	4.5	16.9	55.3
20	80	20	30.8	-3.3	10.4	62.5	6.2	37.5	16.9
21	82	60	20.6	-17	55.8	96.9	1.8	3.1	4

In Table 4-5, 'PT 1' and 'T' were the overpressure and temperature of saturated CO_2 mixtures prior to the pipe opening/failure. A 'Test No.' in **bold** in Table 4-5 suggests an explosion, according to the criterion of 'PT 2/PT 3 > 0.1 bar' as described in Subsection 4.1.2 and Table 4-3 'Classification II of CO_2 BLEVE tests' on page 52. The average percentages of liquid and vapor of tests with explosion and tests with no explosion are summarized in Table 4-6. Test 1 and test 3 were excluded from SET 1'.

Table 4-6: Average liquid and vapor CO_2 percentages of tests with/without explosion.

SET No.	Tests	Explosion?	Average liquid CO_2 [wt-%]	Average vapor CO_2 [wt-%]
1'	2,5,7,8,10,12,13,14,20	NO	77.8	22.2
2'	4,6,9,11,15,16,17,18,19,21	YES	93.3	6.7

Recall the point of interest with phase composition of CO_2 mixture. It would be great to know to what extent liquid CO_2 contributes to an explosion and to what extent vapor CO_2 contributes. Table 4-6 suggests that tests with explosion had significantly higher percentages

of liquid on average (93.3%) than tests without explosion (77.8%), prior to the opening or failure of the experimental pipe. This observation thus suggests two points. First, liquid CO_2 might contribute more than vapor CO_2 to an explosion. Second, the potential of explosion may increase with increase of liquid CO_2 percentage in the two-phase mixture.

4.4 CO$_2$ Tests with no fragments

This Subsection includes results and discussion of experiments with no fragments (SET 1 as in Table 4-2 on page 51). SET 1 includes test 1 to test 20. Subsection 4.4.1 describes test 1 separately as background for other tests. Subsections 4.4.2, 4.4.3 and 4.4.4 discuss results of test 2 to test 20 from aspects of CO$_2$ filling level, pipe opening speed and bubble nucleation inside.

4.4.1 Background test (Test 1)

Test 1 was a background test, aiming to investigate the magnitude of system noise and make sure the noise signal was in an acceptable range when performing CO$_2$ BLEVE tests. Pressure record of test 1 is shown in Figure 4-7 below. Pressure records of all tests could be found in Appendix I. All pressure values are overpressures.
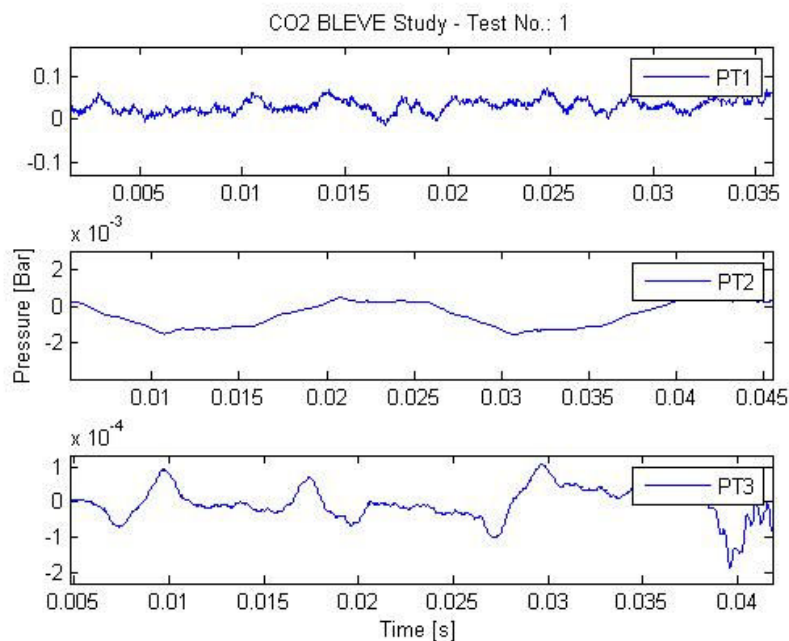
Figure 4-7: Pressure signals of Test 1.

As shown in Figure 4-7 above, the magnitudes of noise signals from PT 1, PT 2, PT 3 are around 0.05 bar, 0.001 bar, 0.0001 bar respectively.

As recorded in Table 4-5 on page 60, overpressures inside the experimental pipe in all tests were around or above 20 bar, 400 times higher than this background PT 1 (0.05 bar).

As defined in Subsection 4.1.2 'Classification II', only a test with either PT 2 or PT 3 or both higher than 0.1 bar was considered as an explosion. This threshold of 0.1 bar is 100 times higher than background PT 2 (0.001 bar) and 1000 times higher than background PT 3 (0.0001 bar).

PT 4 was not recorded in test 1. As an additional pressure transducer mounted 2.1 m away from the experimental pipe and only used in test 21, it had an overall scale (0.02 bar/V) of 100 times higher than both PT 2 and PT 3 (2 bar/V) (see Table 3-4 on page 39). As a result, its response to background noise would not be a problem.

Comparison above suggests that background noise during experiments was within an acceptable range and was indeed neglected.

4.4.2 CO_2 filling and pressure buildup

With experimental data of CO_2 tests 2 to 20 of varied CO_2 filling, first and easiest to come into mind are following two questions: Is there a relationship between CO_2 filling level and pressure buildup (PT 1) inside the experimental pipe? Will more CO_2 filling increase the possibility of having an explosion (PT 2/PT 3 > 0.1 bar)?

Figure 4-8 plots CO_2 filling levels in tests 2 to 20 with PT 1. Figure 4-9 plots CO_2 filling level with a maximum value of PT 2/PT 3, to tolerate the malfunction of either PT2 or PT3 as it happened sometimes during experiments. Tests with explosion and tests with no explosion have been indicated in both figures. To be more precise, due to gas leaking in most experiments performed, the REAL weight of CO_2 mixture right before the opening/failure of pipe as a sum of weights of liquid CO_2 with vapor CO_2 in Table 4-5 on page 60 were used to plot, instead of using the weight of dry ice initially placed into the pipe. With no video record, test 3 was excluded from both Figure 4-8 and Figure 4-9.
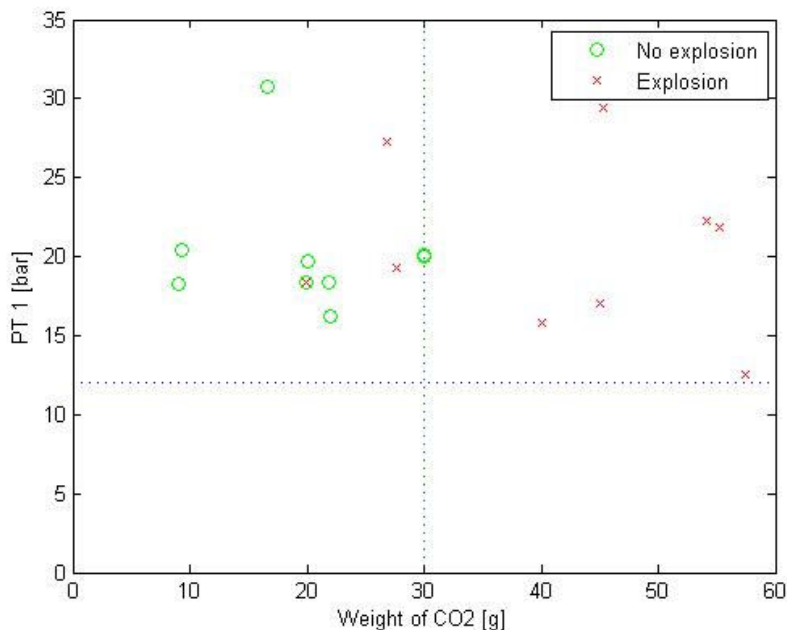
Figure 4-8: CO_2 filling level – PT 1 (Test 2 to 20, except test 3).
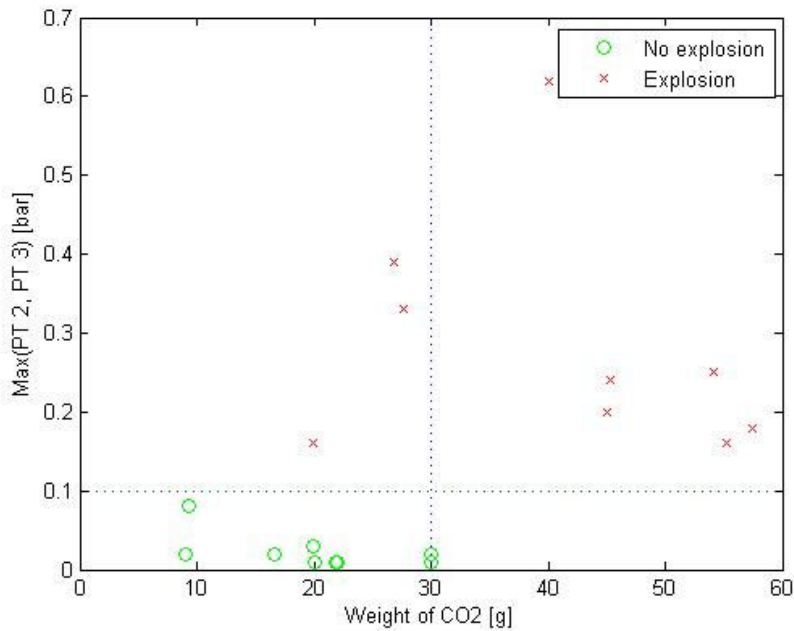
Figure 4-9: CO$_2$ filling level – max(PT 2, PT 3) (Test 2 to 20, except test 3).

Figure 4-8 and Figure 4-9 above suggests two things: 1) there was no obvious connection between CO$_2$ filling level and the pressure build-up inside the experimental pipe. 2) However, it is clear that it was not very likely to have an explosion when CO$_2$ filling was less than 30 g in a pipe volume of 80 cm^3 (an overall density of 375 kg/m^3). The explosion did happen every time with no exception when CO$_2$ filling was more than 30 g.

Based on observations above, we have assumed that a certain amount of two-phase flow splashing out of the experimental pipe is one of the pre-conditions for an explosion. Recall the analysis of phase composition with calculation results in Subsection 4.3.2, liquid CO$_2$ was considered to be more capable than vapor CO$_2$ to lead to an explosion. Observations above and indications from phase composition analysis together might explain why an explosion was unlikely to occur if the quantity of CO$_2$ was too little, say, less than 20 g in a volume of 80 cm^3 (an overall density of 250 kg/m^3). With less CO$_2$ filling, pressurized liquid within the pipe may have been completely vaporized before it was able to reach out of pipe and contribute to an explosion. A small quantity of liquid CO$_2$ in such a situation would possibly deter the occurrence of an explosion.

4.4.3   Inner pressure and opening speed

The inner pressure refers to PT 1, the over pressure inside the experimental pipe. This Subsection aims to find out if the initial PT 1 before pipe opening and the speed of opening is related.

As observed from both pressure records (Appendix I) and test videos, PT 1 in test 2 to test 20 followed a similar varying route with time since the very beginning of pipe opening. In most cases, PT 1 had a large drop when pipe opened, then had a short increase instead of

continuously decreasing. This decrease and increase repeated 2 or 3 times within 50 ms after triggering. This happened most probably because of the time delay needed for the air cylinder to build up pressure from an opposite direction to retract the piston. As of our first concern, the time it took to open the pipe for the first time for all tests was found to be 5 to 10 ms.

Test 17 was used as an example in Figure 4-10 to show the several pressure drops since the first pipe opening. Other tests had very similar curves. Figure 4-11 shows PT 1 of all tests (Test 2 to test 20) with the time period the first pipe opening (first pressure drop) had lasted for, indicating a difference in opening speeds.
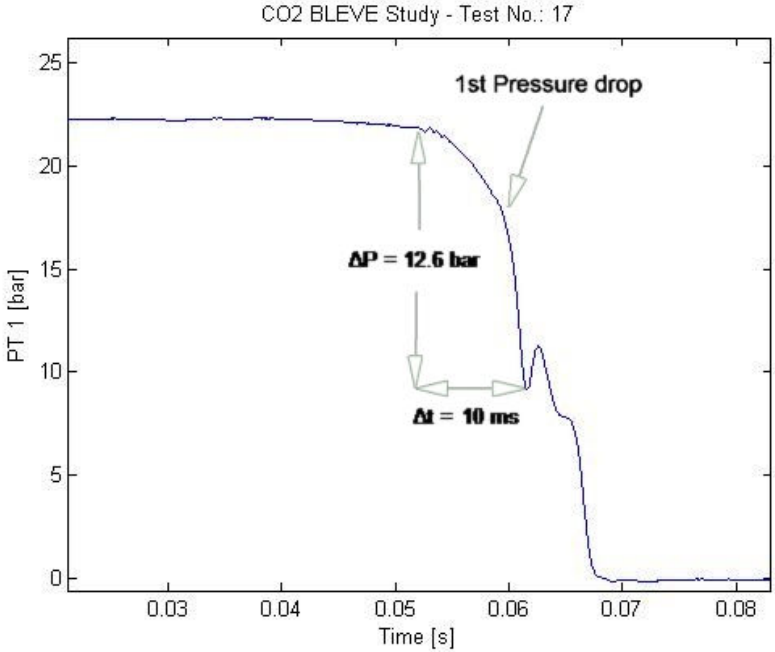
Figure 4-10: Pressure drops since the first pipe opening (Test 17 as example).
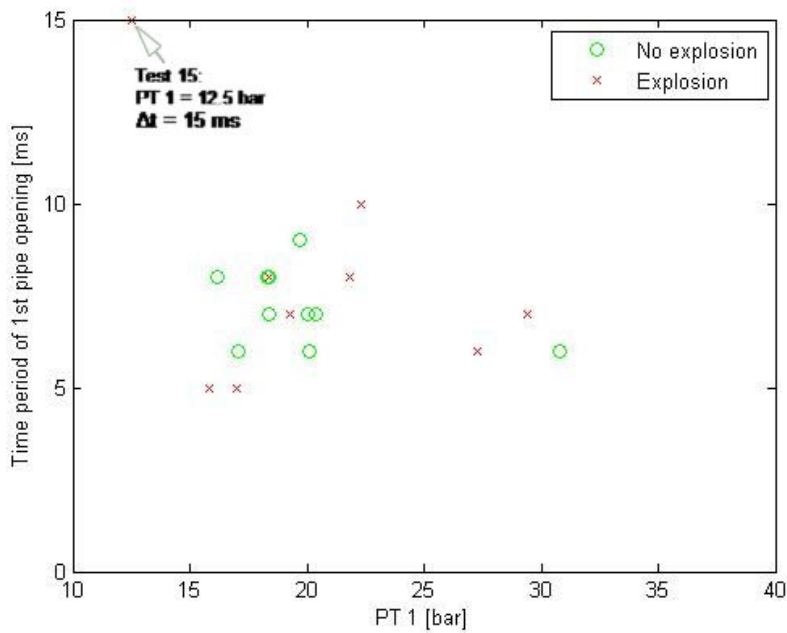
Figure 4-11: PT 1 – time of 1st pipe opening for tests 2-20.

Figure 4-11suggests that PT 1 and the time period of 1st opening were not related. A higher pressure in pipe did not necessarily fasten the opening (Test 15 was just a coincidence with both the lowest PT 1 and the longest opening time). This indicates that the time it took to open the pipe depended mainly on the speed of pressure buildup in the air cylinder and the piston's retraction. As a result, the opening time was expected to be shortened significantly when a higher pressure in the air cylinder was applied. This was what really happened when Compressor 2 replaced Compressor 1 in test 21, as will be described in Subsection 4.5.

4.4.4   Bubble nucleation

As mentioned in Subsection 2.2 'CO$_2$ BLEVE', homogenous bubble nucleation is considered as a pre-condition for a BLEVE. However, fast and furious bubbling may interrupt the nucleation process itself and may therefore deter the occurrence of a BLEVE. It is not easy to find a criterion that is widely accepted for deciding to what extent the bubble nucleation is 'homogenous' and to what extent it is not.

This Subsection tries to find out how the increase of initial pressure (PT 1) inside the experimental pipe has influenced the growth rate of bubble before opening or failure of the pipe, and whether the growth rate of bubble has played a role in the formation of blast wave.

For simplicity, the bubble growth rate was measured as the height of growing bubble against time. A representative figure with bubble growing inside the experimental pipe is as Figure 4-12 (Test 18). Below the yellow horizontal line inside the pipe was liquid CO_2 and above it the white, foam-like substance was newly nucleated and nucleating CO_2, the bubble.
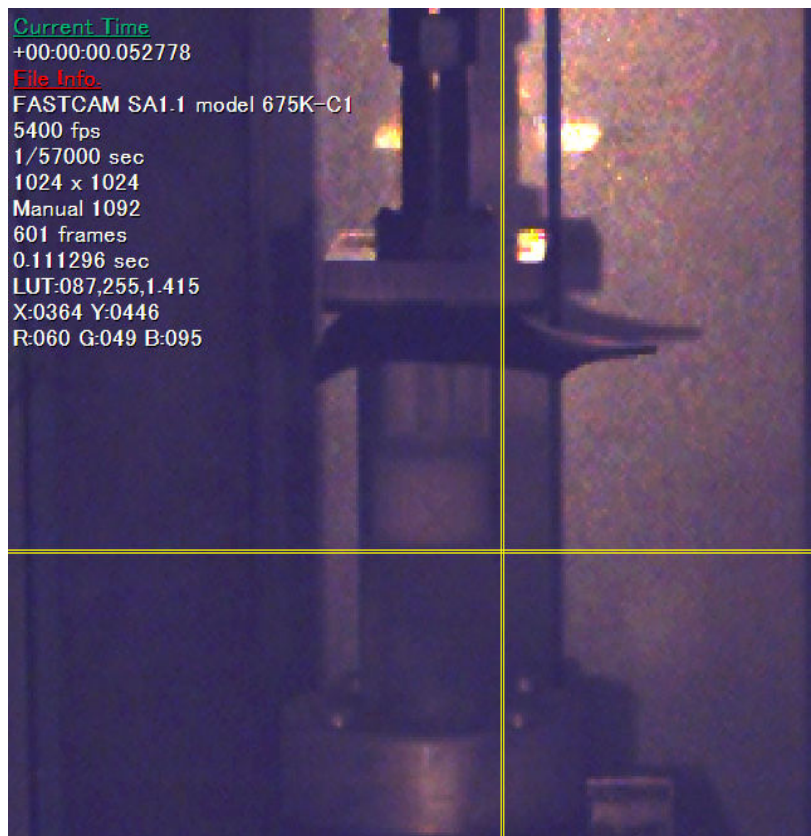
Figure 4-12: Bubble nucleating above liquid CO_2 in the experimental pipe (Test 18).

To help comparing bubble growing speeds among different tests, test 18 (with explosion) and test 14 (no explosion) have been chosen. Basic experiment information of test 18 and test 14 is picked up in Table 4-7. Data points of bubble height [mm], PT 1 [bar] and PT 2 [bar] from both experimental videos and pressure records have been selected with a constant frame step. With a frame speed of 5400 fps, data points were selected every 6 frames (approximately 1.11 ms) starting from the very beginning of the first pressure drop. A total of 16 data points and 14 data points were prepared for test 18 and test 14 respectively for plotting, as recorded by Table 4-8. The bubble heights were computed with pixel manipulation, a method that has been used in Subsection 4.2 the 'Balloon test'.

Table 4-7: Experimental data of test 14 and test 18.

Test No.	Pipe Volume [cm3]	Dry ice [g]	PT 1 [bar]	T [°C]	Phase composition at PT1 / T				
					Liquid CO2 [g]	Percentage [wt-%]	Vapor CO2 [g]	Percentage [%]	CO2 loss by leakage [wt-%]
14	80	30	20	-17.8	27.2	90.7	2.8	9.3	0.0
18	80	62	29.4	-5	37.3	91.6	3.4	8.4	34.4

Table 4-8: Growing bubble heights with pressures, frame No. and time (Test 14 and test 18).

Frame No.	Time [ms]	Test 18			Test 14		
		PT 1 [bar]	PT 2 [bar]	Bubble height [mm]	PT 1 [bar]	PT 2 [bar]	Bubble height [mm]
88	44.1	29.3	0.001	0	19.9	0.001	8
94	45.2	28.9	0.003	0	19.4	0.002	8
100	46.3	27.9	0.001	0	18.1	0.001	8
106	47.4	25.6	0	0	15.6	0	9.5
112	48.5	22.8	0.003	0	12.7	0.001	17.5
118	49.6	20.2	0.006	9.5	10.8	0.006	27.7
124	50.7	18.8	0.007	19	10.3	0.003	35.8
130	51.9	18.7	0.007	22	11.7	0	43.1
136	53.0	19.1	0.003	25	13.5	0.002	45.3
142	54.1	19.4	0.003	25	14.2	0	45.3
148	55.2	19.5	0.002	25	14.5	0.003	45.3
154	56.3	19.6	0	25	14.5	0.003	48.9
160	57.4	19.5	0.008	25	13.5	0	52.6
166	58.5	18.7	0.007	29.2	12.2	0.001	62.8
172	59.6	17.7	0.003	31.4	/	/	/
178	60.7	16.7	0.002	42.4	/	/	/

Figure 4-13 and Figure 4-14 plot bubble heights, PT 1 and PT 2 against time [ms] for test 18 and test 14. Plots of bubble heights and pressures against frame numbers could be found in Appendix J, in case a plotting with frame numbers is preferred by readers.
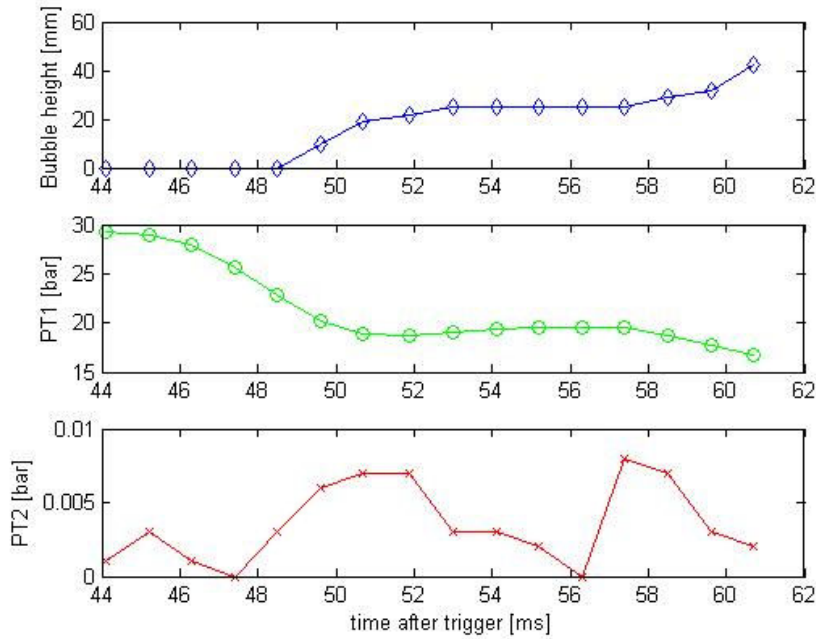
Figure 4-13: Bubble heights, PT 1 and PT 2 against time (Test 18: explosion).
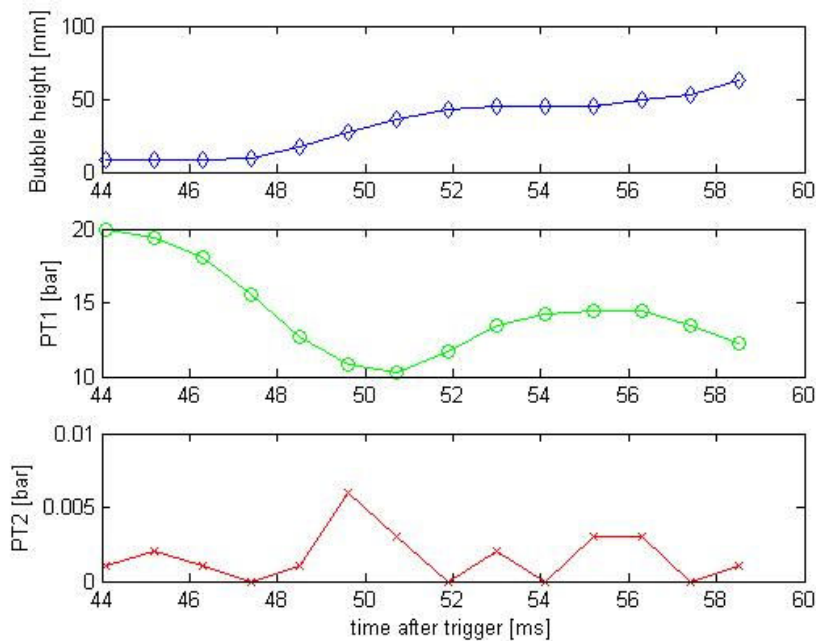
Figure 4-14: Bubble heights, PT 1 and PT 2 against time (Test 14: no explosion).

As shown in Figure 4-13, PT 1 in test 18 started decreasing from 44 ms until 51 ms then kept relatively constant for another 6 ms. A 2nd drop started from 57 ms. Within this same time period, the bubble height remained 0 mm for over 4 ms then started increasing to over 20 mm. After that, it remained there as PT 1 kept constant. And then, with a 2nd pressure drop (57 ms), the bubble height started to increase again at exactly the same time with pressure decreasing.

As shown in Figure 4-14, things in test 14 were a little different. First, the bubble height remained 8 mm when PT 1 started to decrease and stayed there for 3 ms. With continuous pressure drop, the bubble height started to increase. When PT 1 had already reached the first bottom and started to increase again since 53 ms, the bubble height was still increasing at that point and lasted for about 3 ms.

It is hard to know what really caused the difference as observed above. One thing that worth mentioning is that the pressure drop inside pipe may not necessarily bring down the temperature, partly because the liquid-vapor mixture had become superheated at that moment and no longer went through the saturation curve of CO_2 as shown in phase diagrams in Appendix A, partly because more heat inflow from ambient air was expected when the pipe opened slightly. As a combined consequence, bubble nucleation could be attenuated or on the contrary, further enhanced.

Homogenous bubble nucleation might be achieved with attenuation of bubbling to some extent and might therefore cause an explosion in the end, as might be the case of test 18. Enhanced bubble nucleation may gradually turn into furious bubbling, interrupt the nucleation process itself and deter the occurrence of a potential explosion, as might be the case of test 14.

Besides observations of bubble growing with PT 1, it was indeed less significant to look into PT 2, since the pressure peak of PT2 did not appear until later, which was not shown in Figure 4-13 and Figure 4-14. A closer look into the formation of blast waves with bubble nucleation is not discussed in this work, but turned out to be possible in further study.

4.5 CO$_2$ Test with fragments

As classified in Subsection 4.1, test 21 was the only CO$_2$ test performed in lab while the experimental pipe ruptured in an explosion with fragments and experimental data of both pressure signals and video record was captured and stored. It offers a unique opportunity to look into spontaneous vessel rupture with storage of pressurized liquid and vapor.

Subsection 4.5.1 analyzes the pressure record of test 21 with comparison to previous tests described in Subsection 4.4. Subsection 4.5.2 tries to find out how fast the contact surface between two-phase CO$_2$ mixture and the ambient air was moving when the pipe ruptured. Subsection 4.5.3 calculates the kinetic energy of fragments that can be related to the overall explosion energy.

4.5.1 Pressure signals

Experimental data of test 21 is picked up as Table 4-9.

Table 4-9: Experimental data of test 21.

Test No.	Pipe Volume [cm3]	Dry ice [g]	PT 1 [bar]	PT 2 [bar]	PT 3 [bar]	T [°C]	Phase composition at PT1 / T				
							Liquid CO2 [g]	Percentage [wt-%]	Vapor CO2 [g]	Percentage [wt-%]	CO2 loss by leakage [wt-%]
21	82	60	20.6	**0.24**	**0.23**	-17	55.8	96.9	1.8	3.1	4

Pressure signals from all four pressure transducers mounted in test 21 are shown in Figure 4-15.
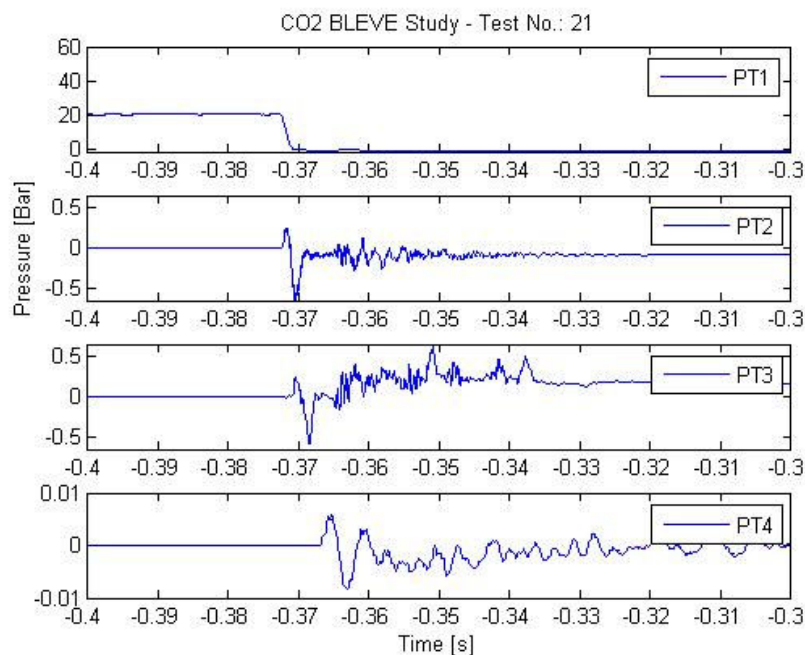
Figure 4-15: Pressure record of test 21 with PT 1, PT 2, PT 3 and PT 4.

Figure 4-15 shows that all four pressure transducers had worked properly with signals of significance recorded. To start from PT 1, Figure 4-16 gives a closer look.
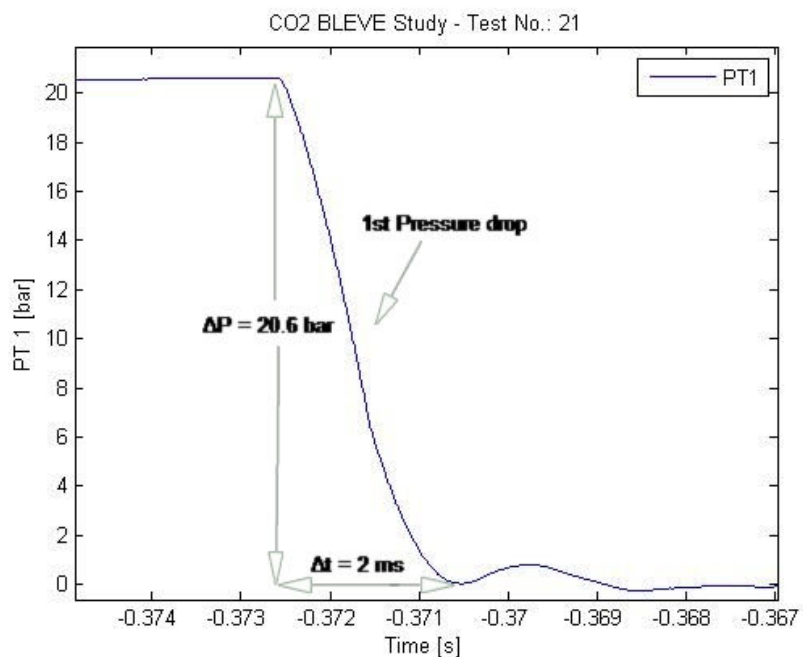
Figure 4-16: Pressure drop in PT 1 with pipe ruptured (Test 21).

a) PT 1.

Comparing Figure 4-16 (test 21) with Figure 4-10 on page 65 (Pressure drops in test 17) which was a non-explosion test yet had very representative pressure signals among test 2 to test 20, at least three differences were observed.

1) The pressure jump from top to bottom during the 1st pressure drop (ΔP) in test 21 and test 17,

ΔP_{21} = 20.6 bar, ΔP_{17} = 12.6 bar.

ΔP_{21} was almost twice higher than ΔP_{17}.

2) The time ΔP took in test 21 and test 17,

Δt_{21} = 2 ms, Δt_{17} = 10 ms.

Δt_{21} was five times shorter than Δt_{17}.

3) The 2nd pressure drop in test 17 as shown in Figure 4-10 was about 10 bar, a same magnitude as ΔP_{17} (12.6 bar) and represented clearly pipe opening for a second time. The 2nd pressure drop in test 21 as shown in Figure 4-16 was as small as 1 bar and could simply be caused by the oscillation of the piston as well as the steel pedestal and thus could be neglected.

Although a faster pressure buildup in the air cylinder and a faster retraction of the piston could significantly reduce the time for a pressure drop, a bigger pressure drop and a faster time it took in test 21 had absolutely nothing to do with the air cylinder or the movement of the piston, because the piston was retracted AFTER the pipe had ruptured. This may be due to

the fact that if a spherical pipe ruptures along multiple directions to form fragments, the contact surface between the pressurized liquid/vapor mixture and the ambient air is larger than the case when a pipe is only opened from the top.

A simple calculation is done to help explain this assumption clearer.

Table 3-2 on page 27 has given pipe sizes used in different tests. Test 17 used an experimental pipe with a length of 100 mm and an inner diameter of 32 mm. Test 21 used an experimental pipe with a length of 80 mm and an inner diameter of 36 mm. Geometrical parameters of the pipes used in test 17 and test 21 are summarized in Table 4-10.

Table 4-10: Geometrical parameters of the pipes used in test 17 and test 21.

Test No.	D_{pipe} [mm]	L_{pipe} [mm]	S_{top} [mm^2]	$S_{surface}$ [mm^2]
17	32	100	804	10048
21	36	80	1017	9043

D_{pipe}, L_{pipe}, S_{top}, $S_{surface}$ in Table 4-10 are the inner diameter, the length, the area of pipe top and the surface area of the pipe respectively.

$S_{top} = (1/4)*\pi* D_{pipe}^2$.

$S_{surface} = \pi* D_{pipe}* L_{pipe}$.

As in test 17, the area of contact surface at the very beginning of pipe opening was the top area of the experimental pipe. That was 804 mm^2. When it came to test 21, since the piston still kept the pipe top closed and the aluminum pedestal sealed the pipe bottom at the moment of pipe rupturing, the area of contact surface became the surface area of the pipe which was 9043 mm^2. With a same CO_2 filling level of 60 g and very close initial pressures and temperatures in both tests ([PT 1, T] = [22.3 bar, -14.3 °C] in test 17 and [20.3 bar, -17 °C] in test 21), an initial contact surface with more than 10 times larger area in test 21 than that in test 17 was supposed to be one important reason for the faster pressure drop.

b) PT 2/PT 3.

Figure 4-17 gives a closer look into PT 2 and PT 3 in test 21. Based on the assumption that 'PT 2/PT 3 > 0.1 bar' proves an explosion as described, both the peak of PT 2 (0.24 bar) at t_2 and that of PT 3 (0.23 bar) at t_3 indicated the occurrence of an explosion in test 21.
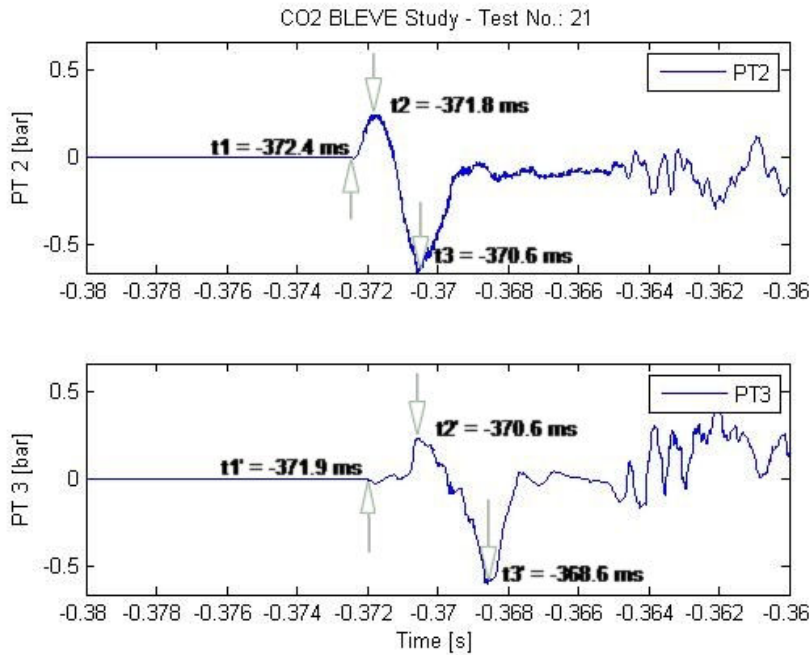
Figure 4-17: Pressure signals of PT 2 and PT 3 in test 21.

As shown in Figure 4-17, t_1 and t_1' were the time when PT 2 and PT 3 started to response. t_2 and t_2' were the time when PT 2 and PT 3 reached their peaks. t_3 and t_3' were the time when PT 2 and PT 3 reached their bottoms. Two observations based on Figure 4-17 include:

1) The time difference between the response of PT 2 and PT 3,

   $\Delta t_1 = t_1$'$- t_1 = 0.5$ ms.

With a sound speed of about 220 m/s in vapor CO_2 at 20.3 bar and -17 °C (Appendix H), the time a pressure wave propagated through the distance between PT 2 and PT 3 (10 cm),

   $\Delta t = 0.1$ m/(220 m/s) $= 0.45$ ms, very close to Δt_1.

2) After the peaks of PT 2 and PT 3 at t_2 and t_2' respectively, a bottom for both PT 2 and PT 3 was reached at t_3 and t_3' with absolute overpressures of 0.65 bar and 0.6 bar respectively. These two bottom points might be caused by an overlapped pressure wave as a sum of the first pressure wave plus a reflection wave from the steel pedestal, or the back wall where the testing rig was mounted, or the plastic coverings beside the testing rig where pneumatic valve and signal amplifiers were placed in and protected from pressure waves, or other devices nearby (Figure 3-6 and Figure 3-7 on page 29). It is not easy to locate a reflection source since many devices or obstacles may have participated.

c) PT 4

Figure 4-18 gives a closer look on PT 4 of test 21.
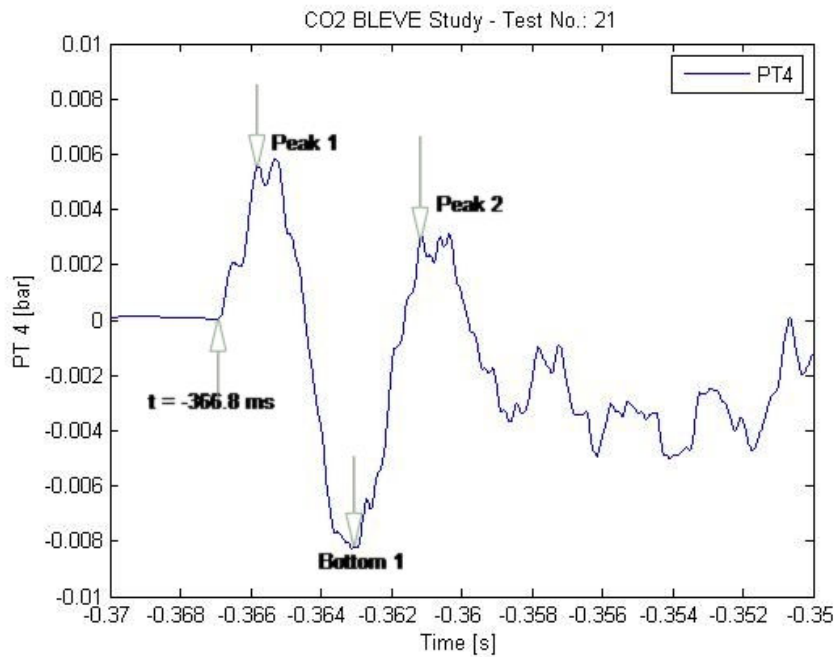
Figure 4-18: Pressure signal of PT 4 in test 21.

Pressure wave from explosion in test 21 propagated to PT 4 at -366.8 ms followed by two pressure peaks with a bottom in between, as marked in Figure 4-18. Two observations on PT 4 signals include:

1) Compared with Figure 4-16, the time when PT 4 started to response and measure (t = - 366.8 ms) was 5.7 ms later than that when the first pressure drop in PT 1 started (t = - 372.5 ms). Mounted near the ground as shown in Figure 3-20 on page 38, PT 4 was 2.1 m away from the pipe center. With a sound speed in air of 340 m/s, the time the pressure wave took to propagate from pipe center to PT 4 through the air was 2.1 m/(340 m/s) = 6.2 ms, very close to the 5.7 ms delay.

2) Similar with the observations of PT 2/PT 3, the 'Bottom 1' and 'Peak 2' as marked in Figure 4-18 could be used to calculate the time gap and pressure change, however, it is not easy to find out in an accurate way which obstacles around PT 4 had participated in the formation of 'Bottom 1' and 'Peak 2'. It could only be assumed to be caused by some kinds of overlapped pressure waves.

4.5.2 Contact surface

The contact surface during an experiment refers to the surface of contacting area where the liquid/vapor CO_2 mixture splashing out of the experimental pipe met the ambient air.

This Subsection tried to find out how fast such a contact surface was moving into a wider space around the experimental pipe after it ruptured in test 21.

Figure 4-16 shows that the pipe started to rupture from -372.5 ms (frame No.: -2012). At this point, the contact surface remained invisible because the liquid/vapor CO_2 mixture had

not yet splashed out and come into the ambient air, as shown in Figure 4-19. 6 pictures with contact surfaces are collected in Figure 4-20, starting from frame -2007 with a frame step of 4. The place and dynamic development of the contact surface are marked with a closed white line. The developing route of such a contact surface is assumed as a spherical emission for simplicity and convenience of video processing. A straight line connecting two points with a longest distance on the contact surface is treated as the diameter as of a spherical object.

Figure 4-19: The beginning of pipe rupture in test 21 (Frame No.: -2012).
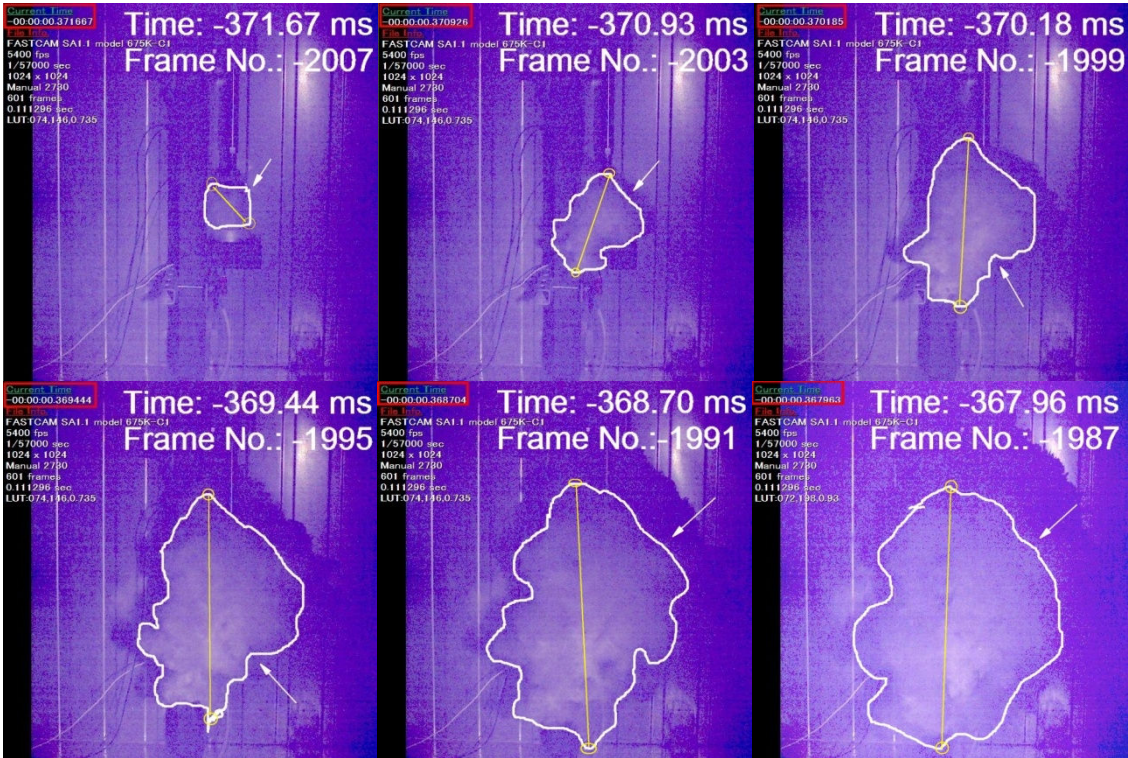
Figure 4-20: Growing contact surface in test 21 (From frame -2007; frame step: 4)

As in the first sub-photo on the top left of Figure 4-20, the imagined diameter (D_1) happens to be of about the same length as the length of the experimental pipe (100 mm). For simplicity, D_1 = 100 mm = 0.1 m.

With same method as used in Subsection 4.2 'Balloon test', the imagined diameters of the contact surface in the rest five sub-photos (D_2 to D_5) can then be calculated by pixel counting with same software, Photron FASTCAM Viewer.

The time when the pipe started to rupture (-372.5 ms) as in Figure 4-19 has been set to be time zero for growth of the contact surface when there was no contact surface at time zero.

Table 4-11 gives information about the development of the contact surface in both diameter and volume against time by processing the contact surface as a spherical object.

Table 4-11: Growth of contact surface with time in test 21.

Time [ms]	Diameter [m]	Surface area [m^2]	Volume [m^3]	Growing speed		
				1-D [m/s]	2-D [m^2/s]	3-D [m^3/s]
0	0	0	0	120.5	37.8	0.6
0.83	0.10	0.031	0.001	135.1	127.3	5.0
1.57	0.20	0.126	0.004	160.0	261.2	17.3
2.32	0.32	0.322	0.017	148.6	350.1	33.1
3.06	0.43	0.581	0.042	81.1	234.2	27.0
3.80	0.49	0.754	0.062	13.5	42.0	5.2
4.54	0.50	0.785	0.065	/	/	/

Surface area S = πD^2; Volume V = (1/6)* πD^3.

Growing speeds are calculated from 1-D to 3-D, each representing the speed of increase in the diameter, surface area and volume of the contact area.

For example, the 1-D, 2-D and 3-D speeds at time 0,

v_D = (D2 – D1)/(t2 – t1).

v_S = (S2 – S1)/(t2 – t1).

v_V = (V2 – V1)/(t2 – t1).

Figure 4-21 shows the variation of diameter, surface area and volume of contact surface with time. Figure 4-22 shows the growth rate of diameter, surface area and volume of contact surface with time.
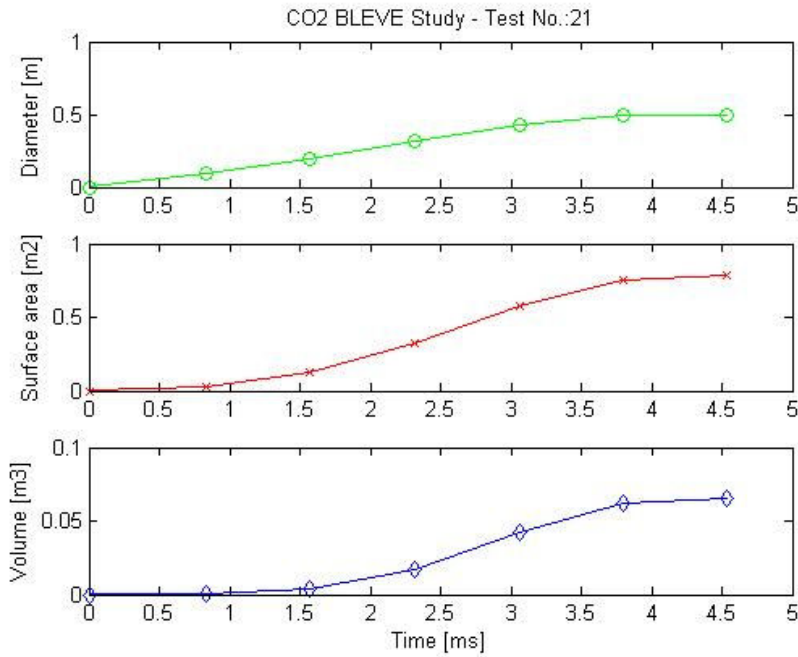
Figure 4-21: Variation of diameter, surface area and volume of contact surface.
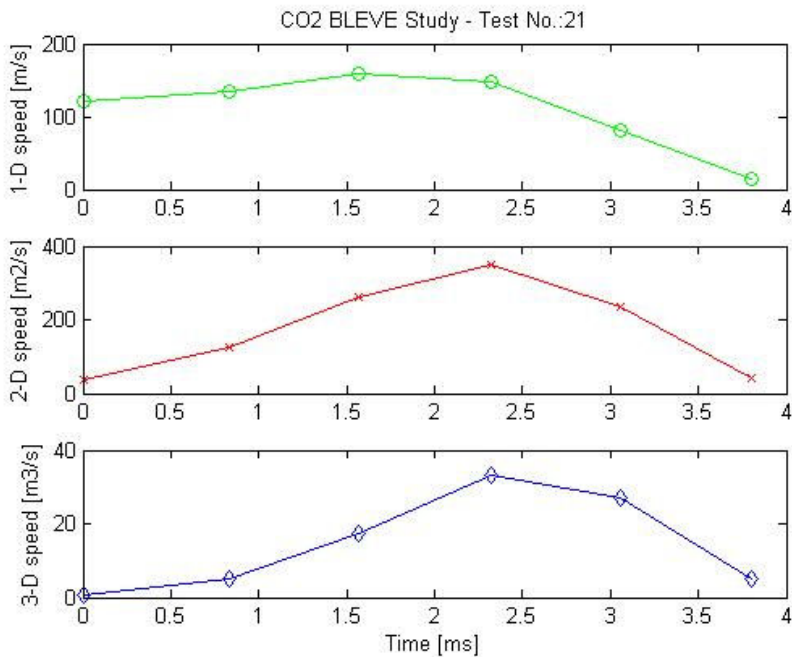
Figure 4-22: Growing speed of diameter, surface area and volume of contact surface.

Figure 4-21 and Figure 4-22 show that the contact surface between two phase CO_2 mixture that splashed out of the experimental pipe in an explosion and the ambient air was capable of growing itself extremely fast to gain a volume of around 0.1 m^3 within 5 milliseconds. However, the growth rate of the contact surface's magnitude would not last long at a high level and would decrease quickly after the first 2 or 3 milliseconds. As a result, the contact surface was expected to stay and remain at a point for a very short time then vanished quickly while CO_2 molecules had been mixing with ambient air.

The growth rate of contact surface in other tests was not computed. This work could be done and may reveal a relationship between initial pressure/temperature (PT 1/T) and 3-D speed of the contact surface (speed of volume growth). An assumption about this could be that a higher initial temperature that is close to or above the superheat limit temperature of CO_2 (-13.8 °C) would fasten the volume growth of the contact surface and strengthen the pressure wave. The possibility of having an explosion may thus be increased.

4.5.3　Fragments and explosion energy

Many mathematical models and methods have been developed for calculation of explosion energy, such as TNT equivalent method, SVEE method etc. as mentioned in Chapter 2. This Subsection tries to suggest a simpler way for estimating explosion energy. It is easy to understand that when an explosion occurs with fragments formed, as the case of test 21 in this work, the total kinetic energy of all fragments must be part of the explosion energy, which, if tracked back one step further, must have been part of the internal energy of the explosives before anything happened. In our case, a 2-phase mixture of pressurized CO_2 was the explosive. It did not necessarily lead to an explosion. But when it did, and even better, exploded with fragments, it becomes feasible and reasonable to relate the kinetic energy of the fragments with the overall explosion energy released.

Figure 4-23 shows a corner near the testing rig in the explosion scene after test 21. Numerous fragments of very small pieces were found everywhere in the laboratory. Three fragments of different weights and locations have been collected, as shown in Figure 4-24.
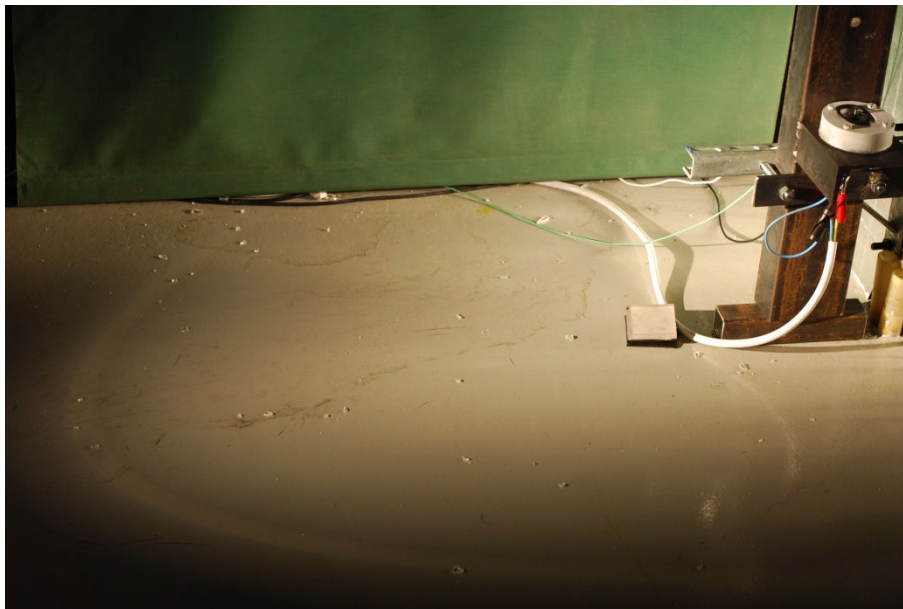
Figure 4-23: A corner with fragments in the explosion scene of test 21.
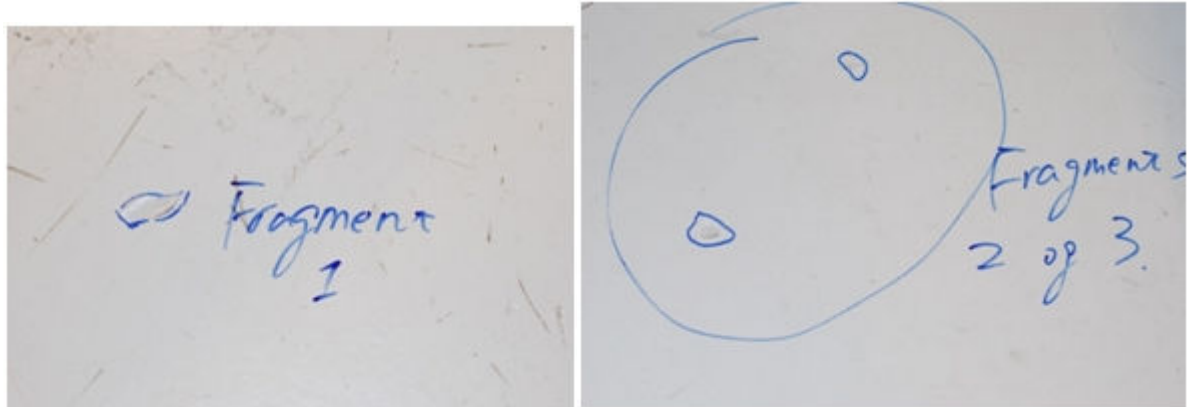
Figure 4-24: Three fragments in test 21 collected for analysis.

Information of the three fragments is given in Table 4-12.

Table 4-12: Three fragments collected in test 21.

Fragment No.	Weight [g]	Distance [m]
1	1.14	4.5
2	0.37	6.0
3	0.13	6.1

The column 'Distance [m]' refers to the distance from a fragment's location to the center of the experimental pipe.

The method used in this Subsection to relate kinetic energy of fragments with the overall explosion energy is based on three assumptions listed in Table 4-13.

Table 4-13: Assumptions for calculation of explosion energy in test 21.

Assumption	Description
1	Fragments of different sizes and weights from rupture of the experimental pipe had a same initial speed v along horizontal direction.
2	The horizontal speed of all fragments v kept constant during flying regardless of any friction or disturbance or irregular flying route through the air. Only gravity worked on fragments.
3	An average of 10% of the explosion energy was transformed into kinetic energy of fragments.

With assumptions above, procedures of calculating explosion energy goes as following.

a) Assumptions 1 and 2 simplified the situation into a standard 'Horizontal Projectile Motion'. Figure 4-25 shows a 'Horizontal Projectile Motion' with a fragment.
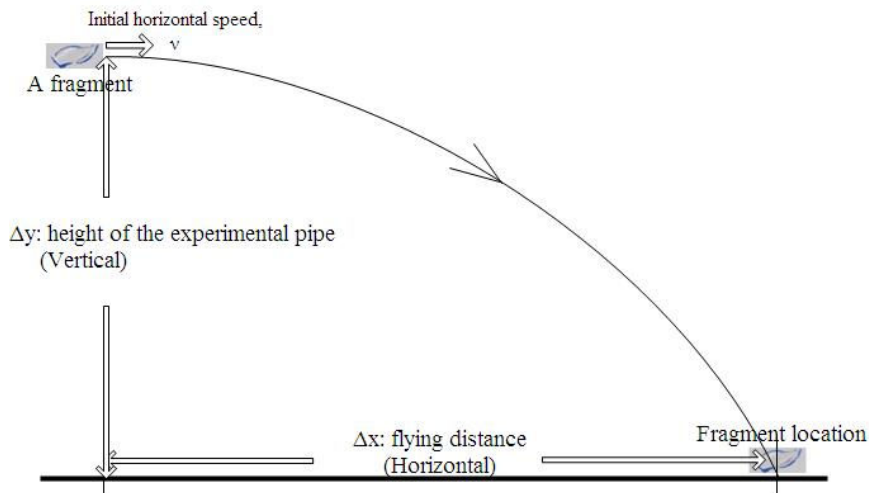
Figure 4-25: A sketch showing a horizontal projectile motion with a fragment.

b) Formulas of horizontal projectile motion could be used to calculate the initial horizontal speed of fragments, v. For the three fragments listed in Table 4-12, they shared a same Δy (Pipe height) in Figure 4-25 while having different Δx (flying distance). The experimental pipe in test 21 was mounted 0.38 m above the ground, so,

$\Delta y = 0.38$ m.

The formula of calculating total flying time t with given vertical height Δy is:

$\Delta y = (1/2)*g*t^2$. g is the acceleration of gravity with a value of 9.8 m/s^2 used here.

With flying time calculated from formula above, the initial horizontal speed for a fragment is available by,

$v = \Delta x/t$.

Table 4-14 gives results of calculation for the three fragments. Since it is assumed that al fragments share a same initial horizontal speed, an average of horizontal speeds of the three fragments is used instead for all fragments in next step.

Table 4-14: Calculation results of horizontal speed for fragments collected in test 21.

Fragment No.	Flying distance Δx [m]	Pipe height [m]	Flying time [s]	Horizontal speed, v [m/s]	Average v [m/s]
1	4.5	0.38	0.28	16.1	
2	6.0	0.38	0.28	21.4	19.8
3	6.1	0.38	0.28	21.8	

c) The average horizontal speed for all fragments is used to calculate the overall kinetic energy of all fragments (assume there were a total of n fragments),

81

$K = K_1 + K_2 + \ldots + K_n$

$\quad = (1/2)*m_1*v^2 + (1/2)*m_2*v^2 + \ldots + (1/2)*m_n*v^2$

$\quad = (1/2)*m_{pipe}*v^2.$

The weight of the experimental pipe in test 21 was measured,

$m_{pipe} = 40.6$ g, so the overall kinetic energy of fragments,

$K = (1/2)*0.041 \text{ kg}*(19.8 \text{ m/s})^2$

$\quad = 8$ J.

d) With assumption 3 as listed in Table 4-13, the kinetic energy of all fragments took 10% of the overall explosion energy. So an estimation for simplicity of the explosion energy in test 21,

$E = 10*K = 80$ J.

One thing that worth mentioning is that this method to estimate explosion energy is very coarse and could only be used when a rough estimation is good enough. An alternative approach may start from the internal energy of CO_2. A more quantitative calculation on explosion energy involves systematic modeling and complex calculations. Further study could be made if estimation of explosion energy is required to be more accurate.

4.6 Fitness with 'Superheat limit temperature' theory

As reviewed in Subsection 2.2.3 'Mechanisms of BLEVE', Reid et al [2] think that the superheat limit temperature for all pressurized liquefied gas is a temperature threshold for the occurrence of a BLEVE. See also Figure 2-1 on page 15. Some researchers follow Reid and continue their study with this theory, partly because of its simplicity. Besides them, Prugh [4]stated that BLEVE can also occur when the initial temperature of the two phase mixture in vessel is well below its superheat limit temperature; except that the explosion energy for this type of BLEVE is considerably lower than BLEVEs that occur when initial temperature is higher than SLT.

This Subsection does not aim to do theoretical deductions, but tries to relate the superheat limit temperature theory with our experimental results, and see to which extent the theory fits practice.

4.6.1 Superheat limit temperature

Figure 4-26 shows the superheat limit curve of CO_2 together with its vapor pressure line. It has included a starting point, dry ice, which was also a starting point in our experiments.
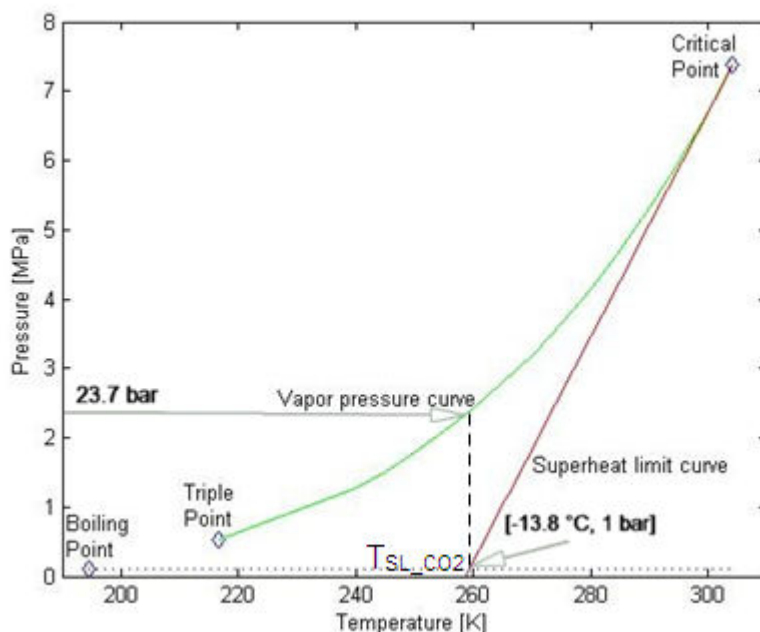
Figure 4-26: Vapor pressure line and Superheat limit curve of CO_2.

Figure 4-26 above shows that at atmospheric pressure, the superheat limit temperature for CO_2 is 259.3 K (-13.8 °C). The saturation pressure at this superheat limit temperature is 23.7 bar, as also marked in Figure 4-26. A MATLAB script for plotting it has been attached as Appendix K.

According to Reid's SLT theory, tests with initial temperature (T) higher than -13.8 °C before the opening/failure of vessel were supposed to have explosions while tests with initial temperatures (T) lower than -13.8 °C were not expected to. Another way of expression is, based on SLT theory, tests with PT 1 > 23.7 bar were supposed to have explosions while tests with PT 2 < 23.7 bar were not expected to.

Is that what really happened in laboratory? Not exactly.

Figure 4-27 below shows data points of tests 2 to test 21 on the saturation vapor pressure curve of CO_2 with superheat limit temperature (SLT) for CO_2 at 1 bar (-13.8 °C) and saturation pressure at SLT (23.7 bar) also marked with dotted lines.
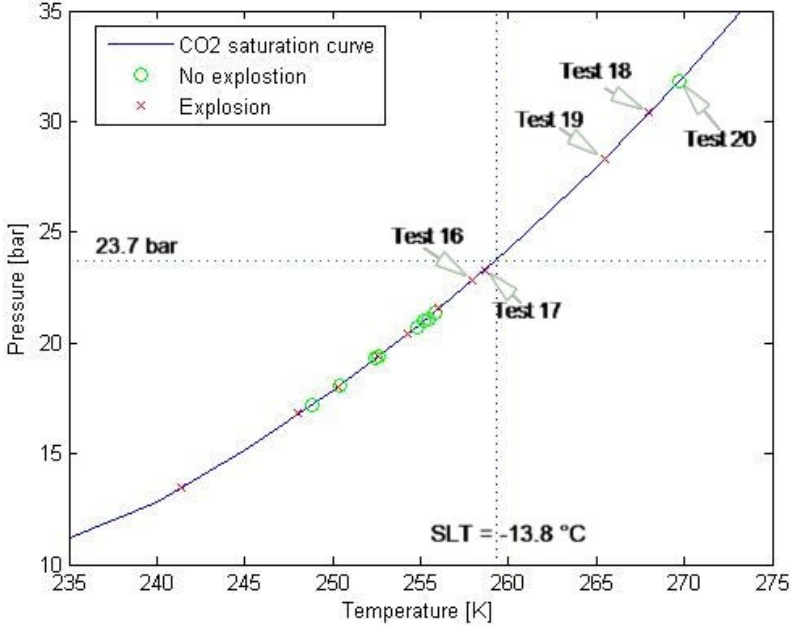
Figure 4-27: CO₂ tests along CO₂ saturation curve (test 2 to test 21).

As shown in Figure 4-27 above, when the initial temperature was near or above SLT (-13.8 °C), test 16, 17, 18, 19 had BLEVEs as expected. Their initial temperatures are -15.1 °C, -14.3 °C, -5 °C and -7.5 °C respectively, all close to or above the SLT of CO_2. A test of exception with no explosion was test 20. Based on previously analysis, the most possible reason could be that the weight of CO_2 was only 20 g (an overall density of 250 kg/m³). We have assumed previously in Subsection 4.3 'Phase composition of CO_2 mixtures' that when CO_2 filling quantity with an overall density of less than 375 kg/m³ would not have enough two phase flow splashing out of pipe and be less likely to have an explosion.

On the other side, when the initial temperature was clearly below SLT, more exceptions were observed. They were test 4, 6, 9, 13, 15 and 21, with initial temperatures of -22.7 °C, -20.4 °C, -25 °C, -20.6 °C, -31.6 °C and -17 °C respectively. They had explosions. There is no good explanation to this so far. Recalling the opinion of Prugh [4], when this 'below SLT BLEVE' happens, the explosion energy might be lower than those BLEVEs that occurred above SLT. Explosion energy of test 21 has been estimated in Subsection 4.5.3. The

explosion energy of 80 J in test 21 could be used in further study to compare with other explosion tests that occurred above SLT.

So far, hints or indications for 'directing' a CO_2 BLEVE by analysis of pressure signals and video records include: 1) Certain amount of CO_2 filling. As in our case, with a volume of around 80 cm^3, 30 g dry ice (that is, an overall density of 375 kg/m^3) appears to be a filling level that very likely may lead to an explosion. When less than 20 g CO_2 were filled ina same volume of 80 cm^3(an overall density of 250 kg/m^3), BLEVE seldom occurred. 2) High initial pressure and temperature. Although a set of initial pressure and temperature higher than SLT requirements does not guarantee the occurrence of an explosion, the possibility is supposed to be increased. 3) No gas leakage. Serious gas leaking from inside the pipe will lose CO_2 fast and be unable to keep building up pressure. Besides, the CO_2 escaped around the pipe can further cool down the experimental rig and bring down the temperature. According to the Superheat Limit Temperature theory, the decrease of temperature would reduce the possibility of having an explosion.

4.6.2   Degree of superheat

An alternative way to look into the 'Superheat Limit Temperature Theory' is through degree of superheat. An example has been shown in Subsection 2.2.3 with pressure liquefied gases like ammonia. When it comes to CO_2, will its degree of superheat correlate to the intensity of pressure wave in an explosion? The answer is supposed to be yes, if the superheat limit temperature theory is assumed reasonable. The degree of superheat is the difference between the initial temperature prior to the opening/failure of the experimental pipe and the boiling point, which, fundamentally, depends still on the initial temperature.

To make it clearer, events happening inside the pipe are reviewed. It may be seen from Figure 4-26 on page 83 that, values of boiling point and superheat limit temperature at 1 bar for CO_2 are 194.5 K and 259.3 K respectively. The temperature difference between the two (259.3 K − 194.5 K = 64.8 K) is called the 'Nominal degree of superheat limit'. When a sudden depressurization takes place due to the opening/failure of the pipe, the liquid/vapor CO_2 mixture which was in thermodynamic equilibrium undergoes a sudden pressure drop and turns itself to be superheated. Depending upon the degree of superheat, violent flashing of two-phase CO_2 mixture might take place with pressure waves, causing an explosion and possibly, fragments also with pipe rupture. Figure 4-28 plots degrees of superheat for test 2 to test 21 against the maximum over pressures of PT 2 and PT 3, in case one of them happened to have a malfunction.
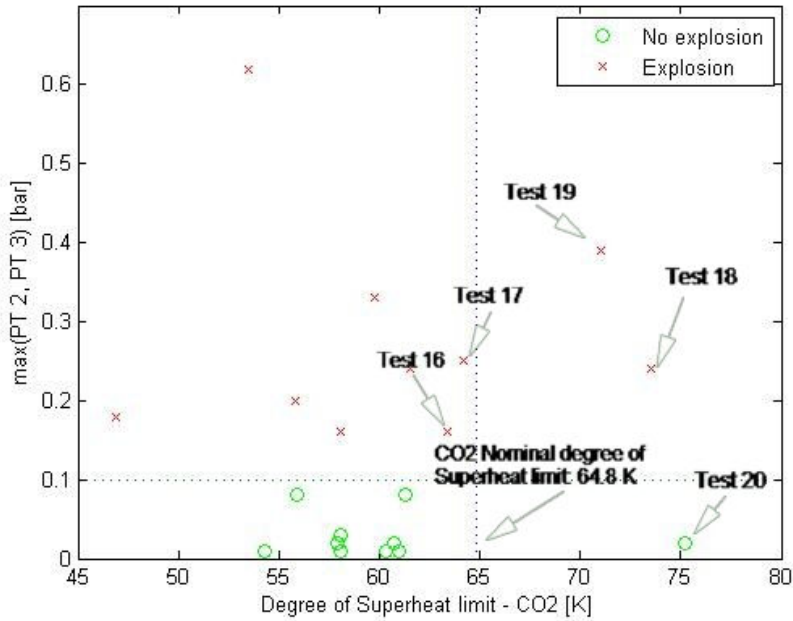
Figure 4-28: Degree of superheat with max(PT 2, PT 3) (Test 2 to Test 21).

Fundamentally, Figure 4-28 and Figure 4-27 express similar things in different points of view and they support each other with additional information for a greater understanding.

Results and discussion above in Subsections 4.6.1 and 4.6.2 indicate that the SLT theory is not completely consistent with experimental results. However, considering all influencing factors during tests, including CO_2 filling, gas leaking, heating rate, 2-phase flow of CO_2 mixtures with varied phase composition, the SLT theory may still be acceptable within a certain range. More research on both theories and experiments is needed in order to further improve the SLT theory or have new theories developed for BLEVE study.

4.7 Dry ice formation

Subsection 2.3.2 'Thermodynamics' in Chapter 2 has described an 'Icing Route' with an assumption that there might be dry ice formation after the opening of a storage vessel containing pressurized liquid CO_2, if depressurization process takes a considerable time instead of being infinitely fast. The formation of dry ice after pipe opening was indeed observed in experiments. This Subsection discusses more on this phenomenon.
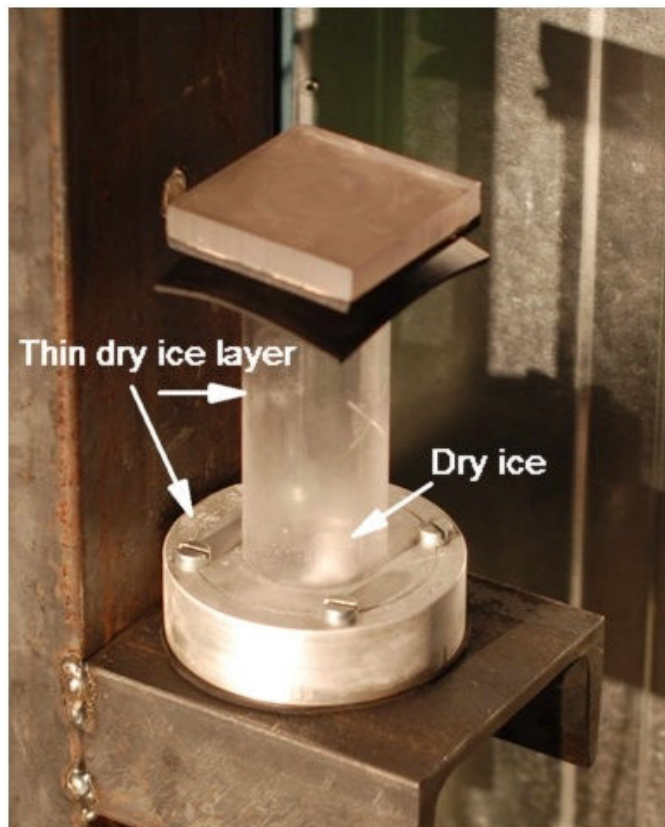
Figure 4-29: Dry ice formed after pipe opening.

Figure 4-29 shows an experimental pipe on aluminum pedestal in a test not recorded with this work (no data saved except the picture). Dry ice formed like a small tablet inside the pipe and as a thin layer on the outer wall of the pipe and the aluminum pedestal. Among recorded tests, test 7 and test 10 were observed with dry ice formation. This additional experimental information could be found in Appendix G. More specifically, small amount of dry ice formed at pipe bottom in test 7 and a thin layer of dry ice formed around the outer wall of the pipe at test 10, both with similar appearance as in figure above. This information was unfortunately incomplete. There might be one or two more tests with dry ice formed but not recorded. Figure 4-30 is used again (as also in Subsection 2.3.2) for the following discussion.
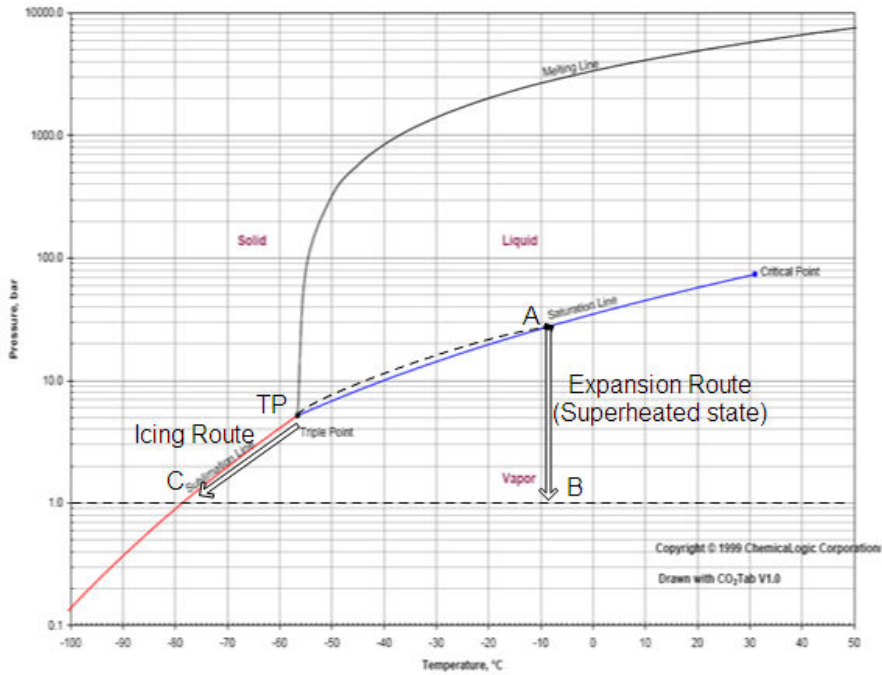
Figure 4-30: Pressure – Temperature diagram of CO_2.

The 'Superheat Limit Temperature' theory with isothermal assumption leads to the 'Expansion Route' through which liquid/vapor CO_2 splashes out of the vessel and the main process is the vaporization of pressurized liquid and expansion of generated vapor. The theory suggests that lower initial temperature would reduce the possibility of having an explosion.

Alternatively, 'Icing Route' with quasi-equilibrium assumption suggests that a considerable time the depressurization takes will bring down the temperature as well as pressure and thus dry ice would start to form when vapor temperature manages to get across the triple point (-56.6 °C, 5.17 bar). A first question with experimental data is: how long exactly did the depressurization take in these tests? Is there a relationship between the time and dry ice formation?

Table 4-15 lists two time periods t_1 and t_2 for test 3 to test 21. t_1 represents the time of depressurization from initial pressure (PT 1) to room pressure (1 bar). This time is considered approximately as the total time of vaporization and expansion. t_2 is the time of pressure drop from triple point pressure (5.17 bar) to 1 bar. Theoretically, this is the time when low-temperature vapor is able to form dry ice. Test 2 is not listed because the time of depressurization in this test was about 10 times longer (390 ms) than in other tests (40 ms on average), probably due to failure of pressure buildup in the air cylinder.

Table 4-15: Depressurization time from PT 1/Triple point to 1 bar, test 3 to test 21.

Test No.	PT 1 [bar]	T [°C]	t_1 [ms]	t_2 [ms]
3	17.1	-22.6	30	10
4	17	-22.7	34	6
5	20.4	-17.2	42	16
6	18.4	-20.4	49	20
7	19.7	-18.2	54	23
8	20.1	-17.5	54	17
9	15.8	-25	28	7
10	18.4	-20.4	50	15
11	19.3	-18.7	52	11
12	18.4	-20.4	49	18
13	18.3	-20.6	49	21
14	20	-17.8	51	16
15	12.5	-31.6	22	8
16	21.8	-15.1	30	10
17	22.3	-14.3	14	2
18	29.4	-5	47	8
19	27.3	-7.5	38	3
20	30.8	-3.3	58	13
21	20.6	-17	2	0.7

Since the idea on temperature is the main difference between 'Expansion Route' deducted from SLT theory and 'Icing Route' deducted with quasi-equilibrium assumption, the initial temperature (T in Table 4-15) is used to plot against t_1 and t_2 respectively, see Figure 4-31 and Figure 4-32.
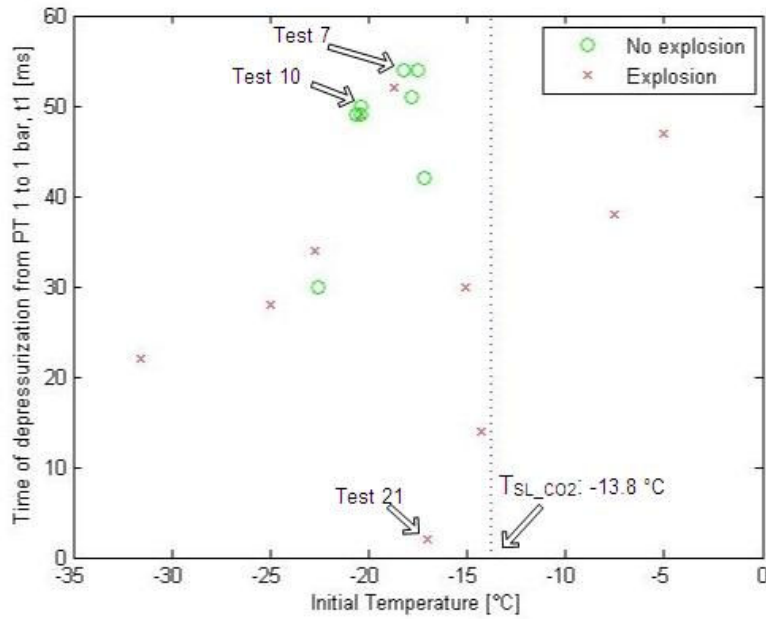
Figure 4-31: Time of depressurization from PT 1 to 1 bar, test 3 to test 21.
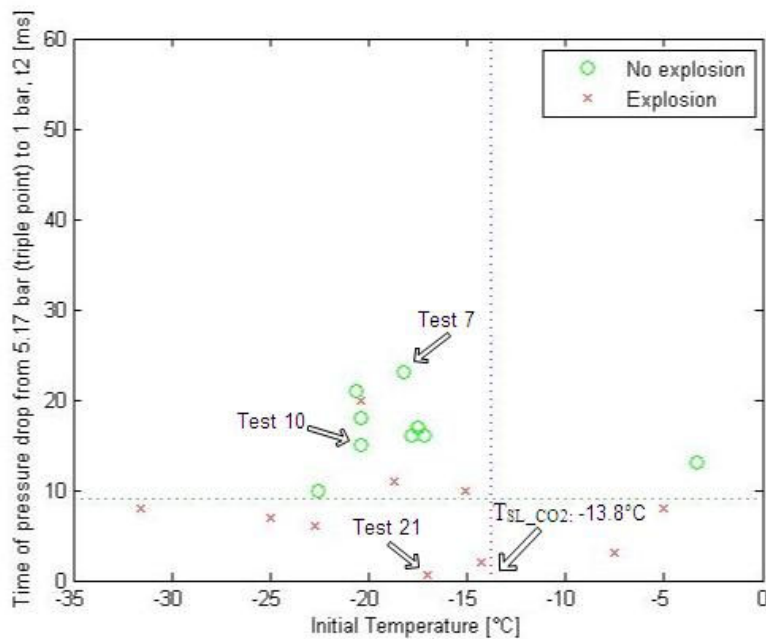
Figure 4-32: Time of pressure drop from 5.17 bar to 1 bar, test 3 to test 21.

Combining Figure 4-31 and Figure 4-32, it is seen that test 7 with dry ice formation had both a longest total time of vaporization (t_1 = 54 ms) and a longest time since the vapor started to form dry ice below the triple point (t_2 = 23 ms). t_1 and t_2 in test 10 were a little shorter, but still higher than average (t_1 = 50 ms, t_2 = 15 ms). As assumed for dry ice formation through 'Icing Route', a longer time of vaporization may keep the temperature decrease, and the triple point temperature (-56.6 °C) may thus be reached; meanwhile, a longer time of keeping the temperature below -56.6 °C may allow more vapor to form dry ice.

If dry ice starts to form, it will most probably form inside the storage vessel and/or around the outer wall of the vessel, since these places are cooled down most efficiently by the large amount of low temperature vapor; besides, the vapor around the vessel can also 'protect' the cooled vessel with dry ice from the ambient air for while so that the heat inflow from air could not sublimate the dry ice immediately. In this way, dry ice could be found after pipe opening, as probably in the cases of test 7 and test 10.

On the other hand, test 21 as also indicated in Figure 4-31 and Figure 4-32 had an extremely short time of depressurization ($t_1 = 2$ ms) and a shorter time that was available to form dry ice ($t_2 = 0.7$ ms). As a result, the lowest temperature the vapor could reach may still lie above the triple point temperature (-56.6 °C) and unable to form dry ice. Even if the temperature was low enough, the tiny amount of dry ice formed within t_2 (0.7 ms) would sublimate into vapor again when the temperature started to increase very soon, with heat inflow from ambient air. In this situation, no dry ice would be observed after vessel opening, as probably in the cases of test 21 and other tests without dry ice formation.

As a summary, key influential factors for dry ice formation may include:

1. Initial temperature (T).

2. Speed of depressurization.

3. CO_2 filling level.

The idea is: with more CO_2 filling in the storage vessel, more vapor may be generated during depressurization. If liquid CO_2 depressurizes with a relatively low speed, vapor temperature would keep decreasing. If the initial temperature is relatively low, close to the triple point temperature of -56.6 °C, there is then a great chance for dry ice formation.

Now that the first question of 'how depressurization and dry ice formation is related' is answered, a second question comes immediately:

Will the formation of dry ice influence the occurrence of an explosion? If yes, how?

Figure 4-32 may be used to explain or 'guess' what is going on when dry ice forms. A very interesting observation from that figure is that there were in total 7 tests which had a pressure drop from 5.17 bar to 1 bar in less than 9 ms, including test 21. Exclusively, all these 7 tests had no dry ice observed after pipe opening and all of them had explosions.

This observation seems to suggest that, dry ice formation that 'consumes' part of the generated vapor would probably decrease the strength of pressure wave and thus reduce the possibility of having an explosion. If no dry ice forms, as in those 7 tests mentioned above, an explosion would be more likely to occur.

When it comes to industrial CO_2 storage, discussion above offers two possible approaches to reduce the risk of a CO_2 explosion during storage or transportation.

First, the safe valve on a storage vessel may be further improved so that if a sudden opening of the vessel occurs, the speed of inner pressure drop is lowered down with further decreased temperature and part of vapor may form dry ice to reduce the strength of pressure wave. If the depressurization process is slow enough, there might be only one leaking point with a 'peaceful' emission of CO_2 vapor into ambient air, instead of an explosion with rupture of the whole vessel and flying fragments.

Second, a more accurate control on the initial pressure/temperature inside the vessel could be applied. Take temperature as the parameter. In Figure 4-31, tests with too high (near or above T_{SL_CO2}, -13.8 °C) or too low initial temperature exploded, while most tests with initial temperature between -22 °C and -17.5 °C (data points near test 7 and test 10) were with no explosions. The saturation pressure for this temperature range is approximately 18 bar to 21 bar. 2 MPa could be an appropriate storage pressure for liquid CO_2 in industry. Further study is required to reduce risk of an explosion.

5 Conclusions

This Chapter summarizes the main conclusions from the experimental work performed on CO_2 BLEVE tests. A brief summary of the work is given in Subsection 5.1 before the main conclusions listed in Subsection 5.2. A few recommendations on future work for further understanding of CO_2 BLEVE issues are described in Subsection 5.3.

5.1 Summary

Experimental work on CO_2 BLEVE studies has been performed in laboratory. The main objective of this work was to construct a functional experimental rig for CO_2 BLEVE experiments and to gain further knowledge on the mechanism and consequences of CO_2 BLEVE by analyzing experimental data.

The experimental rig has been tested with a considerable amount of CO_2 experiments. The rig has been proved to be robust for carrying out fluid BLEVE experiments with a possibility of further modifications.

A total of 21 CO_2 experiments have been carried out on circular, plastic pipes with varying experimental parameters. Pressure signals were primarily used to study pressure waves along time scenarios of a controlled opening or sudden failure of the experimental vessel. Experimental videos offered an additional channel to gain extra insights. Fragments formed in an explosion were analyzed and a simple method based on fragments has been utilized to estimate explosion energy.

A fundamental theory of the mechanism of BLEVE formation, the 'Superheat Limit Temperature' theory has also been discussed and examined with experimental results.

5.2 Main conclusions

Conclusions of this thesis are chosen mainly for practical applications, that is, to reduce the risk during CO_2 storage and transportation. They are listed below in a prioritized order.

1. An experimental rig has been constructed for CO2 BLEVE tests. It is functional and robust and capable to be modified for BLEVE tests with other PLGs.

2. Two possible approaches for a safer CO2 storage include using an initial storage pressure of around 2 MPa and developing a safety valve that can further slow down pressure drop when an unexpected vessel opening and depressurization occurs.

3. A certain amount of two-phase flow splashing out of a storage vessel is required to an explosion. Pressurized liquid CO2 may contribute more to an explosion than vapor CO2. A less quantity of liquid CO2, by lower CO2 filling level in a storage vessel could possibly deter the occurrence of an explosion. On the contrary, an explosion would be favored with a CO2 filling of an overall density of 375 kg/m^3 or higher.

4. The 'Superheat Limit Temperature' theory for predicting occurrence of a BLEVE was not supported with experiments in this work. A CO_2 BLEVE can also occur when the initial temperature is below the superheat limit temperature of CO_2 (-13.8 °C). Nevertheless, considering influencing factors including CO_2 filling level, potential gas leaking and CO_2 mixture with different phase compositions, the theory may still be acceptable. It may also be fine to assume that a higher degree of superheat limit makes it more possible to have an explosion with stronger pressure waves.

5. Kinetic energy of fragments in en explosion could be related to the overall explosion energy for a coarse estimation on potential damages the explosion may lead to.

5.3 Future work

Several recommendations in general for further research are listed below.

1. Liquid CO_2 filling worth to be tried instead of dry ice to better simulate the real industrial CO_2 storage. As for laboratory research, one specific advantage of filling with liquid CO_2 is that the filling level becomes more controllable. Theoretically, a storage vessel for testing can be fully filled with liquid CO_2. It will be interesting to see if an explosion occurs with varying levels of liquid CO_2. Further insights on initial storage conditions and possibility of an explosion could be available.

2. Experimental setup described in this work could be further modified for other purposes. A new set of experimental device and storage vessel of enlarged sizes can upgrade lab-scale experiments into semi-industrial or industrial scale, where conclusions from experimental investigations might be closer to and applied directly to industrial activities.

3. The relationship between bubble nucleation and strength of pressure waves could be further studied. One possibility is to find with experiments more reasonable definitions for 'homogenous' bubble nucleation and 'non-homogenous' nucleation as well as more accurate descriptions on their corresponding consequences.

4. More theoretical study on various models for estimation of explosion energy could be performed in combination with experimental data. A classification of models/theories with suitable experimental circumstances would be of great interest. Besides, implementation and development of existed models with CFD (Computational Fluid Dynamics) and experimental simulation with RCM (Random Choice Method) would bring more insights in BLEVE phenomenon.

References

[1] Tasneem Abbasi, S,A.Abbasi. The boiling liquid expanding vapour explosion (BLEVE): Mechanism, consequence assessment, management. Journal of Hazardous Materials 141 (2007) 489-519.

[2] C.R.Reid et al. Possible mechanisms for pressurized-liquid tank explosions or BLEVEs. Science 203 (1979) 1263-1265.

[3] G.A.Pinhasi et al. 1D plane numerical model for boiling liquid expanding vapor explosion (BLEVE). International Journal of Heat and Mass Transfer 50 (2007) 4780–4795.

[4] R.W.Prugh. Quantify BLEVE Hazards. Chemical Engineering Progress 87 (1991) 66-72.

[5] M.R.Baum. Failure of a horizontal pressure vessel containing a high temperature liquid: the velocity of end-cap and rocket missiles. Journal of Loss Prevention in the Process Industries 12 (1999) 137–145.

Appendices

A: Thermodynamic diagrams of Carbon Dioxide

A Pressure-Temperature diagram and a Pressure-Enthalpy diagram of Carbon Dioxide are given below (Copyright @1999, ChemicaLogic Corporation).
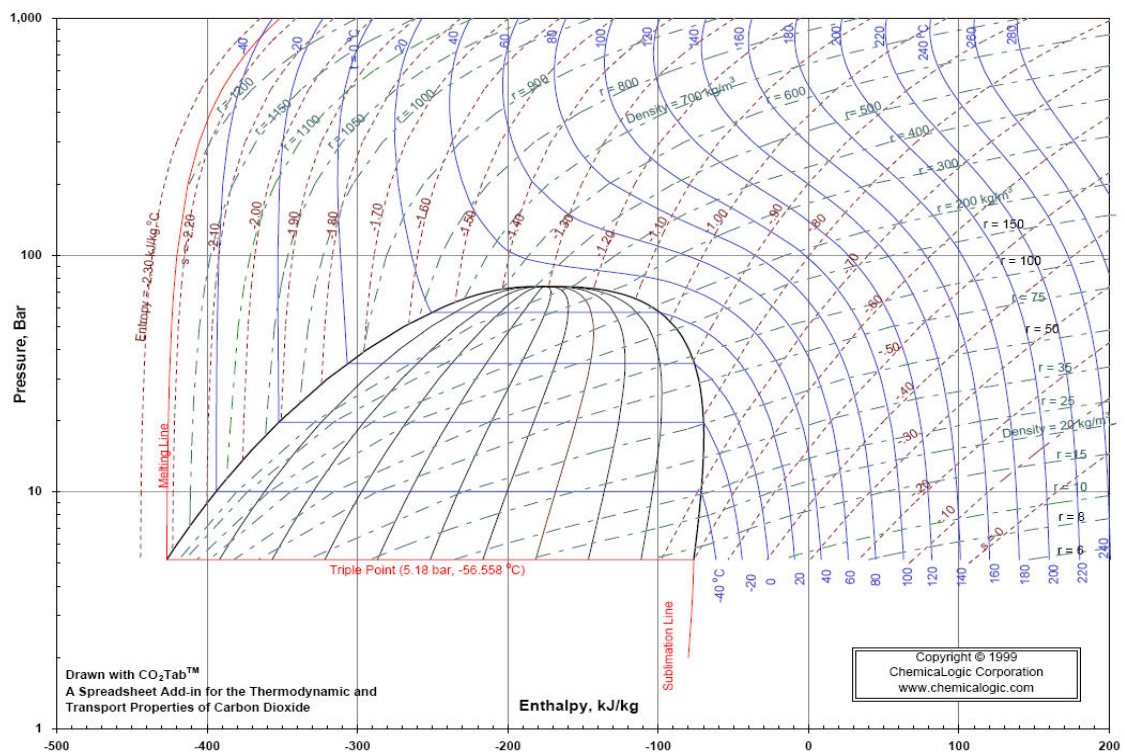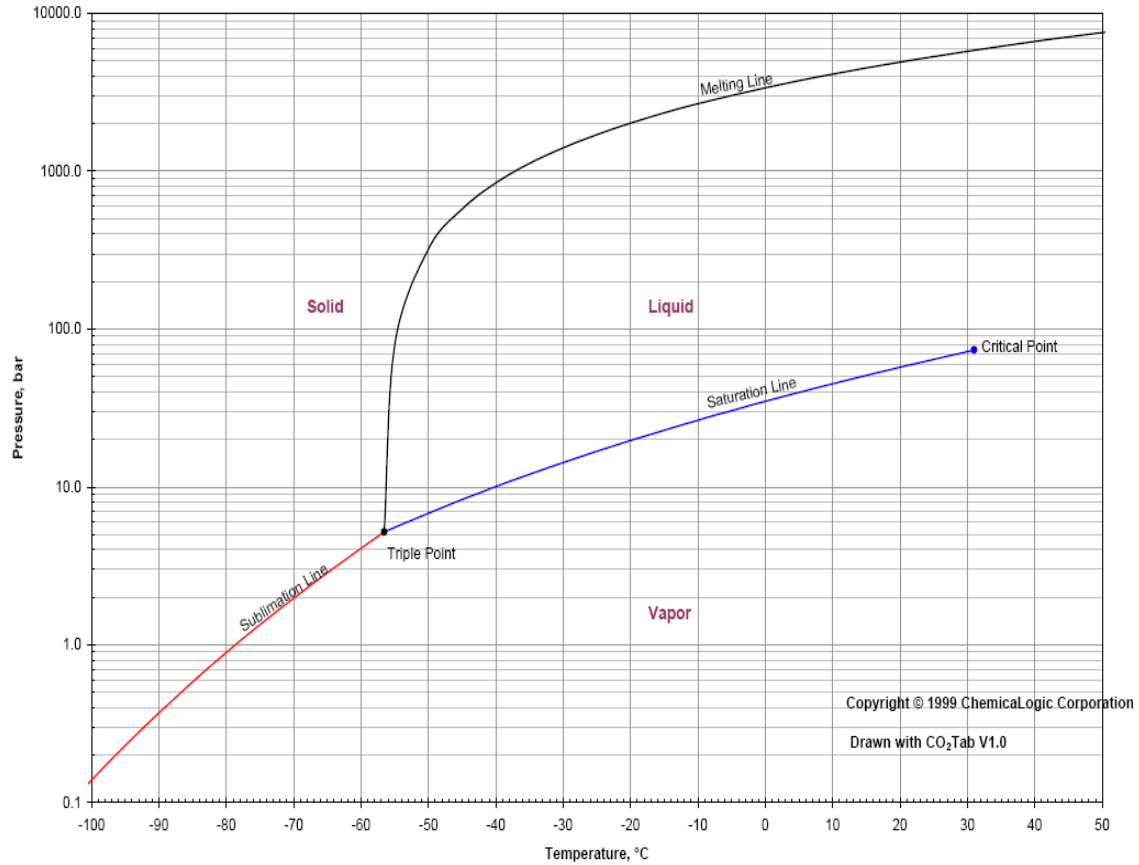
B: A list of major BLEVEs (1926-2004)

An original table summarized by Tasneem Abbasi et al [1] with major BLEVE accidents in history is cited in a full version below. Accidents with CO_2 BLEVE are marked in red.

Date	Location	Cause	Material	Quantity (tonnes)	Death (d), injured (i)
13 December 1926	St. Auban, France	Overfilling	Chlorine	25	19d
28 May 1928	Hamburg, Germany	Runaway	Phosgene	10	11d, 171i
10 May 1929	Syracuse, NY, USA	Explosion (H2)	Chlorine	25	1d
24 December 1939	Zamesti, Romania	Overfilling	Chlorine	10	60d
29 July 1943	Ludwigshafen, Germany	Overfilling	Butadiene	16	57d
5 November 1947	Rauma, Finland	Overfilling	Chlorine	30	19d
28 July 1948	Ludwigshafen, Germany	Overfilling	Ethyl ether	33	209d
7 July 1951	Port Newark, NJ, USA	Fire	Propane (70)	2600	14i
4 April 1952	Walsum, W. Germany	Overfilling	Chlorine	15	7d
4 June 1954	Institute, WV, USA	Runaway	Acrolein	20	–
1955	Ludwigshafen, FRG	Railroad accident	LPG	a	2i
1955	Cottage Grove, OR, USA	Storage vessel failure	LPG	a	12d, 13i
8 January 1957	Montreal, Canada	Fire	Butane	5100	1d
1958	Michigan, USA	Overfilling	Butane	55	1d
28 June 1959	Meldrin, GA, USA	Damage (Derail)	Propane	55	23d
18 August 1959	Kansas City, MO, USA	Fire	Gasoline	70	5d
1959	McKittrick, CA, USA	LPG	Storage cylinder (six on site)	a	2i
17 April 1962	Doe Run, KY, USA	Runaway	Ethylene oxide	25	1d
4 January 1966	Feyzin, France	Fire	Propane	1000	18d, 83i
1 January 1968	Dunreith, IN, USA	Fire (Derail)	Ethylene oxide	NA	5i
21 August 1968	Lieven, France	Mechanical	Ammonia	20	5d
2 January 1969	Repcelak, Hungary	Overfilling	Carbon dioxide	35	9d
25 January 1969	Laurel, MS, USA	Fire (Derail)	Propane	65	2d, 976i
18 February 1969	Crete, NB, USA	Damage (Derail)	Ammonia	65	8d
1969	Cumming, IA, USA	Damage (Derail)	Ammonia	a	a
11 September 1969	Glendora, MS, USA	Fire	Vinyl chloride	55	–
21 June 1970	Crescent City, IL, USA	Fire (Derail)	Propane (5)	275	66i
19 January 1971	Baton Rouge, LA, USA	Overpressure	Ethylene	4	–
19 October 1971	Houston, TX, USA	Fire (Derail)	Vinyl chloride	50	1d, 50i
9 February 1972	Tewksbury, MA, USA	Collision	Propane	28	NA
30 March 1972	Rio de Janeiro, Brazil	Fire	Propane	1000	37d
21 September 1972	NJ Turnpike, NJ, USA	Collision	Propylene	18	2d
27 November 1972	San Antonio, TX, USA	Corrosion	Carbon dioxide	0.01	–
1972	Lynchburg, VA, USA	Propane	Road tanker	9	2d, 5i
1972	Rio de Janeiro, Brazil	LPG	Storage spheres (five on site) and cylinders	a	37d, 53i
5 July 1973	Kingman, AZ, USA	Fire	Propane	100	13d, 95i
11 January 1974	W. St. Paul, MN, USA	Fire	Propane	27	4d
12 February 1974	Oneonta, NY, USA	Fire (Derail)	Propane (4)	288	25i
29 July 1974	Pueblo, CO, USA	Fire (test)	Propane	80	–
29 April 1975	Eagle Pass, TX, USA	Collision	Propane	18	16d
14 December 1975	Niagara Falls, NY, USA	Runaway	Chlorine	20	4d
1975	Des Moines, IA, USA	LPG	Rail tank car	a	3i
11 May 1976	Houston, TX, USA	Collision	Ammonia	20	6d
31 August 1976	Gadsden, AL, USA	Fire	Gasoline	4	3d
1976	Belt, MN, USA	LPG	Rail tank car	80	22i
1977	Cartegna, Columbia	Overpressure	Ammonia	a	30d
1977	Dallas, TX, USA	Isobutene	Rail tank car	a	1i
1977	Goldona, VA, USA	LPG	Rail tank car	70	2d, 9i
22 February 1978	Waverly, TX, USA	Damage (Derail)	Propane	45	16d, 43i
11 July 1978	San Carlos, Spain	Overfilling	Propylene	25	211d
30 May 1978	Texas City, TX, USA	Fire	Butanes (6)	1500	7d, 10i
1978	Donnellson, IA, USA	LPG	Pipeline	435	2d, 2i
30 August 1979	Good Hope, LA, USA	Ship collision	Butane	120	12d
1979	Pazton, TX, USA	Chemicals	Rail tank car	a	8i
1979	Los Angeles, CA, USA	Gasoline	Road tanker	a	2d, 2i
1 August 1981	Montanas, Mexico	Damage (Derail)	Chlorine (2)	110	29d
19 January 1982	Spencer, OK, USA	Overheating	Water	0.3	7d
11 December 1982	Taft, LA, USA	Runaway	Acrolein	250	–
12 July 1983	Reserve, LA, USA	Runaway	Chlorobutadiene	1	3d

Date	Location	Cause	Material	Quantity (tonnes)	Death (d), injured (i)
4 October 1983	Houston, TX, USA	Overfilling	Methyl bromide	28	2d
19 November 1984	Mexico City, Mexico	Fire	Propane (20)	3000	650d, 6400i
1984	Romeoville, IL, USA	Propane	Process vessel	a	15d, 22i
28 January 1986	Kennedy Space Center, FL, USA	Fire	Hydrogen	115	7d
1 April 1990	Boral LPG distribution depot, Sydney, Australia	Fire	LPG	>240	35,000 affected
1 April 1990	Cairns gas terminal, Queensland, Australia	Fire	LPG	a	1d
28 August 1992	Japan	Damage	Nitrogen	a	$5 million loss
August 1993	Panipat, India	Pressure build-up	Ammonia	a	6d, 25i
19 April 1993	Waco, TX, USA	Fire	LPG	a	–
27 June 1993	Quebec, Canada	Fire	Propane	2.3	4d, 7i
4 March 1996	Weyauwega, WI, USA	Derailment	Propane, LPG	a	–
18 March 1996	Palermo, Italy	Collision in a highway tunnel	Propane	a	5d, 25i
2 October 1997	Burnside, IL, USA	Fire	LPG	3.8	2d, 2i
9 April 1998	Alberta City, IA, USA	Fire	Propane	40	2d, 7i
30 April 1999	Between Athens and Lamia, Greece	Traffic accident	LPG	a	4d, 13i
23 September 1999	Toronto, Canada	Derailment	LPG	>60	–
30 December 1999	Quebec, Canada	Derailment, collision	Hydrocarbons	2700	2i, 350 evac.
27 May 2000	Eunice, LA, USA	Derailment	Flammable PLGs	a	2000 evac.
19 July 2000	Ohio, USA	Overfilling	Propane	66	3i
7 January 2001	Kanpur, India	Highway accident	LPG	a	12d, 6i
20 October 2000	Downey, CA, USA	Leak	Propane	2	2d
22 October 2000	Texas, USA	Improper unloading	Propane	17	2d
1 July 2001	Jamnagar, India	Damage	LPG	*	12d
20 February 2002	Cairo, Egypt	Fire caused in a passenger train by a butane tank BLEVE	Butane	*	373d, 7500i
22 June 2002	Tivissa, Spain	Overturned	LNG	48 m^3	1d, 2i
25 June 2002	Gronton, CT, USA	Overheating	Borane-tetrahydrofuran	0.1	2i
11 April 2003	Louisville, USA	Overheating	Maltodextrin and other chemicals	*	1d
13 January 2004	Baltimore, Washington Highway, USA	Traffic accident	Propane	*	10d
19 January 2004	Skikida, Algeria	Explosion	LNG	*	13d, 74i
9 August 2004	Mihama, Japan	Steam pipe depressurization	Steam	*	4d, 7i

[a] Information not available.

C: Methods of estimating explosion energy

An original table summarizing methods of explosion energy estimation by Tasneem Abbasi et al [1] is given in a full version as below.

Methods of estimating BLEVE explosion energy

Identification of the method	Basis of the method	The key expressions	Explosion energy estimates relative to Prugh's method (kJ)	Reference
Prugh's method or the TNT equivalent method	(1) Assumes that the flashing fraction of the liquid and the pressurized gas expand isentropically as an ideal gas in a BLEVE; (2) equates the work done by the expanding vapour with a charge of TNT; (3) Works out the explosion energy, W_{TNT}, as if it is caused by that charge of TNT	$W_{TNT} = \dfrac{2.4 \times 10^{-4} PV^*}{k-1}\left[1 - \left[\dfrac{10.1}{P}\right]^{(k-1)/k}\right]$ where $V^* = V_T + W_L\left[\dfrac{f}{D_{V,T}} - \dfrac{1}{D_{L,T}}\right]$, $f = 1 - \exp\left[-\Omega\dfrac{C}{L}(T_c - T_b)\right]$. $\Omega = 2.63\left(1 - \left[\dfrac{T_c - T_0}{T_c - T_b}\right]^{0.38}\right)$	If the burst energy of a vessel filled with propane is 1 KJ as per Prugh's method, according to other methods it is:	Prugh [16]
SVEE (specific volume, entropy and enthalpy) method	(1) Does not assume ideal gas behavior; (2) assumes isentropic expansion; (3) explosion energy, e_{ex}. is computed from the difference in internal energy of the expanding gas between its initial and the final stage of expansion	$e_{ex} = m_{f1}u_{f1} - m_{f2}u_{f2} + m_{g1}u_{g1} - m_{g2}u_{g2}$ where $m_{f2} = (1 - X_f)m_{f1} + (1 - X_g)m_{g1}. \ m_{g2} = X_f m_{f1} + X_g m_{g1}.$ $u_{f1} = h_{f1} - p_1 v_{f1}, \ u_{g1} = h_{g1} - p_1 v_{g1}, \ u_{f2} = h_{f2} - p_a v_{f2}.$ $u_{g2} = h_{g2} - p_a v_{g2}. \ X_g = \left(\dfrac{s_{g1} - s_{f2}}{s_{g2} - s_{f2}}\right). \ X_f = \left(\dfrac{s_{f1} - s_{f2}}{s_{g2} - s_{f2}}\right)$	1.1	CCPS [8] and TNO [73]
Irreversible adiabatic expansion method of Planas-Cuchi et al.	(1) Does not assume ideal gas behavior; (2) expansion is considered to be an adiabatic, irreversible process; (3) the change in internal energy due to the adiabatic irreversible expansion is equated to the work done by the fluid expanding at constant atmospheric pressure. The expressions for both are solved for getting x, the vapour fraction at the final state of the expansion process. This is then substituted in the expression for change in internal energy; (4) from the change in internal energy, the TNT equivalent mass is calculated	$e_{ex} = -\Delta U = P_0 \Delta V$ where $\Delta U = (u_L - u_G)m_T x + m_T u_L + U_l,$ $P_0 \Delta V = P_0[(v_G - v_L)m_T x + m_T v_L - V_l].$ $x = \dfrac{m_T P_0 v_L - V_l P_0 + m_T u_L - U_l}{m_T[(u_L - u_G) - (v_G - v_L)P_0]},$ $W_{TNT}\ (kg) = 2.14 \times 10^{-7} \times \beta \times \Delta U$	0.4	Planas-Cuchi et al. [59]

C: Average specific heat of the liquid over temperature interval T_0 to T_b (J/kg K); f: Fraction of liquid flashing into vapour (no unit); h_{f1}: Enthalpy of the liquid at the initial state (J/kg); h_{f2}: Enthalpy of the liquid at the final state (J/kg); h_{g1}: Enthalpy of the vapour at the initial state (J/kg); h_{g2}: Enthalpy of the vapour at the final state (J/kg); k: Ratio of specific heats at constant pressure and constant volume (no unit); L: Average latent heat of vaporization over temperature interval T_0 to T_b (J/kg); m_{f1}: Mass of the liquid at the initial state (kg); m_{f2}: Mass of the liquid at the final state (kg); m_{g1}: Mass of the vapour at the initial state (kg); m_{g2}: Mass of the vapour at the final state (kg); m_T: Total mass of the vessel contents (kg); P: Pressure in the vessel at the time of burst (KPa); p_1: Pressure in the vessel at the time of burst (Pa); P_0, p_a: Atmospheric pressure (Pa); s_{f1}: Entropy of the liquid at the initial state (J/kg K); s_{f2}: Entropy of the vapour at the initial state (J/kg K); s_{g1}: Internal energy of the vessel contents (K); s_{g2}: Entropy of the vapour at the initial state (J/kg K); u_{f1}: Internal energy of the liquid at initial state (J/kg); U_l: Initial temperature of the vessel contents (K); u_{f1}: Internal energy of the liquid at initial state (J/kg); u_{f2}: Internal energy of the liquid at the final state (J/kg); u_{g1}: Internal energy of the vapour at the initial state (J/kg); u_{g2}, u_G: Internal energy of the vapour at the final state (J/kg); v_{f1}: Specific volume of the liquid at initial state (m³/kg); v_{g1}: Specific volume of the vapour at the final state (m³/kg); v_{f2}: Fraction of liquid flashing into vapour (kg); X_f: Fraction of liquid flashing into vapour; X_g: Fraction of vapour condensing into liquid; V: Total vapour volume (m³); v_G: Specific volume of the vapour at the initial state (m³/kg); v_{g2}, v_G: Specific volume of the vapour at the final state (m³/kg); V_l, V_T: Volume of the vessel (m³); W_L: Mass of liquid in the vessel (kg); W_{TNT}: Equivalent mass of TNT of the explosion energy (kg); X_f: Fraction of liquid flashing into vapour; X_g: Fraction of vapour condensing into liquid; β: Fraction of explosion energy converted into a pressure wave; ΔU: Change in internal energy (J); ΔV: Change in volume (m³); Ω: Correction for flash fraction f.

Note: Initial state: At the instant of explosion. Final state: After explosion.

D: Technical information of selected devices

Sub-appendices on selected devices with more technical information.

D.1 Bosch Rexroth 5/3 –way valve, Series RA 14

Directional valves → Electrically operated

5/3-way valve, Series RA14

Qn = 1200 l/min; pipe connection; compressed air connection output: G 1/4; Electr. connection: Plug, ISO 6952, form B; Can be assembled into blocks; ATEX optional

Version	Spool valve, zero overlap
Pilot	internal
Sealing principle	soft sealing
Blocking principle	Single base plate principle
Mounting on manifold strip	P-strip / PRS strip
Ambient temperature min./max.	+0°C / +50°C
Medium temperature min./max.	-10°C / +50°C
Medium	Compressed air
Particle size max.	5 μm
Oil content of compressed air	0 mg/m³ - 5 mg/m³
Connector standard	ISO 6952
Duty cycle	100 %
Materials:	
Housing	Polyamide
Seals	Acrylonitrile Butadiene Rubber
Front plate	Polyamide
Threaded bushing	Brass
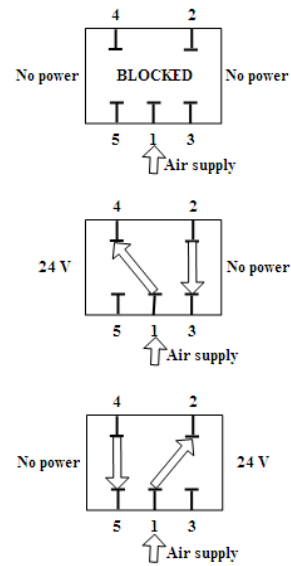
Operating voltage			Voltage tolerance			Power con-sumption	Switch-on power		Holding power	
DC	AC 50 Hz	AC 60 Hz	DC	AC 50 Hz	AC 60 Hz	DC	AC 50 Hz	AC 60 Hz	AC 50 Hz	AC 60 Hz
						W	VA	VA	VA	VA
-	24 V	24 V	-	-10% / +10%	-10% / +10%	-	12	9.9	8.5	7.3
24 V	-	-	-10% / +10%	-	-	4.8	-	-	-	-
24 V	-	-	-10% / +10%	-	-	2.6	-	-	-	-
-	110 V	110 V	-	-10% / +10%	-10% / +10%	-	11	9.4	8.5	6.9
-	230 V	230 V	-	-10% / +10%	-10% / +10%	-	11	9.4	8.5	6.9

Dimensions
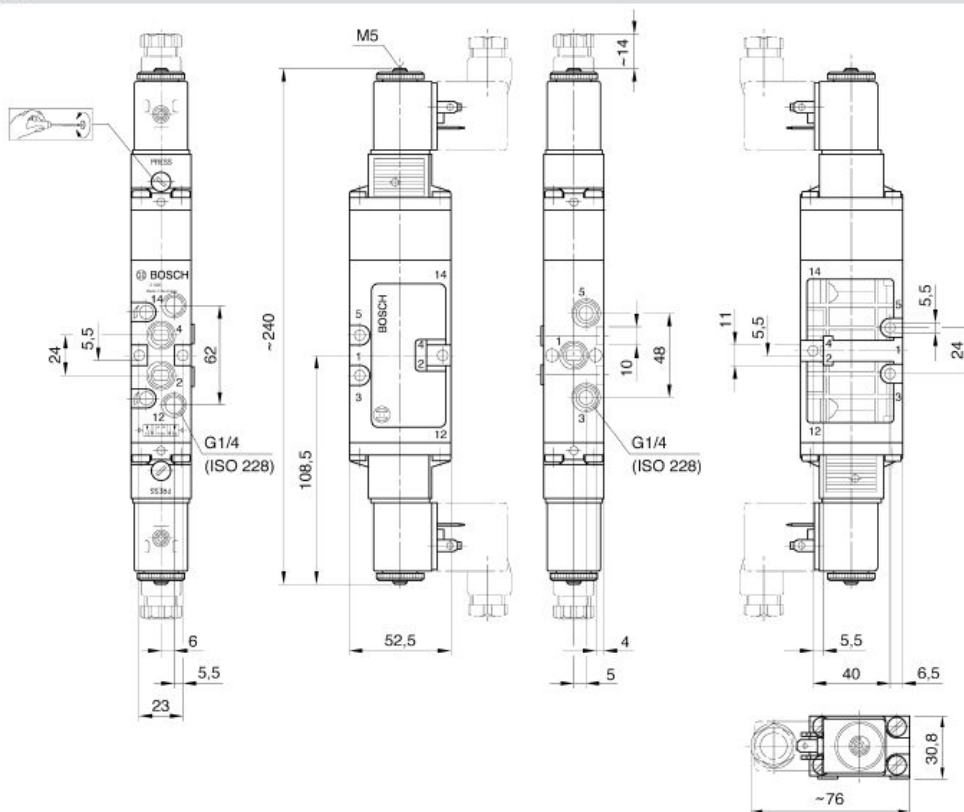
D.2 Bosch Rexroth Series 167 Tie rod cylinder

Piston rod cylinders → Tie rod cylinders

● Series 167

Ø 25 - 320 mm; Ports: G 1/2 - G 1; double-acting; with magnetic piston; cushioning: pneumatic, adjustable; piston rod: external thread

Standards	ISO 15552
Compressed air connection	internal thread
Working pressure min./max.	1.5 bar / 10 bar
Ambient temperature min./max.	-20°C / +75°C
Medium temperature min./max.	-20°C / +75°C
Medium	Compressed air
Particle size max.	50 µm
Oil content of compressed air	0 mg/m³ - 5 mg/m³
Pressure for determining piston forces	6 bar

Materials:

Cylinder tube	Aluminum, anodized
Front cover	Aluminum
End cover	Aluminum
Seal	Acrylonitrile Butadiene Rubber

Piston Ø		[mm]	80
Retracting piston force		[N]	2720
Extending piston force		[N]	3000
Cushioning length		[mm]	19.5
Weight	0 mm stroke	[kg]	2.5
	+10 mm stroke	[kg]	0.072
Stroke max.		[mm]	1700

Dimensions
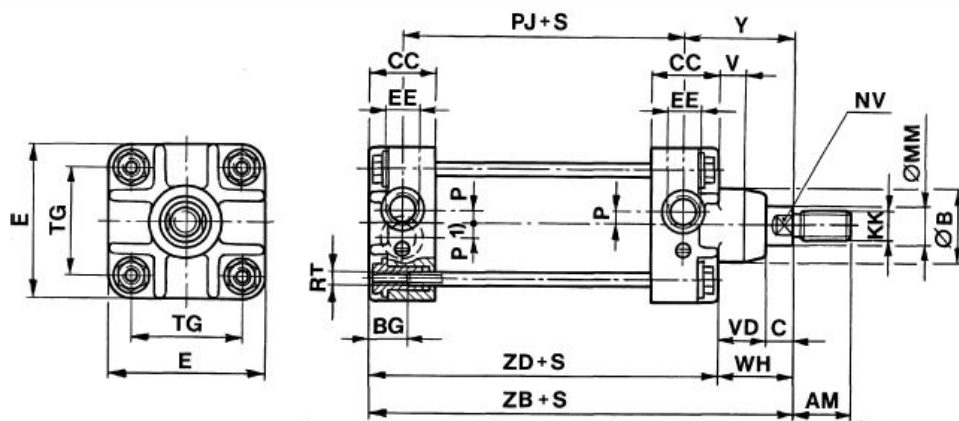
S = stroke
P 1) = for cylinder Ø 250 and 320 mm

Piston Ø	AM	Ø B h12	BG	C	CC	E	EE	KK	Ø MM	NV	P	PJ	RT
80	40	48	19	16	36,0	95	G 3/8	M20x1,5	25	22	9	86	M8

Piston Ø	TG	TS 1)	V	VD	WH	Y	ZB	ZD
80	73	+2,5/–0	8	32	48	67	172 ±1,4	124

D.3 Beru GN857 glow plug

SR-Set 028	0 120 000 028	GN 857 x 4	**Audi** 80 diesel −7.91** Volkswagen Golf/Jetta/Passat/Bus diesel 7.91** On 5/6 cylinder models add 1 or 2 GN 857

GN 857

0 100 226 173

BERUPARTS.com

Connection stud
Round nut
Insulating washer
O-ring seal
Plug body

Seal

Installation thread

Annular gap

Glow tube

Regulating filament
Insulating filling

Heating filament

Pre-heating 2–5 Secs.
Startglow approx. 2 Secs.
Post-heating approx. 300 Secs.
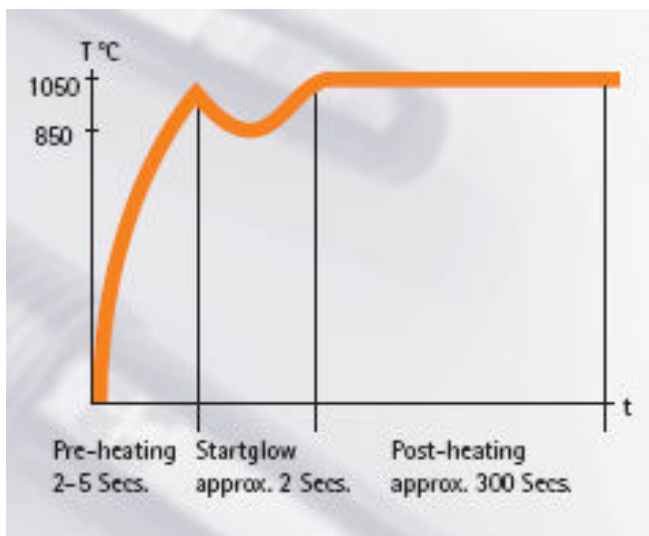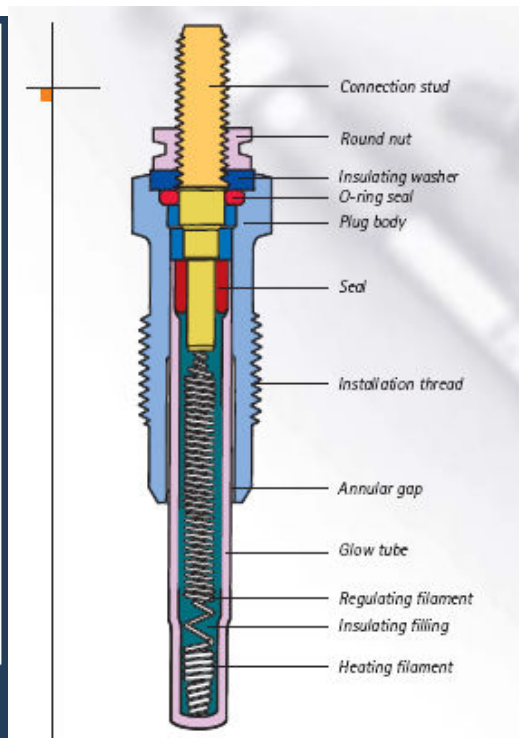
www.beru.com

D.4 Kulite XT-190 (M) Pressure transducer

kulite®

MINIATURE RUGGEDIZED
IS® PRESSURE TRANSDUCER
XT-190 (M) SERIES
- Easy Installation
- High Natural Frequency

The ruggedness of this sensor has not compromised its performance. It was designed for ease of installation.

OPTIONAL CONNECTOR VERSION

.250 MAX. (6.4)

CONNECTOR

NOT AVAILABLE ON DIFFERENTIAL UNIT

CABLE STRAIN RELIEF
PRESSURE REFERENCE TUBE .016 X 1" LONG (.4 X 25.4) FOR PSIG & PSID UNITS
.190 (4.9)
.40 (10.2)
.17 (4.3)
"L"
3/8 HEX (9.5)
THREAD "T"
O – RING .176 I.D. X .040 C.S. (4.5 I.D. X 1.0 C.S.)
HEX PROFILE AFTER CRIMPING
TEMP. COMP. MODULE
4 COND. # 30 AWG SHIELDED CABLE 30" (762) LONG
B SCREEN STANDARD M SCREEN OPTIONAL

CONSULT FACTORY FOR SPECS. ON SEALED GAGE

P/N	"T"		"L"	
190	10-32 UNF-2A	.437	11.1 mm	
190M	M5 X .8	.437	11.1 mm	
190	10-32 UNF-2A	.760	19.3 mm	
190M	M5 X .8	.760	19.3 mm	

WIRING	
COLOR	DESIGNATION
RED	+ INPUT
BLACK	– INPUT
GREEN	+ OUTPUT
WHITE	– OUTPUT

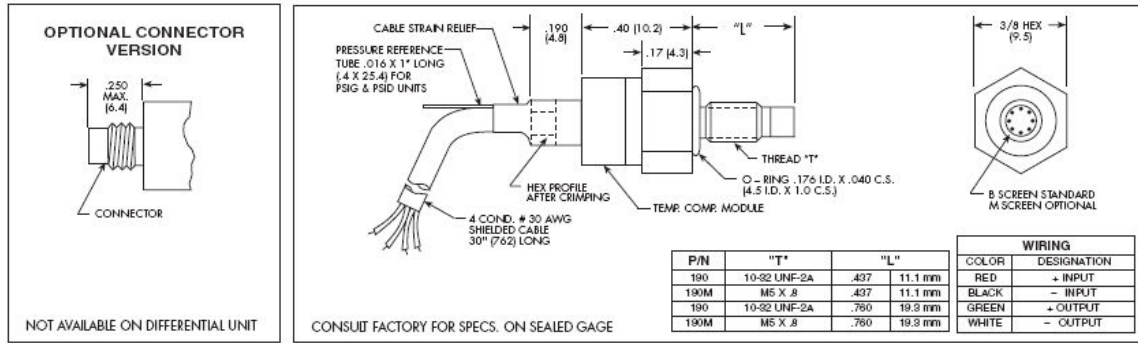| INPUT Pressure Range	0.35 / 5	0.7 / 10	1.7 / 25	3.5 / 50	7 / 100	17 / 250	35 / 500	70 / 1000	140 BAR / 2000 PSI
Operational Mode	Absolute, Gage, Sealed Gage, Differential					Absolute, Sealed Gage			
Over Pressure	2 Times Rated Pressure to a Maximum of 3000 PSI (210 BAR)								
Burst Pressure	3 Times Rated Pressure to a Maximum of 5000 PSI (350 BAR)								
Pressure Media	All Nonconductive, Noncorrosive Liquids or Gases								
Rated Electrical Excitation	10 VDC/AC								
Maximum Electrical Excitation	15 VDC/AC								
Input Impedance	1000 Ohms (Min.)								
OUTPUT Output Impedance	1000 Ohms (Nom.)								
Full Scale Output (FSO)	100 mV (Nom.)								
Residual Unbalance	± 5 mV (Typ.)								
Combined Non-Linearity, Hysteresis and Repeatability	± 0.1% FSO BFSL (Typ.), ± 0.5% FSO (Max.)								
Resolution	Infinitesimal								
Natural Frequency (KHz) (Typ.)	150	175	240	300	380	550	700	1000	1400
Acceleration Sensitivity % FS/g Perpendicular Transverse	1.5×10^{-3} 2.2×10^{-4}	1.0×10^{-3} 1.4×10^{-4}	5.0×10^{-4} 6.0×10^{-5}	3.0×10^{-4} 4.0×10^{-5}	1.5×10^{-4} 2.0×10^{-5}	1.0×10^{-4} 9.0×10^{-6}	6.0×10^{-5} 6.0×10^{-6}	4.5×10^{-5} 3.0×10^{-6}	2.0×10^{-5} 2.0×10^{-6}
Insulation Resistance	100 Megohm Min. @ 50 VDC								
ENVIRONMENTAL Operating Temperature Range	-65°F to +350°F (-55°C to +175°C)								
Compensated Temperature Range	+80°F to +180°F (+25°C to +80°C) Any 100°F Range Within The Operating Range on Request								
Thermal Zero Shift	± 1% FS/100°F (Typ.)								
Thermal Sensitivity Shift	± 1% /100°F (Typ.)								
Steady Acceleration	10,000g. (Max.)								
Linear Vibration	10-2,000 Hz Sine, 100g. (Max.)								
PHYSICAL Electrical Connection	4 Conductor 30 AWG Shielded Cable 30" Long								
Weight	4 Grams (Nom.) Excluding Cable								
Pressure Sensing Principle	Fully Active Four Arm Wheatstone Bridge Dielectrically Isolated Silicon on Silicon								
Mounting Torque	15 Inch-Pounds (Max.) 1.7 N-m								

Note: Custom pressure ranges, accuracies and mechanical configurations available. Dimensions are in inches. Dimensions in parenthesis are in millimeters. Continuous development and refinement of our products may result in specification changes without notice - all dimensions nominal. (C)

KULITE SEMICONDUCTOR PRODUCTS, INC. • One Willow Tree Road • Leonia, New Jersey 07605 • Tel: 201 461-0900 • Fax: 201 461-0990 • http://www.kulite.com

The Specific Model No. of the pressure transducer in the experiments with this work is XT-190-500 SG. Rated pressure: 500 psi (35 bar). Maximum pressure: 750 psi (50 bar). 10V excitation. Sensitivity: 0.200 mV/psi.

D.5   Nicolet Sigma 90 Transient Oscilloscope

Sigma Models

	Number of Channels	Resolution	Maximum Sample Rate	Accuracy	Bandwidth	Input Filter Stages	Input Amplifier Type	Input Range	Number of Timebases
SIGMA 30	4	12-bit	10 MS/s	0.25%	5 MHz	500 kHz	Single ended, switchable to 2 ch diff	5 mV–20 V/div	1
SIGMA 60-4	4	8-bit*	200 MS/s	1%	200 MHz	20 MHz, 1MHz	Single ended	2 mV–5 V/div	1
		10-bit*	2 MS/s	0.5%	870 kHz	870 kHz			
SIGMA 75-8	8	8-bit	100 MS/s	0.25%	25 MHz	5MHz, 500 kHz	Single ended, switchable to 4 ch diff	5 mV–20 V/div	1
SIGMA 90	4,8	12-bit*	10 MS/s	0.25%	5 MHz	500 kHz	Single ended switchable to 2 or 4 ch diff	5 mV–20 V/div	1,2**
		8-bit*	100 MS/s	0.25%	25 MHz	5 MHz, 500 kHz			
SIGMA 100 and 100HV	4,8	12-bit*	100 MS/s	0.25%	25 MHz	5 MHz 500 kHz	Single ended, switchable to 2 or 4 ch diff	5 mV–20 V/div	1,2**
		14-bit*	1 MS/s	0.25%	435 kHz	435 kHz			

*Software selectable

An introduction of this type of oscilloscope is available online at http://www.lb-acoustics.at/lb-acoustics_en/Downloadzone/sigma_serie.pdf

D.6   Photron FASTCAM SA1 high-speed camera with NIKON lens

Photron *FASTCAM-SA1*   **Nikon 50mm f/1.2**

Frame rate / resolution table:
Variable frame rate steps 64 x 16

Vertical resolution

		1024	896	768	640	512	384	256	128	112	96	80	64	32	16
Horizontal resolution	1024	5,400	6,250	7,500	9,000	10,800	15,000	22,500	45,000	50,000	54,000	67,500	86,400	150,000	270,000
	896	6,250	7,500	8,000	10,000	12,500	16,000	25,000	50,000	54,000	62,500	75,000	93,750	150,000	270,000
	768	7,500	8,000	10,000	12,000	15,000	20,000	28,800	54,000	62,500	75,000	86,400	108,000	180,000	300,000
	640	8,000	10,000	10,800	13,500	16,000	22,500	30,000	62,500	75,000	86,400	100,000	120,000	216,000	300,000
	512	10,000	12,000	13,500	16,000	20,000	27,000	40,000	75,000	86,400	100,000	120,000	144,000	250,000	400,000
	384	12,500	15,000	16,000	20,000	25,000	33,750	50,000	90,000	108,000	125,000	144,000	150,000	270,000	450,000
	256	16,000	20,000	22,500	27,000	30,000	45,000	67,500	125,000	135,000	150,000	180,000	216,000	360,000	500,000
	128	27,000	30,000	36,000	40,000	50,000	67,500	100,000	180,000	200,000	225,000	250,000	300,000	450,000	600,000
	64	36,000	40,000	48,000	54,000	67,500	90,000	125,000	225,000	250,000	270,000	300,000	360,000	500,000	675,000

|	
Data Acquisition	Supports Photron MCDL
Cooling	Actively cooled
Operating Temperature	0-40 degrees C
Mounting	1x ¼-20 UNC, 1x 3/8-16 UNC, 6x M6
Dimensions and Weight	286mm L x 156mm W x 191mm H, weight 6.3kg
Power requirements	100V - 240V AC ~ 1.5A, 50-60Hz optional DC operation 18-36 VDC, 90VA

www.photron.com

D.7 Quantum Composers Series 9500 Pulse Generator

Counter Architecture Overview
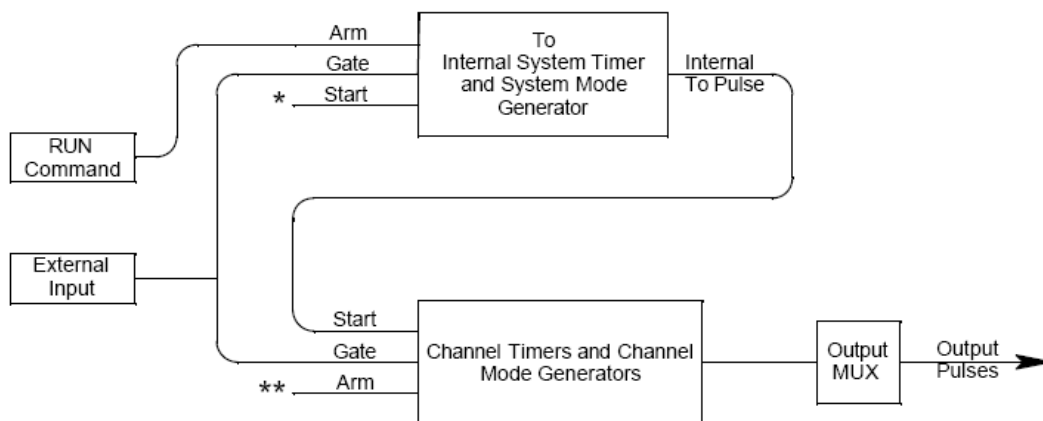
*Start source is: RUN button in Internal Modes
External input in External Trigger modes
*TRG command via Serial/GPIB access

**Channels are armed by the RUN button. In single shot and burst modes channels may be rearmed by pressing the RUN button.

GENERAL

STORAGE	2 channel	4 channel	8 channel
	12	12	12
DIMENSIONS	10.5" x 8.25" x 5.5"		
WEIGHT	8 lbs		
POWER	20 Watts		
	100 - 240 VAC		
	47 - 63 Hz		
	<1 A		
FUSE	(Qty 2) 630 mA, 250 V Time-lag		

PULSE GENERATION

CHANNELS	2, 4 or 8 independent outputs, with digitally controlled delay and pulsewidth
MODES	normal, single, shot, burst, duty cycle
MULTIPLEXER	combine any of the channels
DELAY	0 - 1000 sec
PULSEWIDTH	10 ns - 1000 sec
RESOLUTION	1 ns
ACCURACY	1 ns + .0001 x setpoint
TIMEBASE	50 MHZ
RMS Jitter	< 250 ps
BURST MODE	1 - 1,000,000 pulses

EXTERNAL TRIG / GATE

RATE	DC -5 MHz
THRESHOLD	200 mV - 15 V
INPUT RANGE	0 - 30 V
TRIGGER SLOPE	rising or falling edge
RMS JITTER	< 5 ns
INSERTION DELAY	< 150 ns

OUTPUTS

IMPEDANCE	50 Ohms
RISE TIME	3ns typ TTL
	15ns typ @ 20V (high imp) Adj
	25 ns typ @ 10V (50 ohms) Adj
SLEW RATE	>.5 V/ns TTL
	>0.1 V/ns Adj
OVERSHOOT	< 100 mV + 10% of pulse amplitude

'External trigger' MODE was applied in experiments with this work.

E: HAZOP Study

This appendix offers a report of HAZOP study to our experimental rig where CO_2 experiments have been performed. Subsection E.1 gives an overview on why a HAZOP Study is necessary. Mandatory protections are described in Subsection E.2 that every experimental operator or visitor to the laboratory should obey with no exceptions. Subsection E.3 is a HAZOP report with selected experimental devices.

E.1 Overview

Hazard and operability study (commonly known as HAZOP) was initially issued as a methodology to identify and deal with potential problems in industrial processes, especially those that can bring about hazards to the working environment or working people or a serious damage to the whole process. It is said that HAZOP study is now the most widely used method for hazard analysis.

Potential hazards did exist. Most obviously, the CO_2 BLEVE tests as designed and performed in this thesis work were expected to bring about pressure waves and/or plastic fragments of high speed. Both of the pressure waves and the flying fragments may cause potential damage to the working environment as well as experimental operators. Before any real CO_2 BLEVE tests were performed in laboratory, three questions as following need to be answered.

a) What kinds of potential hazards to the working environment or experimental operators?

b) Which causes may lead to these potential dangers? And,

c) How could they be prevented?

This report of HAZOP Study has applied the methodology of HAZOP to the experimental rig and experimental procedures as described in details in Chapter 3. The purpose was to locate potential hazards during experiments, find out ways of prevention of these hazards as well as ways of protection to experimental operators and to reduce experimental risks as much as possible.

E.2   Mandatory Protections

Before a HAZOP STUDY for selected experimental devices, a MANDATORY set of protection gears for all experimental operators and/or lab visitors should be prepared and used. A pair of eye glasses and a pair of earphones as shown in Figure E-1 are default protection gear for everyone in the laboratory. They will no more be mentioned when it comes to detailed HAZOP Study in Subsection E.3, unless for a speical emphasis.

Figure E-1: A mandatory gear set for protection of experimental operators/lab visitors.

Due to the extremely low temperature of dry ice (-78.5 °C), a pair of gloves with fine heat insulation is an important protection for hands when handling dry ice, cutting, weighing and placing it into the experimental pipe, as shown in Figure E-2.
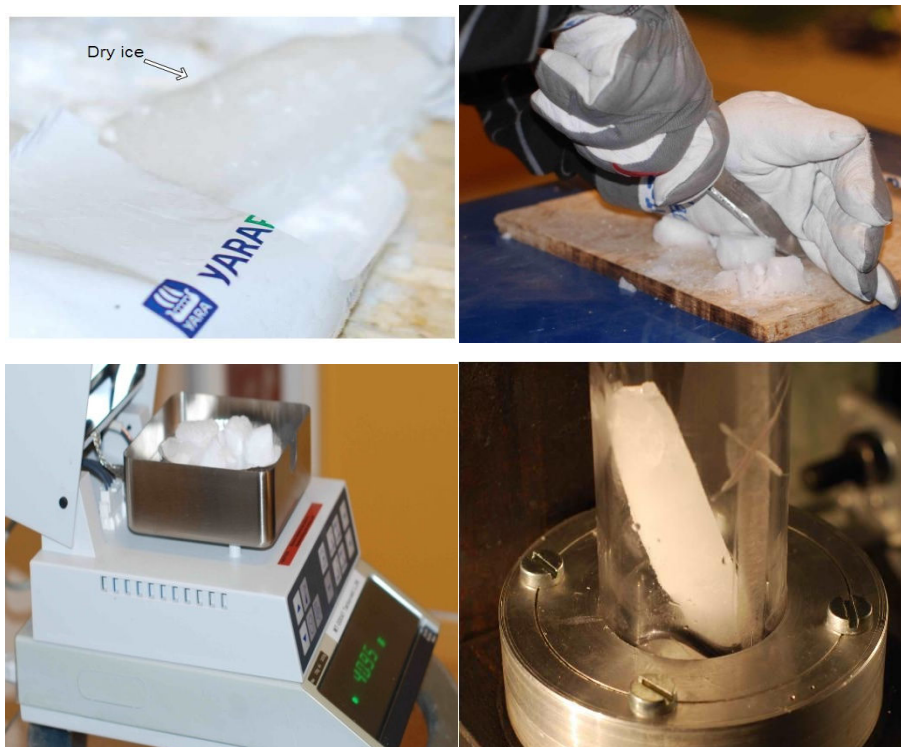
Figure E-2: Dry ice handling. Top left: Dry ice purchased from Yara International ASA, Norway. Top right: Cutting dry ice wearing a pair of gloves with fine heat insulation. Bottom left: Weighing dry ice in an electronic scale. Bottom right: Placing dry ice into the experimental pipe.

Another MANDATORY protection for all experimental operators and/or lab visitors is the 'Safe Zone' where they can protect themselves from pressure waves or flying fragments during experiments. The 'Safe Zone' in our experiments is established by separating people from the experimental center with a strong plastic wall of about 2 m * 2 m, as shown in Figure E-3. When experimental setup is ready with device parameters set and dry ice filled into the experimental pipe, every person in the laboratory should stand within the 'Safe Zone'.

Figure E-3: 'Safe Zone' during experiments.

E.3 HAZOP Study of selected devices

An instrumental diagram of experimental rig as Figure E-4 offers an overall picture of experimental units involved.
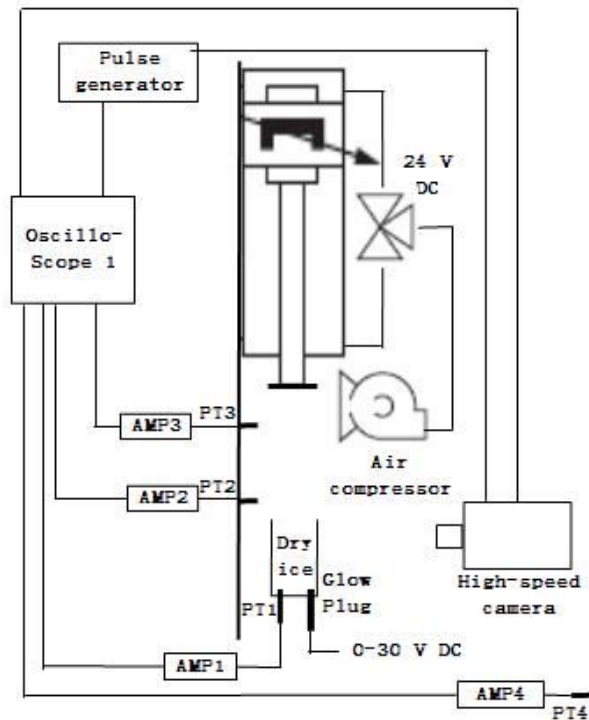
Figure E-4: Instrumental diagram of experimental rig.

Experimental devices analyzed include:

1. Compressor 1 & Compressor 2.
2. 5/3 Pneumatic valve.
3. Air Cylinder.
4. Gasket between the piston and the exprimental pipe.
5. Experimental pipe.

Parameters applied to these study objectives normally include: Flow, Pressure, Temperature, Voltage, Current, Level, Time, Agitation, Reaction, Start-up / Shut-down, Draining / Venting, Inertising, Utility, Instrument air / power failure, DCS failure, Maintenance and Vibrations.

The current standard GUIDE WORDS and their meaning are given in Table E-1.

Table E-1: HAZOP guide words.

Guide Word	Meaning
NONE	Complete negation of the design intent
MORE	Quantitative increase
LESS	Quantitative decrease
AS WELL AS	Qualitative modification / increase
PART OF	Qualitative modification / decrease
REVERSE	Logical opposite of the design intent
OTHER THAN	Complete substitution
EARLY	Relative to the clock time
LATE	Relative to the clock time
BEFORE	Relating to order or sequence
AFTER	Relating to order or sequence

HAZOP Study and Protection approaches for individual devices are described.

1. Compressor 1 & Compressor 2

Main parameters and usage of these two air compressors are listed in Table E-2.

Table E-2: Compressor 1 and Compressor 2.

Compressor No.	Used in	Outlet pressure applied [bar]	Maximum outlet pressure [bar]
1	Tests 1-20 (SET 1)	4	8
2	Test 21 (SET 2)	10	16

FUNCTION: Both compressors aimed to generate pressurized air through the pneumatic valve to air cylinder and to control the movement of the piston in air cylinder.

NOTE: Parameters applicable for the device/devices are chosen and always listed in CAPITAL letters in a HAZOP table as 'PRESSURE' in Table E-3 for compressors. Guide words chosen are always listed in CAPITAL letters in the first row. Consequence and Cause are listed below parameters. Same rules apply to other HAZOP tables of other experimental devices.

Table E-3. HAZOP for Compressor 1 & Compressor 2.

	MORE	LESS	NONE	OTHER THAN
<PRESSURE>	High pressure	Low Pressure	Vacuum	Explosion
Consequence	Higher static pressure in air cylinder	Lower static pressure in air cylinder	Initial state, with 1 atm inside air cylinder	Compressor fails; potential damage to people or devices nearby with high pressure air flow
Cause	Outlet increased	Outlet decreased	No outlet	Breakage on compressor with high inner pressure

HAZOP includes:

1) With an outlet pressure of 4 bar and a maximum of 8 bar for Compressor 1 both within the maximum pressure of the air cylinder (10 bar) and the air tank (10 bar), the only hazard Compressor 1 could possibly bring is the pressurized air flow of 4 bar bursting out that may hurt experimental operators.

2) When using Compressor 2, besides the potential damage of pressurized air flow of 10 bar, with a maximum outlet pressure of 16 bar for Compressor 2, another potential damage will occur if the outlet pressure applied to the air tank and air cylinder is wrongly adjusted to be more than 10 bar. This might cause failure of the air tank and/or the air cylinder that would lead to catastrophic accidents.

Protection approaches include:

1) Operators should wear a pair of thick gloves to protect hands from pressurized air flow when disconnecting pipes from air compressors.

2) Never adjust the outlet pressure of Compressor 2 to be more than 10 bar.

2. 5/3 Pneumatic valve

FUNCTION: Driven by 24 V voltage at either side and a minimum pneumatic pressure of around 4 bar (tested), the Rexroth 5/3 way directional valve could redirect the high pressure air flow from air compressor to an opposite cylinder inlet / outlet, which consequently moves the piston in an opposite direction.

Table E-4: HAZOP for 5/3 way pneumatic valve.

	MORE	LESS	NONE	REVERSE
FLOW	High flow	Low flow	No flow	Reverse flow
Consequence	Higher flow rate through the valve	Lower flow rate through the valve	No air flow through the valve	Air flow redirected and piston moves in an opposite direction
Cause	Outlet pressure from compressor increased	Outlet pressure from compressor decreased	No outlet from compressor; valve blocked; or static pressure inside cylinder reached	Operational voltage charged to the other side, with air pressure over 4 bar.
<VOLTAGE>	Higher voltage	Lower voltage	No voltage	/
Consequence	Higher voltage	Lower voltage	No voltage	/
Cause	Power supply increased	Power supply decreased	Power shut-down / failure / Valve failure	/

HAZOP includes:

1) With increasing pressure, the high flow rate through the valve could bring potential damage to operator or devices nearby when disconnecting the valve from air compressor.

2) Considering an average minimum body resistance of 720 Ω, a nominal operating voltage of 24 V leads to a current of 24 V / 720Ω = 33.3 mA, which makes an operator feel pain and his fingers get numb for a short time but causes no lethal damage to heart. However, with voltage from power supply increasing, the operator is in danger of lethal current attack when it reaches 50 mA (at a voltage of 36 V). A current of 100 mA kills people.

3) An overload voltage higher than the nominal 24 V could also bring damage or break the pneumatic valve.

Protection approaches include:

1) Wear a pair of gloves.

2) Never apply a voltage of higher than 36 V to the pneumatic valve.

3. Air Cylinder

FUNTION: THIS Series 167: 80/200 mm tie rod air cylinder has a maximum working pressure of 10bar. With the piston inside moving downwards by pressurized air flow from Compressor 1 or Compressor 2, the experimental pipe will be closed from the top. With redirection of pneumatic valve, the piston will retract at a fast speed to open the experimental pipe, causing a sudden pressure drop if initially there is a pressure buildup process.

Table E-5: HAZOP for air cylinder.

	MORE	LESS	NONE	OTHER THAN
<PRESSURE>	High pressure	Low Pressure	Vacuum	Explosion
Consequence	Higher static pressure in air cylinder; stronger force on piston	Lower static pressure in air cylinder; weaker force on piston	Initial state, with 1 atm inside air cylinder, same as ambient air	Air cylinder fails and cracks; potential damage to people and devices nearby with cracking fragments
Cause	Outlet pressure from compressor increased	Outlet pressure from compressor decreased	Compressore fails / disconnected; pneumatic valve fails / disconnected	Breakage on cylinder with an inner pressure higher than 10 bar.

HAZOP includes:

1) The cracking of air cylinder might happen if pressurized air flow coming in from compressors has a pressure of more than 10 bar, as in the case of using Compressor 2.

2) A too high pressure inside cylinder also forces the piston to move faster. It remains possible that the piston with a great momentum will break the experimental pipe from the top and cause other damages also, like fragments of the pipe .

3) It is highly dangerous to put hands between the piston and the experimental pipe when the piston is retracted into the air cylinder and the cylinder is filled with pressurized air.

Prevention approaches include:

1) Always keep the outlet pressure of Compressor 2 not higher than 10 bar.

2) It is fine to retract piston back into the air cylinder after the experimental pipe has been closed. However, when the piston is to be moved downwards to close the pipe, make sure the inner pressure in the air cylinder is not too high and that the speed of pistion will not be too fast.

3) Never put hands between the piston and the experimental pipe.

4. Square gasket

FUNCTION: to ensure no gas leakage from the experimental pipe between the piston and the experimental pipe.

Table E-6: HAZOP for square gasket.

	MORE	LESS	NONE	OTHER THAN
<STRENGTH / FLEXIBILITY>	Stronger / more flexible	Weaker / less flexible	Fragile	Wrong material
Consequence	Can stand high pressure / temperature	Can only stand low pressure / low temperature	Useless	Not fit in the tesing system
Cause	Better physical properties in strength / flexibility	Poorer physical properties in strength / flexibility	Infected by Ronaldo's knee	Wrong material

HAZOP includes:

1) If the gasket is not strong enough, that is, can not endure the strong force brought by the piston and/or pressure waves with high energy brought by CO_2 BLEVEs, it will break, generating fragments which would bring damage to the operators or devices nearby.

2) If the gasket is not flexible enough, it will gradually deform itself with repeating usage and eventually become unfit for sealing. A unfit gasket will either prevent the pressure buildup inside the experimental pipe or lead to a sudden breakage that will cause unexpected damage to operators or devices nearby.

Protection approaches include:

1) New gaskets made of different materials could be tested and used. Materials that may suit for a gasket and their working pressure and temperature ranges are listed in Table E-7.

Table E-7: Feasible gasket materials.

MATERIAL	WORKING TEMP (°C)	WORKING PRESSURE
PU (polyurethane rubber)	[-40, 80]	don't know, but has highest tensile strength
PTFE (polytetrafluoroethylene)	[-20, 250]	< 6.4 MPa
PCTFE	[-196, 125]	stronger than PTFE
NBR (Nitrile butadiene rubber)	[-40, 120]	/
EPDM (ethylene propylene diene M-class rubber)	as low as -54	/
SR (silicone rubber)	[-40, 220]	/

NOTE: Some working pressures are not found. For the use of gasket, PTFE sounds good enough, if the VAPOR temperature NEAR gasket all along heating process is within its range, but indeed a short time exceed will do no much harm to the gasket. PCTFE may be even better, but may be more expensive.

2) Wear a pair of gloves when dealing with things like piston, square gasket, etc on the testing rig.

5. Experimental pipe

FUNCTION: To store and create a confined volume for CO2 BLEVE tests.

Table E-8: HAZOP for an experimental pipe.

	MORE	LESS	NONE	AS WELL AS	OTHER THAN
<PRESSURE>	High pressure	Low Pressure	Vacuum	Delta-P	Explosion
Consequence	Higher static pressure in pipe; stronger force on both pipe and the gasket at the open side	Lower static pressure in pipe; weaker force on both pipe and the gasket at the open side	Initial state, with 1 atm inside pipe, same as ambient air	Pressure set with air compressor is not fully reached inside the pipe	Pipe fails and cracks; potential damage to people and devices nearby with high speed cracking fragments
Cause	Outlet pressure from compressor increased	Outlet pressure from compressor decreased	Compressore fails / disconnected; pneumatic valve fails / disconnected	Possible gas leakage at connection pipe / valve 2 / drilling holes / sealing with steel pedestal / gasket at the open side	Anything that causes sudden breakage and depressrization of pipe, with high inner pressure. A sudden hit from outside with great force, for instance

HAZOP includes:

1) As mentioned in HAZOP of the air cylinder, one major potential damage comes from the piston is when it closes the experimental pipe at high speed. This could crash the pipe immediately and generate fragments.

2) Unexpected failure of the testing pipe may also happen due to high internal pressure and also generate gragments for further damage.

Protection approaches include:

1) Never put hands between the piston and the experimental pipe when the air cylinder is filled with pressurized air.

2) For preventing the damage caused by the high-speed fragments, operators should wear protecting glasses and stand behind a transparent plastic wall, several meters away from the experimental center.

End of Appendix E.

F: MATLAB script for reading pressure signals

A MATLAB script 'read.m' was written to transform voltage signals recorded by oscilloscope to overpressures, with an overall scale combining the sensitivity of a pressure transducer and the scale of a signal amplifier. The script was commented for readers.

```matlab
% Originally presented by Andre Vagner Gaathaug. Modified by Wei Ke.
clear ;

test = input('Test [1 2 3...] No.: '); % Input the auto-No. of a test.
ch = [2 3 4]; % Three channels for (PT 1, PT2, PT 3)

filename = '09_KeW_P101_T 00001/CH2_02h.TXT';
tn = num2str(test); % Convert number 'test' into string 'tn'.
filename((20-length(tn)):19) = tn(1:length(tn)); % Select test number.

dl = [1 4 2 6]; % Help locate correct data lines.

for i = 1:length(ch) % Calculation loop for channels selected.

    filename(23) = num2str(ch(i));
    filename(26) = num2str(ch(i));

    fid = fopen(filename, 'r'); % Open a txt.file with voltage signals.
    sample = 100000; % Sampling size of 100000.

    TTime = textscan(fid, '%f', 1, 'headerlines', dl(1)); % Trigger time.
    TT = TTime{:}';

    FSTime = textscan(fid, '%f ', 1, 'headerlines', dl(2)); % Sampling time.
    FST = FSTime{:};

    STime = textscan(fid, '%f ', 1, 'headerlines', dl(3)); % Time per sample.
    ST = STime{:};

    volt = textscan(fid, '%f ', sample, 'headerlines', dl(4));
    V(:,i) = volt{:};

% For PT 1, calculate over pressure by subtracting an average voltage of
% the last 1000 sample points. For PT 2 and PT 3, calculate over pressure
% by subtracting an average voltage of the first 1000 sample points.
    nch2 = find(ch == 2);
    if i == nch2
        V(:,i) = V(:,i) - mean(V(end-1000:end,i));
    else
        V(:,i) = V(:,i) - mean(V(1:1000,i));
    end

    T(:,i) = FST + ST.*((1):(length(V(:,i))))';

end % calculation loop ends here.

% Scaling of Voltage signals.
basescale = [1 24 0.2 0.2]; % bar/Volt.
scale = basescale(ch);
```

```matlab
PRes=V.*(ones(size(V(:,1)))*scale); % Convert voltage to pressure.
% Filtering. Originally presented by Dag Bjerketvedt.
windowSize = 2*50;
F1PRes=filter(ones(1,windowSize)/windowSize,1,PRes);

S1 = size(F1PRes);

FPRes(:,:)=F1PRes(windowSize/2:end,:);
FPRes(S1(1)-windowSize/2:S1(1),:)= F1PRes(end-windowSize/2:end,:);

% Plotting
figure (1)
plot (T,FPRes);
xlabel('Time [s]')
ylabel('Pressure [Bar]')
title(['CO2 BLEVE Study',' - ','Test No.: 18']);
legend('PT1','PT2','PT3');

figure (2)
t = T(80001:90000)'; % to select a time period of 0.1 s
P1 = FPRes(80001:90000,1);
P2 = FPRes(80001:90000,2);
P3 = FPRes(80001:90000,3);

subplot(3,1,1);
plot(t,P1);
title(['CO2 BLEVE Study',' - ','Test No.: 18']);
axis([0,0.1,-1,60]);
legend('PT1');

subplot(3,1,2);
plot(t,P2);
ylabel('Pressure [Bar]')
axis([0,0.1,-0.66,0.66]);
legend('PT2');

subplot(3,1,3);
plot(t,P3);
xlabel('Time [s]')
axis([0,0.1,-0.66,0.66]);
legend('PT3');

% End of the script.
```

G: Experimental data of CO$_2$ BLEVE tests

Test No.	Pipe Volume [cm3]	Dry ice [g]	PT1 [bar]	PT2 [bar]	PT3 [bar]	Temp [°C]	Phase composition at PT1 / T					Additional info.
							Liq_CO$_2$ [g]	Liq wt-%	Vap_CO$_2$ [g]	Vap wt-%	Loss [wt-%]	
1	82	0	0.05	0	0	-78.5	0	0	0	0	0.0	/
2	82	22	16.2	0.01	0.01	-24.2	20.5	93.2	1.5	6.8	0.0	/
3	82	30	17.1	0.02	0.08	-22.6	/	/	/	/	/	/
4	82	45	17	0.02	**0.2**	-22.7	43.5	96.7	1.5	3.3	0.0	/
5	82	9.7	20.4	0.01	0.08	-17.2	5.1	54.6	4.2	45.4	3.7	/
6	80	20	18.4	**0.16**	0.01	-20.4	17.8	89.4	2.1	10.6	0.5	Testing pipe replaced
7	80	20	19.7	0.01	0	-18.2	16.8	84.0	3.2	16.0	0.0	Some dry ice left at pipe bottom
8	80	30	20.1	0.01	0.01	-17.5	27	90.0	3.0	10.0	0.0	/
9	80	45	15.8	**0.62**	**0.1**	-25	38	95.0	2.0	5.0	11.1	/
10	80	30	18.4	0.01	0.01	-20.4	18.6	85.1	3.3	14.9	27.1	Tiny dry ice of a thin layer covering pipe outer wall
11	80	30	19.3	**0.33**	**0.1**	-18.7	24.6	88.8	3.1	11.2	7.6	/
12	80	20	18.4	0.03	0.02	-20.4	16.5	83.1	3.4	16.9	0.7	/
13	80	10	18.3	0.02	0.01	-20.6	5.2	57.2	3.9	42.8	9.0	/
14	80	30	20	0.02	0.02	-17.8	27.2	90.7	2.8	9.3	0.0	/
15	80	60	12.5	**0.18**	**0.16**	-31.6	56.3	98.2	1.1	1.8	4.4	Increased slightly output pressure of air compressor
16	80	62	21.8	**0.16**	**0.16**	-15.1	53.5	96.8	1.8	3.2	10.9	O-ring at pipe bottom broke
17	80	60	22.3	**0.25**	**0.1**	-14.3	52.3	96.6	1.9	3.4	9.7	Using broken O-ring
18	80	62	29.4	**0.13**	**0.24**	-5	37.3	91.6	3.4	8.4	34.4	Cut on pipe surface, weakening pipe strength
19	80	60	27.3	**0.1**	**0.39**	-7.5	22.3	83.1	4.5	16.9	55.3	Deeper cutting on pipe
20	80	20	30.8	0.02	0.01	-3.3	10.4	62.5	6.2	37.5	16.9	Transducer 2 was hit by flying pipe
21	82	60	20.6	**0.24**	**0.23**	-17	55.8	96.9	1.8	3.1	4	Pipe ruptured with fragments in an explosion

H: Thermodynamic data

CO2 properties	P [bar]	T [K]	T [°C]	Density-liq [kg/dm3]	Density-vap [kg/dm3]	Internal Energy-liq [kJ/kg]	Internal Energy-vap [kJ/kg]	Sound Speed-liq [m/s]	Sound Speed-vap [m/s]
	5.18	216.6	-56.4	1.1782	0.0138	79.6136	392.8636	975.85	222.78
	12.83	240	-33	1.0886	0.0333	125.6886	398.0682	806.38	222.96
	15.19	245	-28	1.0676	0.0395	135.7932	398.5909	769.44	222.24
	17.85	250	-23	1.0457	0.0466	146.0364	398.8636	731.78	221.22
	20.84	255	-18	1.0228	0.0549	156.4455	398.8409	693.01	219.87
	24.19	260	-13	0.9987	0.0644	167.0568	398.4545	652.58	218.19
	27.91	265	-8	0.973	0.0755	177.9136	397.6818	610.07	216.15
	32.03	270	-3	0.9456	0.0884	189.0682	396.3864	565.46	213.75
	36.59	275	2	0.9159	0.1036	200.6045	394.5227	519.14	210.96
	41.61	280	7	0.8834	0.1217	212.6364	391.8409	471.54	207.72
	47.12	285	12	0.8469	0.1439	225.35	388.1364	422.75	203.94
	53.18	290	17	0.8045	0.1719	239.0682	382.9091	371.95	199.45
	59.82	295	22	0.7524	0.2097	254.4773	375.2045	315.91	193.84

Data above is from TABLE 2-199 in Perry's Chemical Engineering's Handbook, and data below is real test data by linear interpolation from above.

Note: Test No. 1 is not listed here since it was set as background with no CO2 filling and no heating.

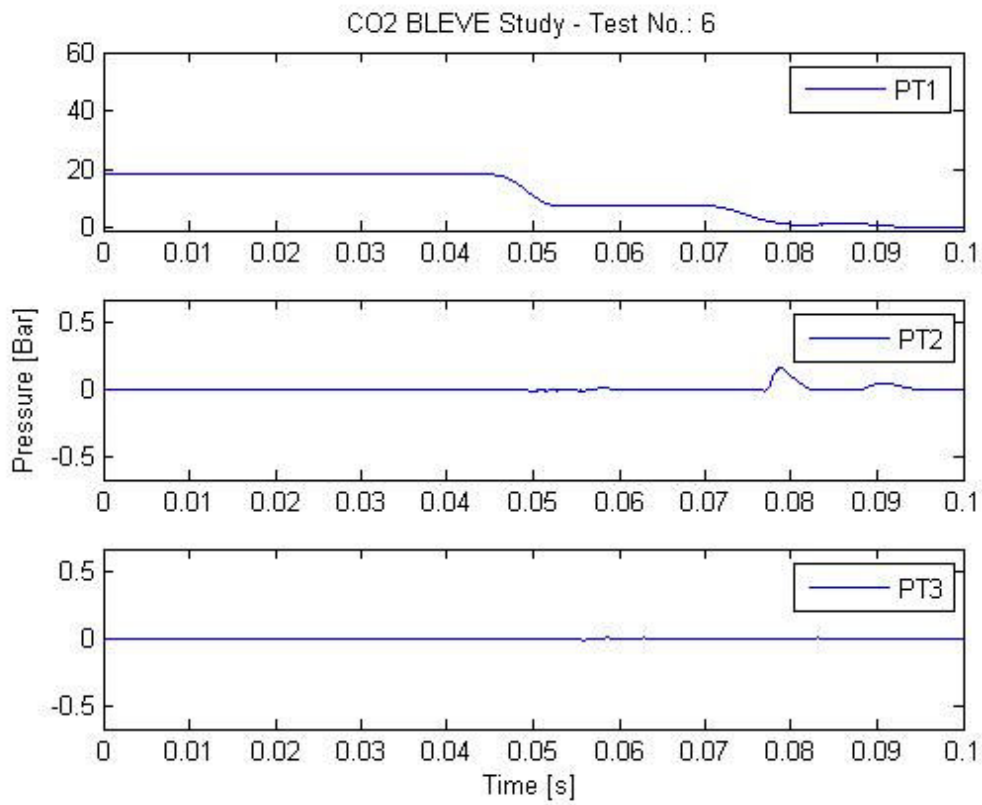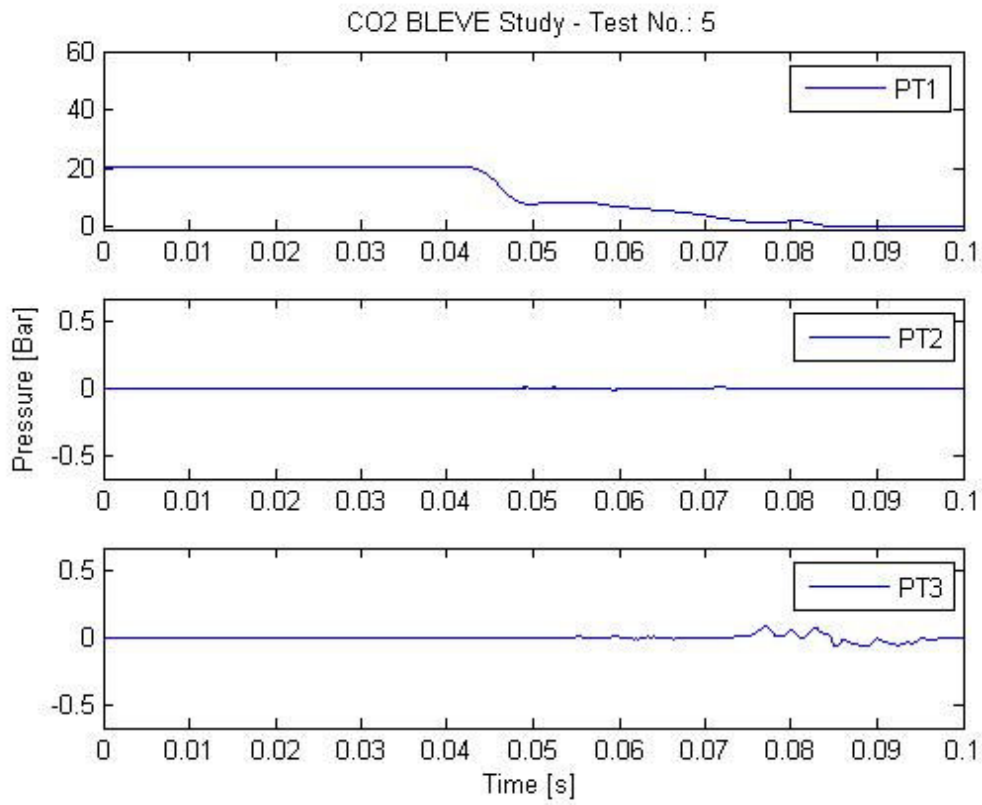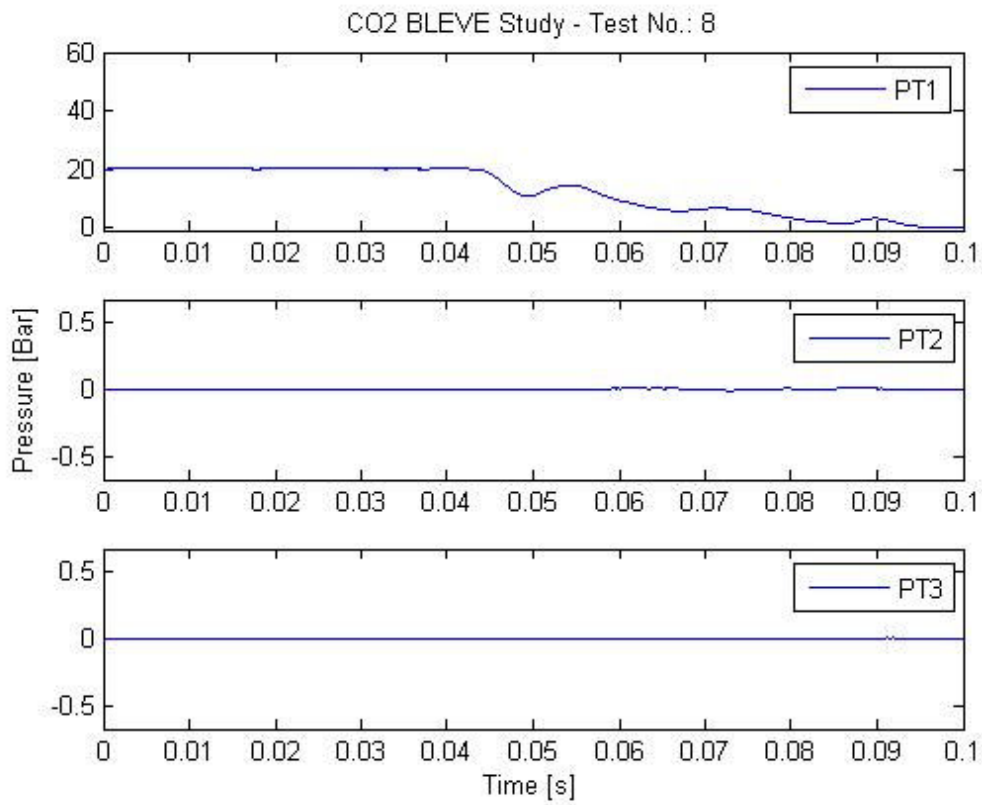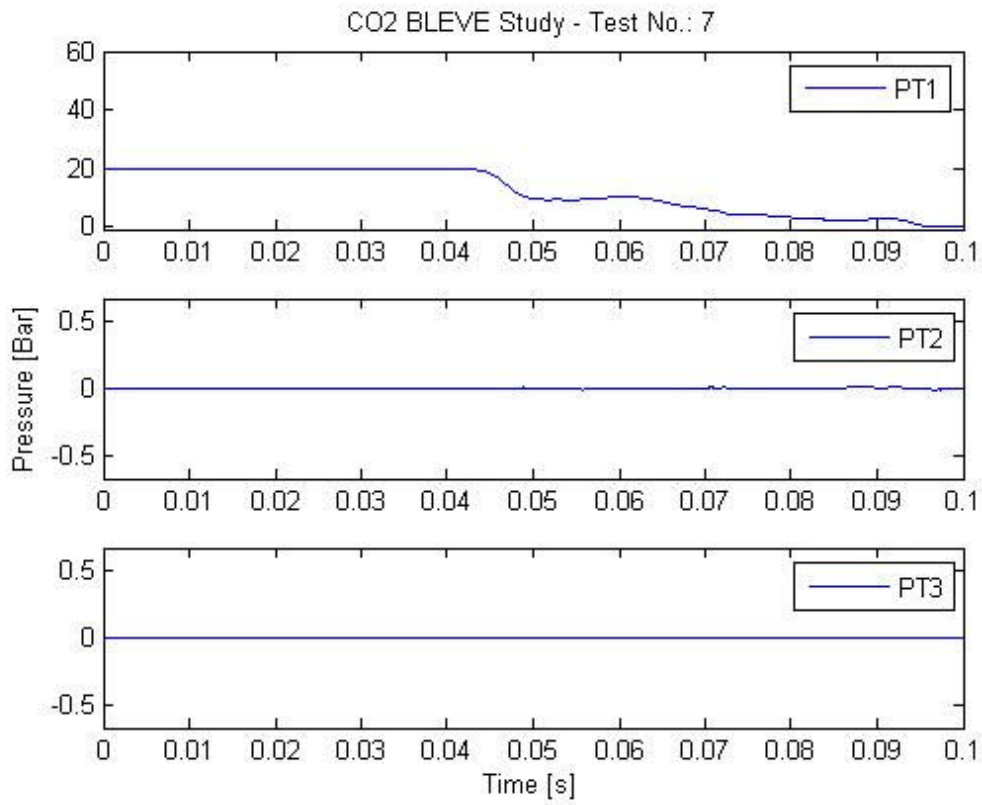| Test No.	PT1 + 1 [bar]								
2	17.2	248.8	-24.2	1.0511	0.0449	143.5334	398.7970	740.98	221.47
3	18.1	250.4	-22.6	1.0438	0.0473	146.9067	398.8617	728.54	221.11
4	18	250.3	-22.7	1.0446	0.0470	146.5586	398.8625	729.84	221.15
5	21.4	255.8	-17.2	1.0188	0.0565	158.2193	398.7763	686.25	219.59
6	19.4	252.6	-20.4	1.0338	0.0509	151.4324	398.8518	711.68	220.52
7	20.7	254.8	-18.2	1.0239	0.0545	155.9581	398.8420	694.83	219.93
8	21.1	255.5	-17.5	1.0209	0.0556	157.2691	398.8109	689.87	219.74
9	16.8	248	-25	1.0543	0.0438	141.9930	398.7560	746.65	221.62
10	19.4	252.6	-20.4	1.0338	0.0509	151.4324	398.8518	711.68	220.52
11	20.4	254.3	-18.7	1.0262	0.0537	154.9137	398.8442	698.72	220.07
12	19.4	252.6	-20.4	1.0338	0.0509	151.4324	398.8518	711.68	220.52
13	19.3	252.4	-20.6	1.0346	0.0506	151.0843	398.8526	712.98	220.57
14	21	255.2	-17.8	1.0216	0.0554	156.9523	398.8224	691.08	219.79
15	13.5	241.4	-31.6	1.0826	0.0351	128.5573	398.2166	795.89	222.76
16	22.8	257.9	-15.1	1.0087	0.0605	162.6539	398.6148	669.36	218.89
17	23.3	258.7	-14.3	1.0051	0.0619	164.2377	398.5572	663.32	218.64
18	30.4	268	-5	0.9564	0.0833	184.6551	396.8989	583.11	214.70
19	28.3	265.5	-7.5	0.9704	0.0767	178.9695	397.5592	605.85	215.92
20	31.8	269.7	-3.3	0.9471	0.0877	188.4455	396.4587	567.95	213.88
21	21.6	256	-17	1.0173	0.0568	158.5678	398.7532	684.92	219.53

I: Pressure records

Test 1 to test 20 had three signal channels: PT 1, PT 2 and PT 3. An additional channel PT 4 was added in test 21, to measure side-on pressures. The time period for plotting for test 1 to test 20 was 0 to 0.1s AFTER trigger. In test 21, -0.4 to -0.3 s was plotted, BEFORE trigger.
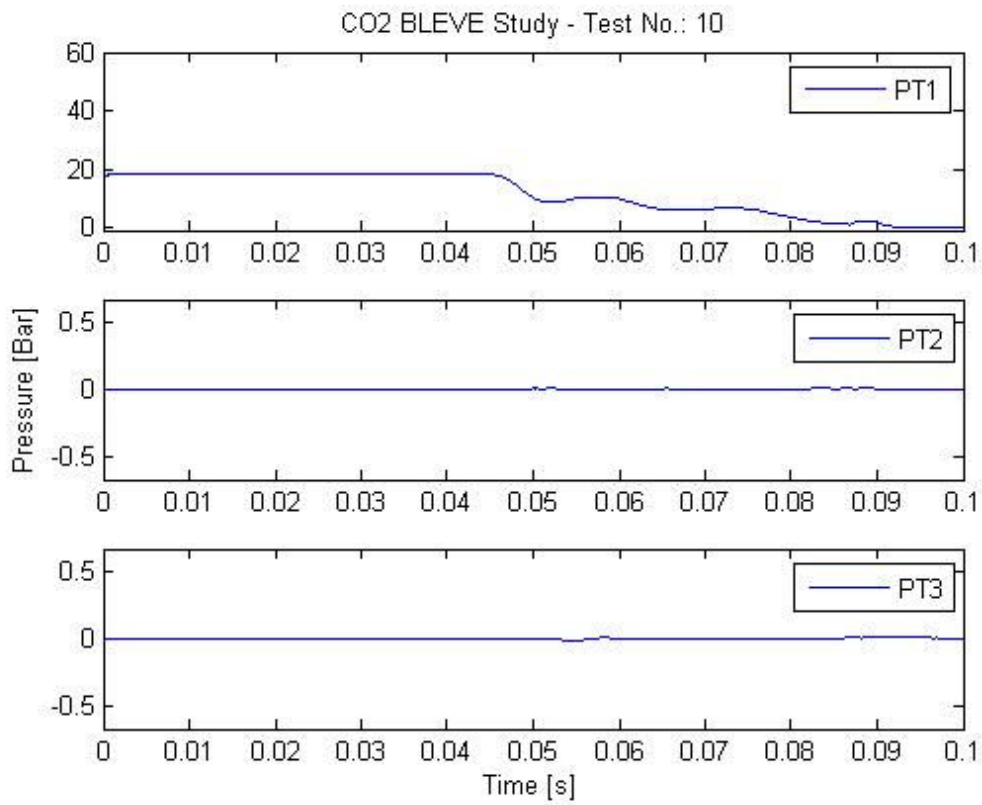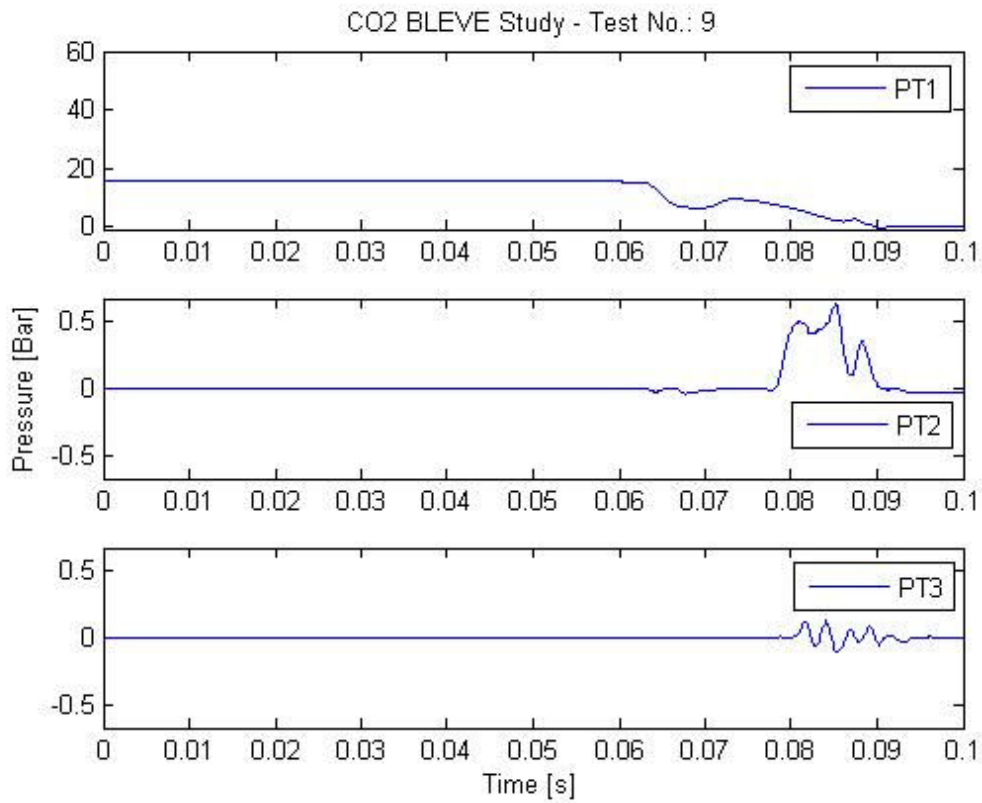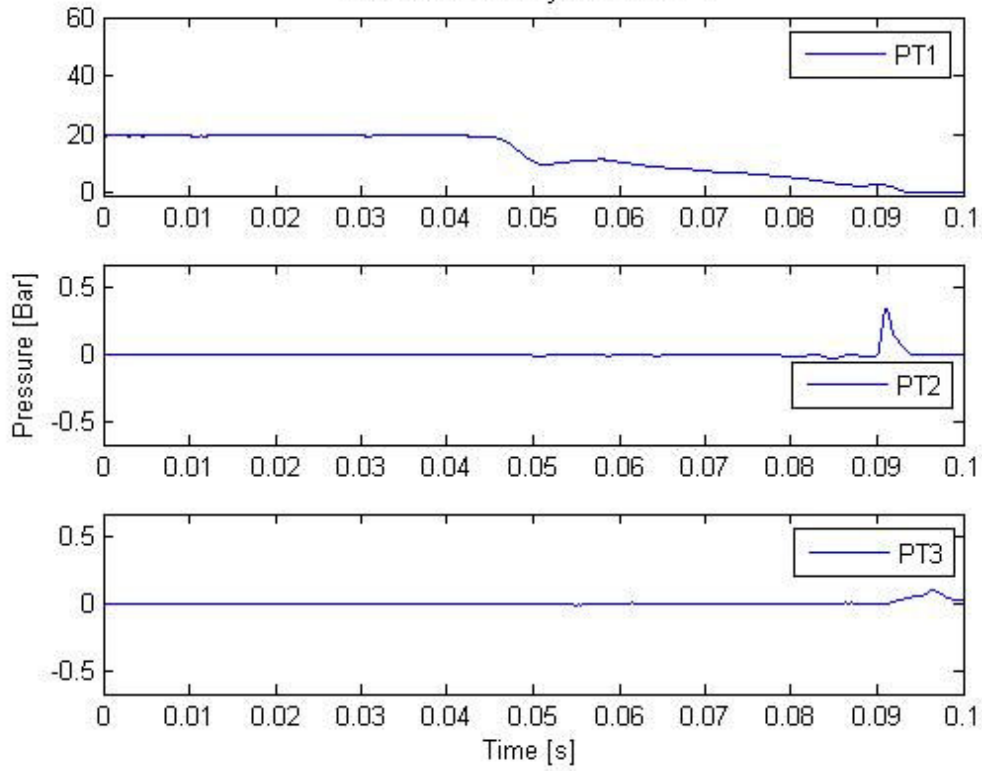
CO2 BLEVE Study - Test No.: 3

CO2 BLEVE Study - Test No.: 4

CO2 BLEVE Study - Test No.: 7

CO2 BLEVE Study - Test No.: 8

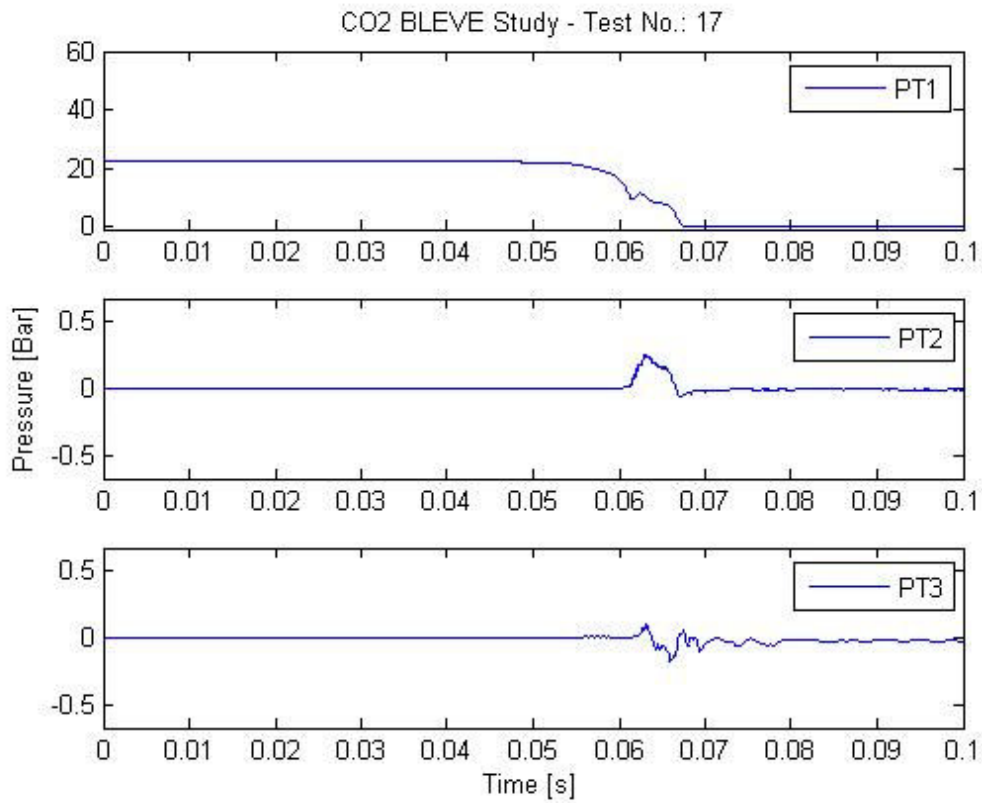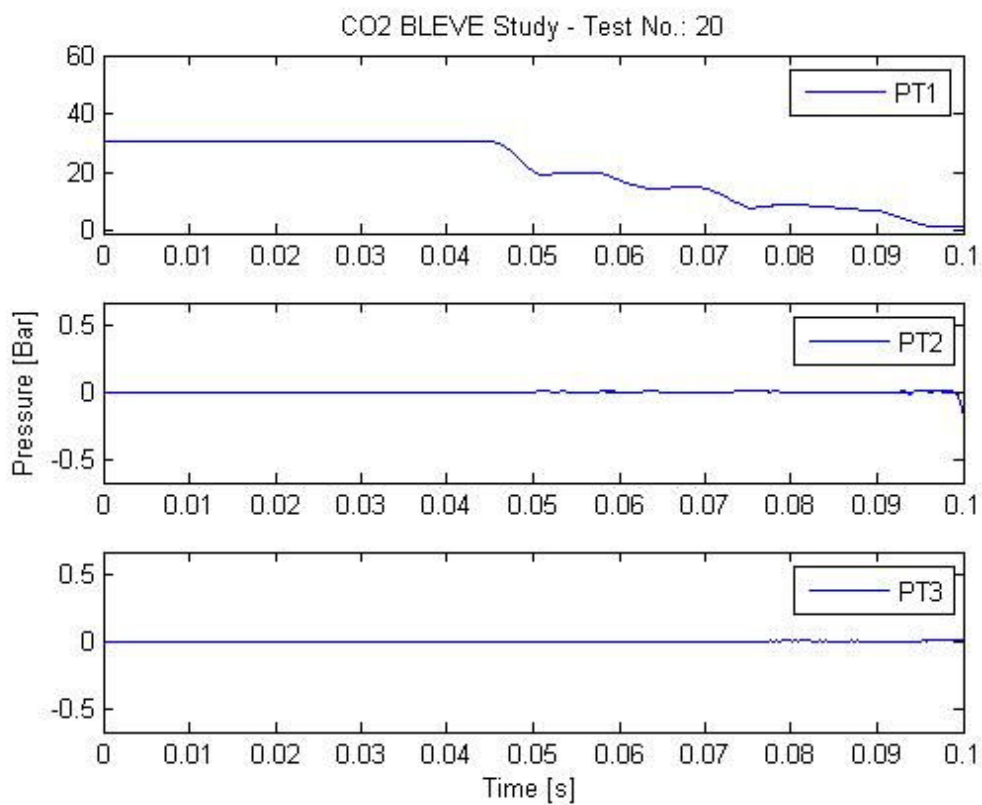CO2 BLEVE Study - Test No.: 9

CO2 BLEVE Study - Test No.: 10
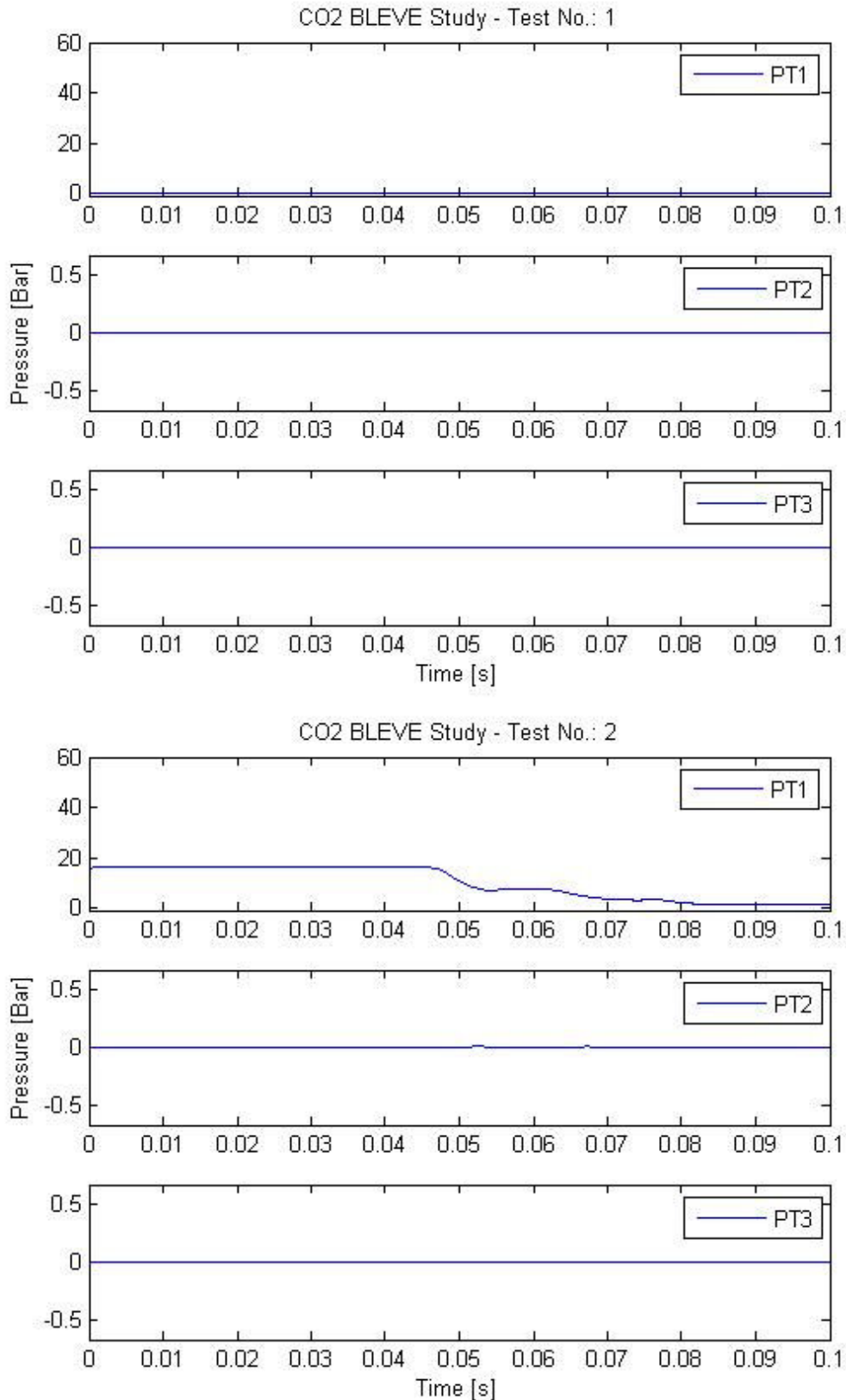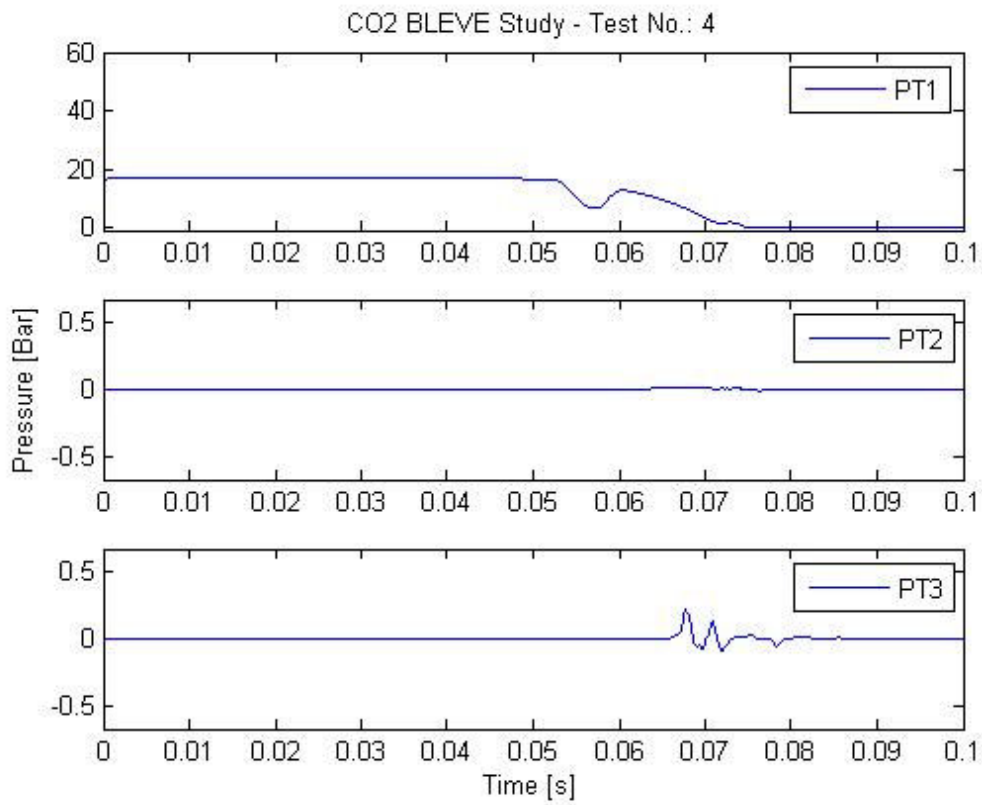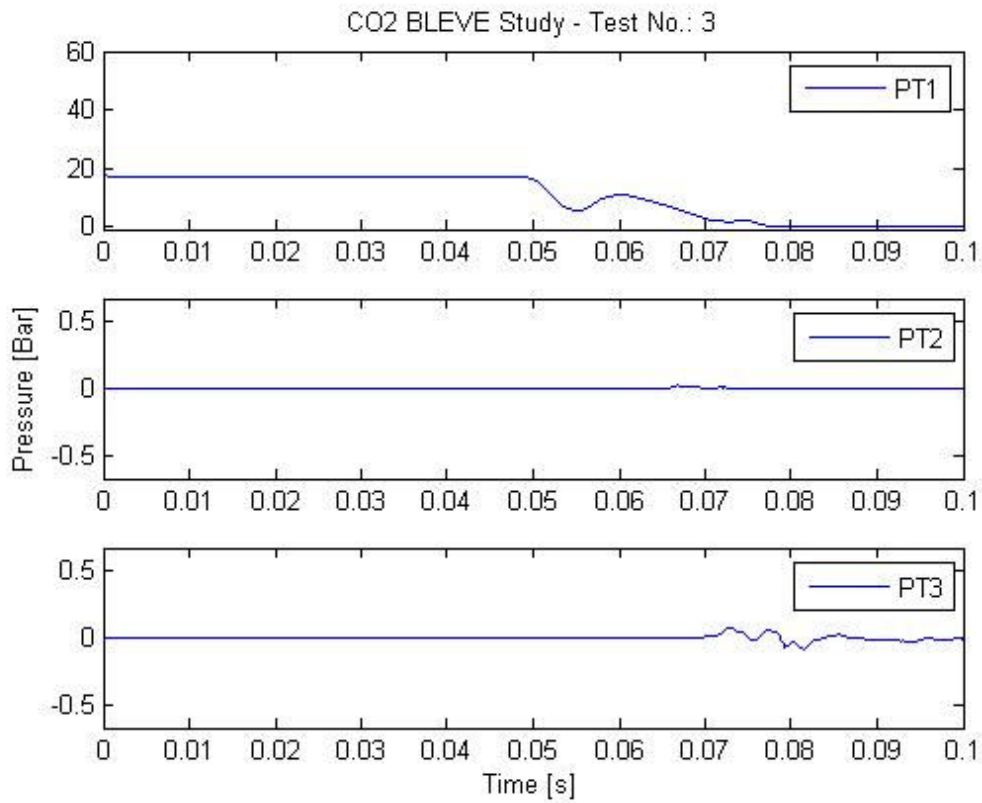
CO2 BLEVE Study - Test No.: 11

CO2 BLEVE Study - Test No.: 12

CO2 BLEVE Study - Test No.: 13

CO2 BLEVE Study - Test No.: 14

CO2 BLEVE Study - Test No.: 15

CO2 BLEVE Study - Test No.: 16

CO2 BLEVE Study - Test No.: 17

CO2 BLEVE Study - Test No.: 18

CO2 BLEVE Study - Test No.: 19

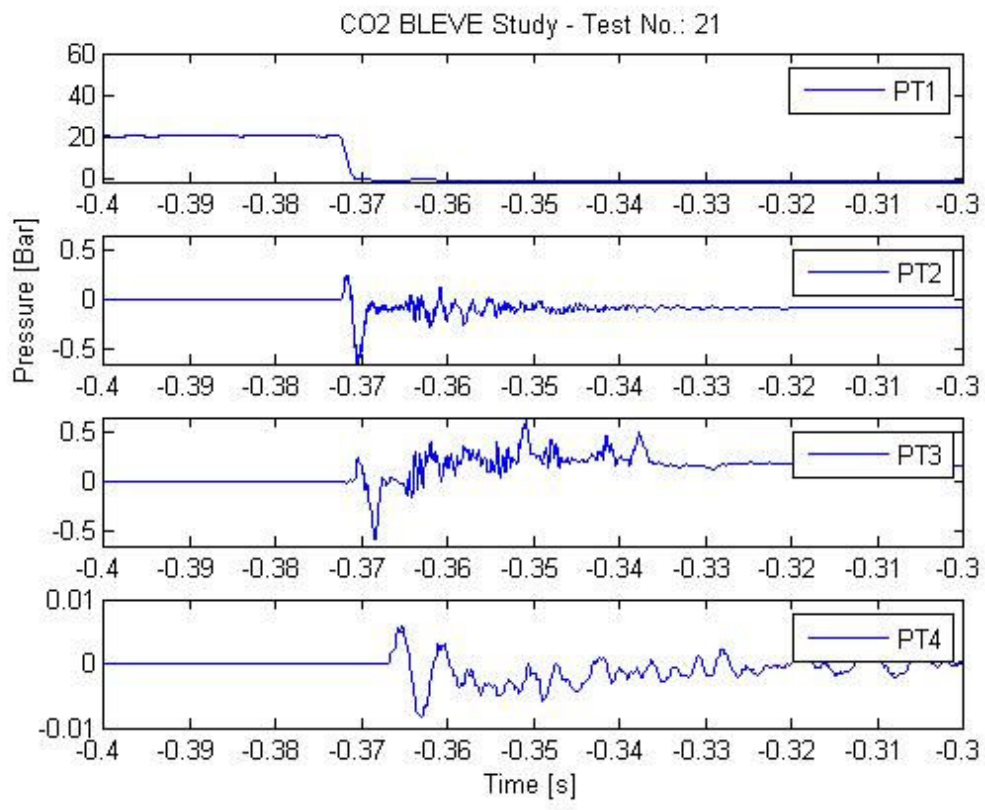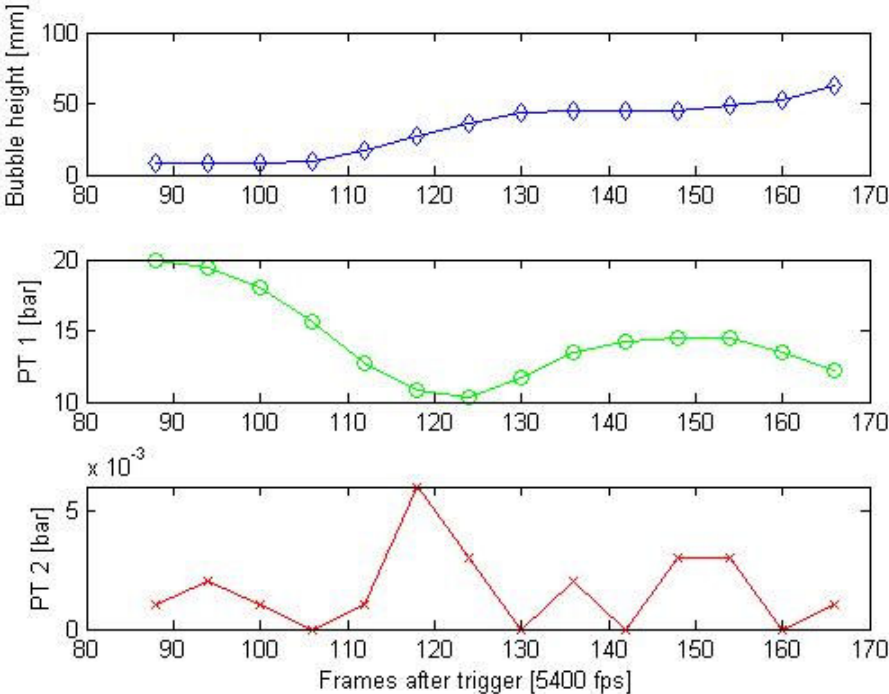CO2 BLEVE Study - Test No.: 20
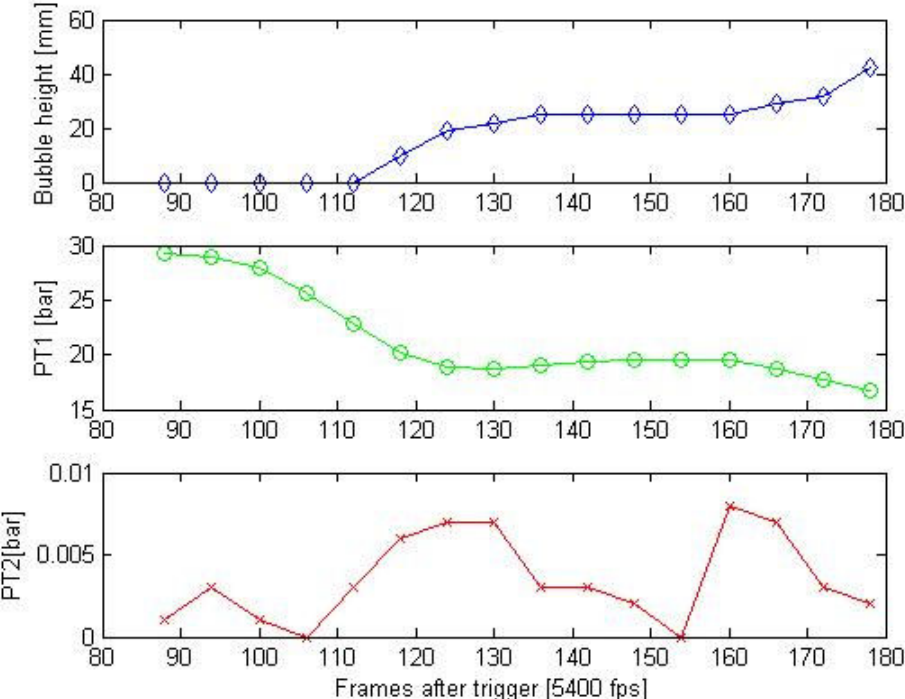
CO2 BLEVE Study - Test No.: 21
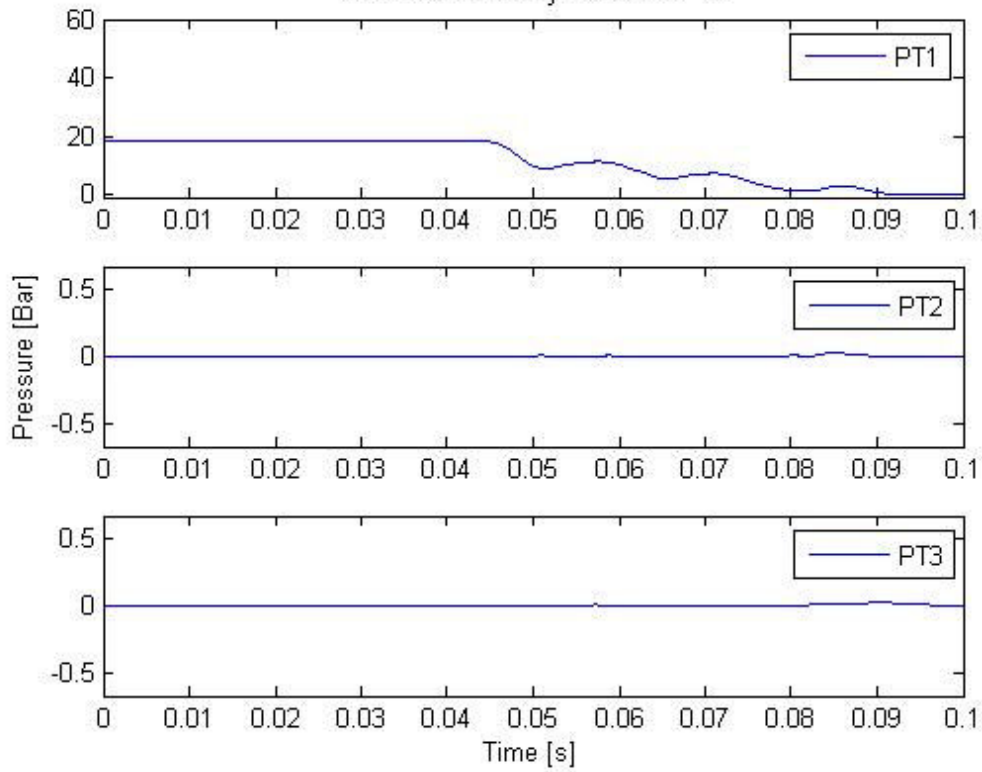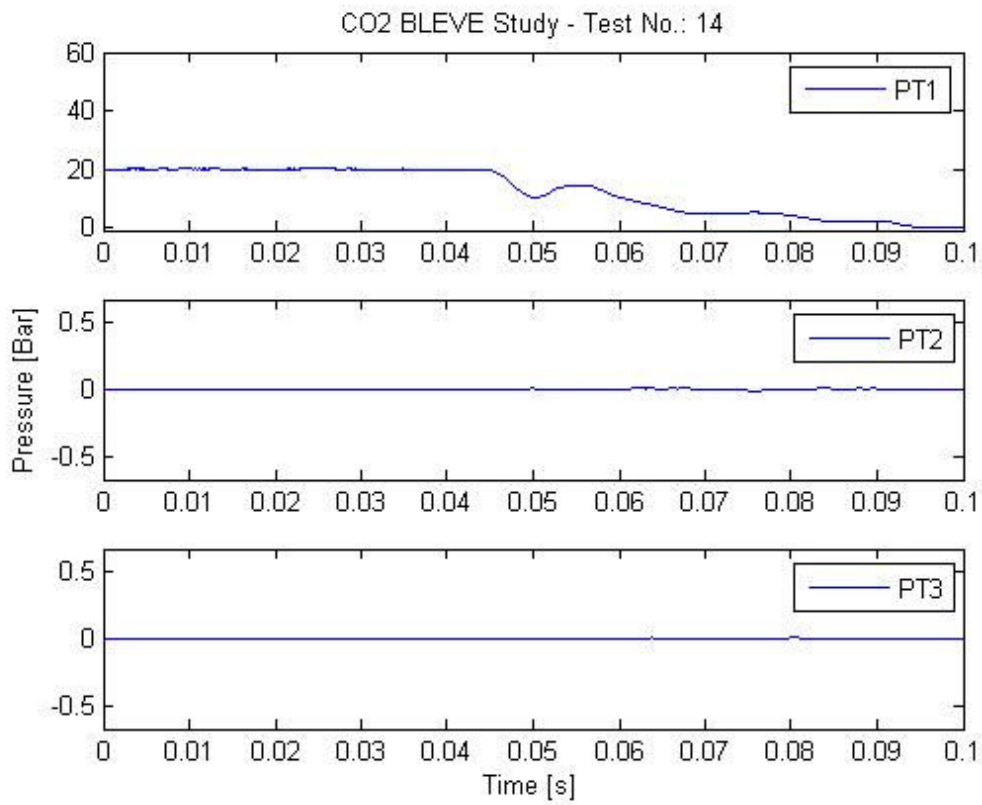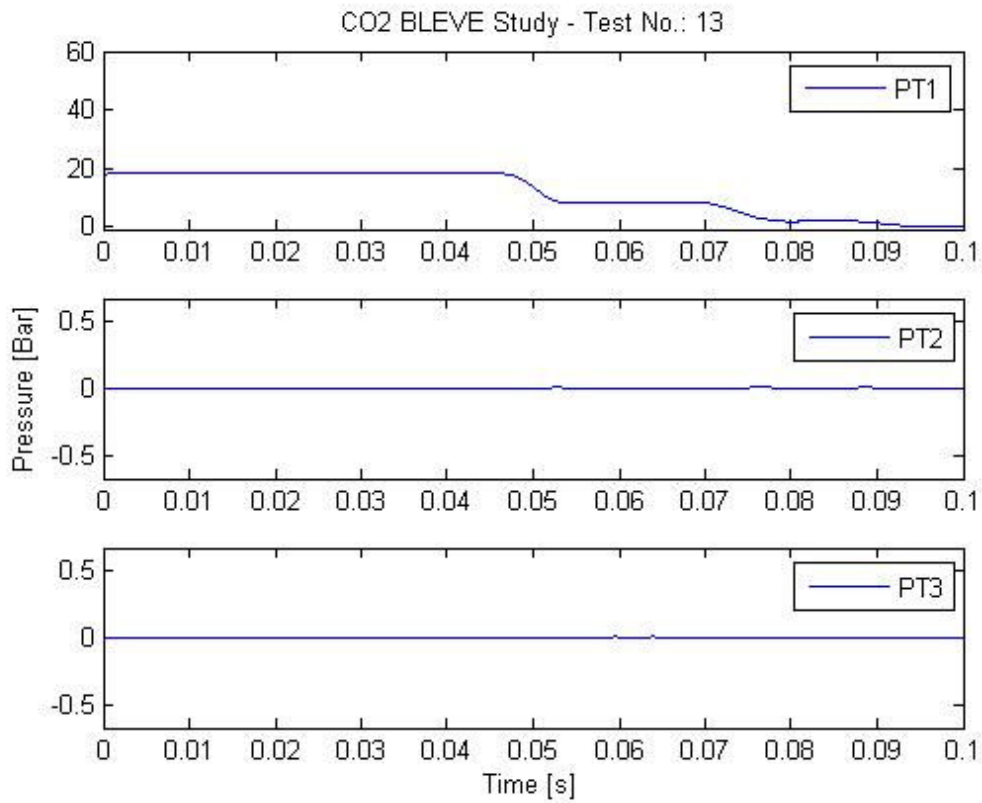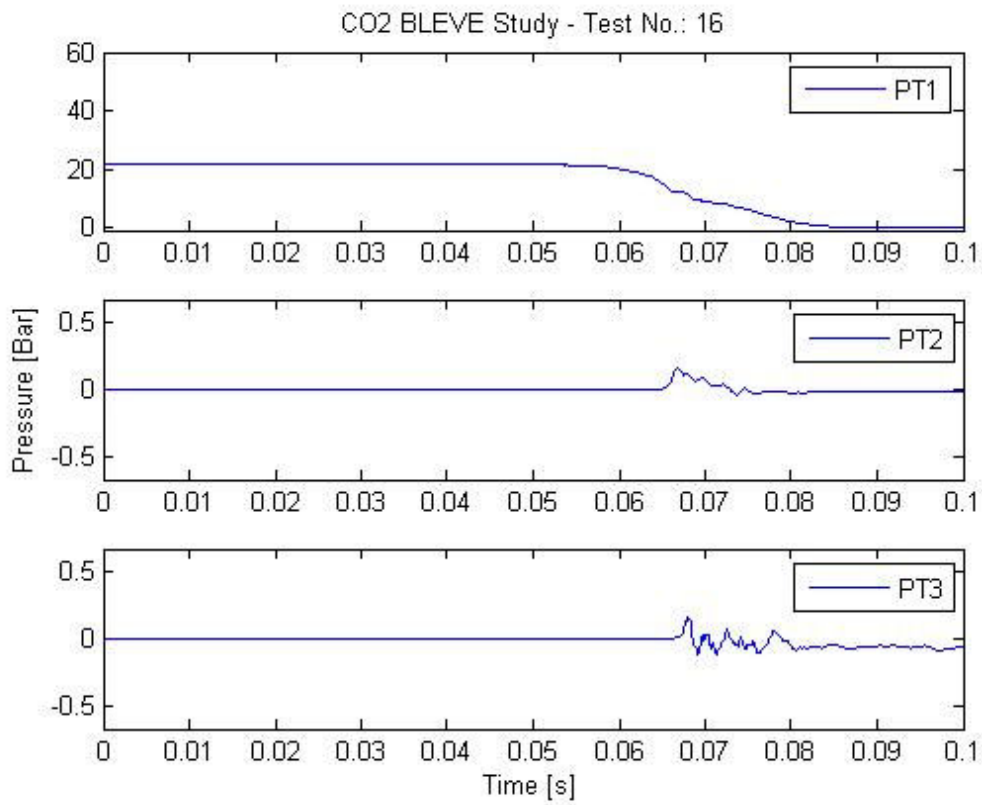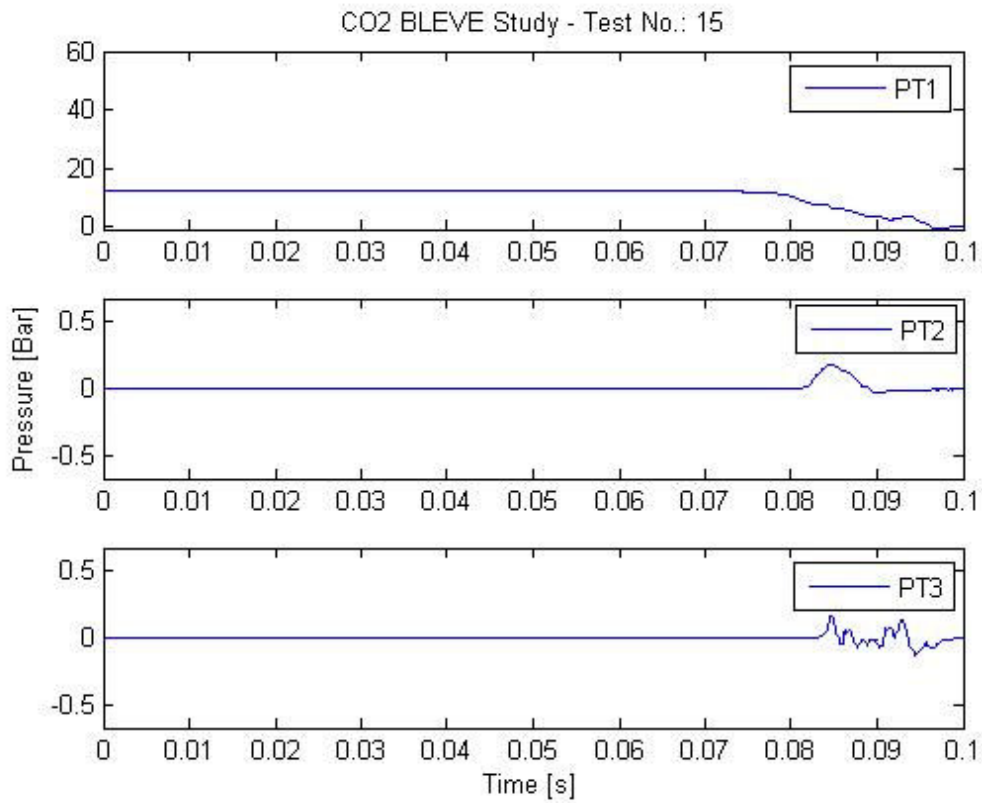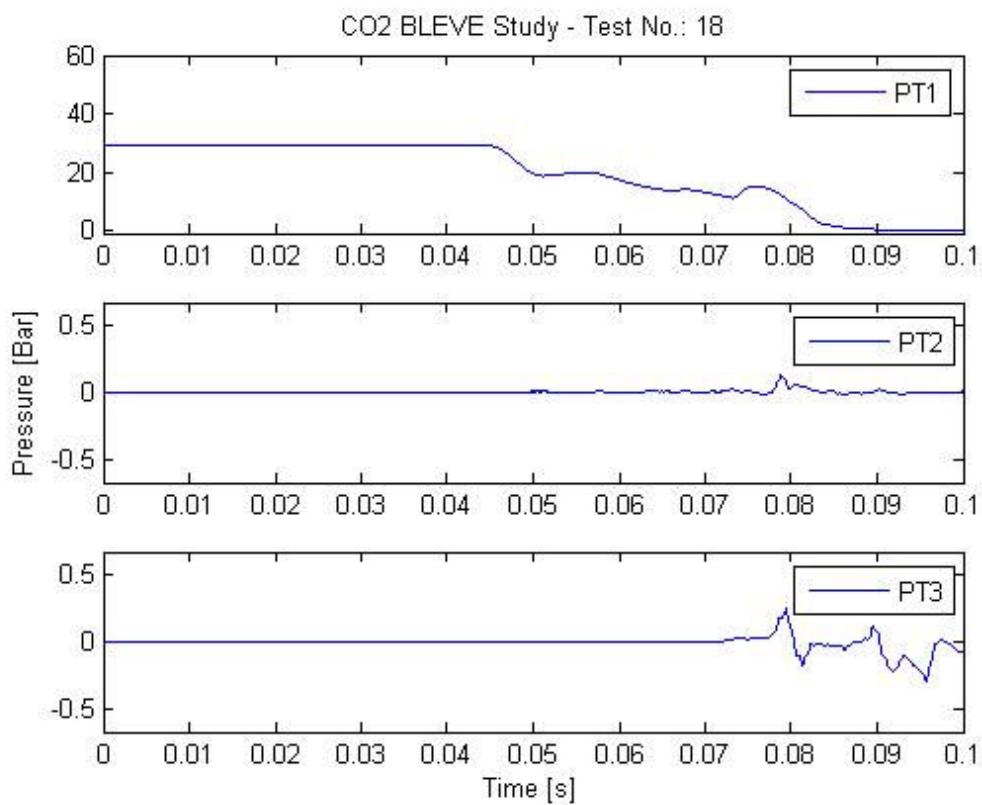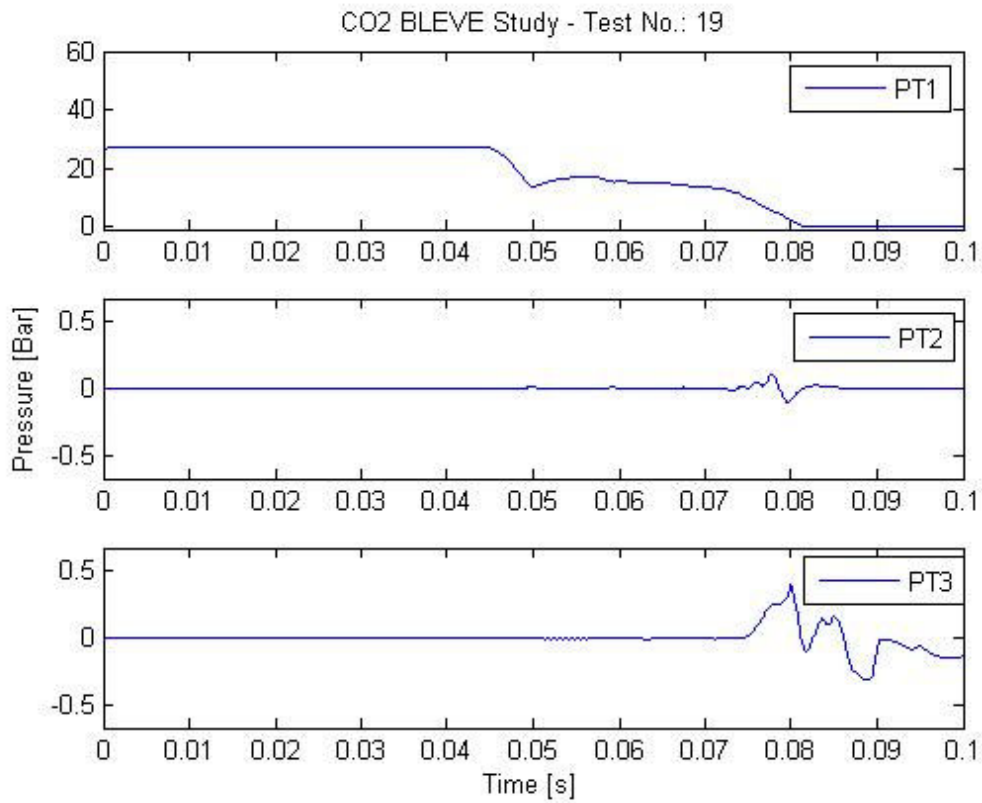
J: Bubble growth with pressures (Test 14/18)

Bubble height against frame number (5400 fps) and PT 1/PT 2 in test 14:

Bubble height against frame number (5400 fps) and PT 1/PT 2 in test 18:

K. MATLAB script for plotting superheat limit curve

A MATLAB script 'superheat curve_CO$_2$' was written for this purpose. Thermodynamic data of saturation pressure and temperature is from Perry's Chemical Engineer's Handbook, Table 2-199 on page 2-240.

```matlab
% Presented by: Dag Bjerketvedt, HiT, 23.09.2008.
% Modified by: Ke Wei, HiT, 20,05,2009.
% CO2 saturation curve - superheat limit curve.

C = (7.377-7.231)/(304.13-303.23); % Tangent at critical point.
T = 220:304;
P = C.*(T-(304.13))+ 7.377;
p0 = [0.1 0.1];
t0 = [0 300];

% Saturation P/T data of CO2 from boiling point to critical point.
T_sat = [194.5 216.6 240 245 250 255 260 265 270 275 280 285 290 295 300
304.13]'; % [K]
P_sat = [1 5.18 12.83 15.19 17.85 20.84 24.19 27.91 32.03 36.59 41.61 47.12
53.18 59.82 67.13 73.77]'/10; % [MPa]

% Plotting
plot(T_sat(1:2),P_sat(1:2),'bd',T_sat(2:16),P_sat(2:16),'g',T_sat(16),P_sat
(16),'bd',T,P,'r-',t0,p0,':');
axis([190 310 0 8]);
xlabel('Temperature [K]')
ylabel('Pressure [MPa]')
text(190,0.4,'Boiling Point')
text(240,2.5,'Vapor pressure curve')
text(270,1.6,'Superheat limit curve')
text(297,7.5,'Critical point')
text(210,1,'Triple Point')

% End of script.
```